LBNL-xxxxxx
September 2009

Final Report for completed IPP-0110 and 0110A Projects:

"High Energy Ion Technology of Interfacial Thin Film Coatings for Electronic, Optical and Industrial Applications"

Summary

The DOE-supported IPP (Initiatives for Proliferation Prevention) Project, IPP-0110, and its accompanying "add-on project" IPP-0110A, entitled "High Energy Ion Technology of Interfacial Thin Film Coatings for Electronic, Optical and Industrial Applications" was a collaborative project involving the Lawrence Berkeley National Laboratory (LBNL) as the U.S. DOE lab; the US surface modification company, Phygen, Inc., as the US private company involved; and the High Current Electronics Institute (HCEI) of the Russian Academy of Sciences, Tomsk, Siberia, Russia, as the NIS Institute involved.

Regular scientific research progress meetings were held to which personnel came from all participating partners. The meetings were held mostly at the Phygen facilities in Minneapolis, Minnesota (with Phygen as host) with meetings also held at Tomsk, Russia (HCEI as host), and at Berkeley, California (LBNL as host) In this way, good exposure of all researchers to the various different laboratories involved was attained.

This report contains the Final Reports (final deliverables) from the Russian Institute, HCEI. The first part is that for IPP-0110A (the "main part" of the overall project) and the second part is that for the add-on project IPP-0110A. These reports are detailed, and contain all aspects of all the research carried out.

The project was successful in that all deliverables as specified in the proposals were successfully developed, tested, and delivered to Phygen. All of the plasma hardware was designed, made and tested at HCEI, and the performance was excellent. Some of the machine and performance parameters were certainly of "world class". The goals and requirements of the IPP Project were well satisfied.

I would like to express my gratitude to the DOE IPP program for support of this project throughout its entire duration, and for the unparalleled opportunity thereby provided for all of the diverse participants in the project to join in this collaborative research. The benefits are superb, as measured in quite a number of different ways.

Ian Brown
Berkeley
Sep 2009

HIGH ENERGY ION TECHNOLOGY OF INTERFACIAL THIN FILM COATINGS FOR ELECTRONIC, OPTICAL AND INDUSTRIAL APPLICATIONS

Subcontract No.6502005
Between

Ernest Orlando Lawrence Berkeley National Laboratory University of California
And
High Current Electronics Institute

Final report

Principal Investigator _____ ***Prof. Efim Oks***

RUSSIA-TOMSK-2003

Source of Plasma with Additional Cold Emitter

“SPACE-2”

Technical description and

Manual

1. Composition and purpose

The SPACE plasma source is designed to produce gas plasma in a vacuum vessel for various technological and scientific applications. It consists of

1. Plasma source (3 pieces).
2. Power supplies of the plasma sources.

2. Basic operating parameters

1. Main discharge voltage		50÷120 V
2. Keeping discharge voltage:	Ignition	600 V
	Operating	15÷50 V
3. Main discharge current (for 1 source)		5÷20 A
4. Keeping discharge current (for 1 source)		5÷20 A
5. Mode of operation		DC
6. Operating gas		Argon
7. Operating pressure		0.4÷2 mTorr
8. Gas flow rate (for 1 source)		40÷80 sccm
8. Maximum density of the plasma produced in a vacuum vessel with volume of 1 m^3		$8 \cdot 10^{10}$ cm^{-3}
9. Maximum density of ion current extracted from the plasma for vacuum vessel with volume of 1 m^3		2 mA/cm^2
10. Plasma density uniformity on a base length of 40 cm near the center of the chamber with volume of 1 m^3		±10%
11.Power supply		3x220 V
12.Minimum pressure of the cooling water		0.2 MPa

3. Plasma source description and principle of operating.

The plasma source is based on tandem high current discharge. The first stage (keeping discharge) serves to generate electron beam. The second stage (main discharge) accelerates the beam and provides effective ionization of gas atoms in a vacuum vessel. Discharges have common electrode. The keeping discharge anode is electrically connected to the main discharge cathode.

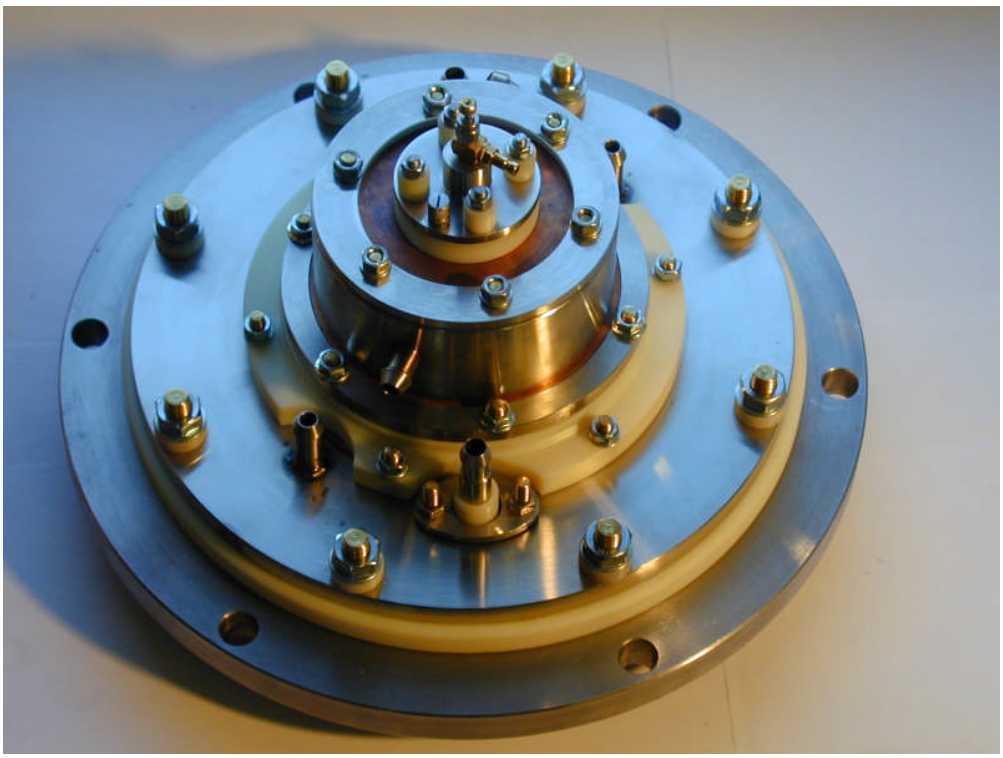

Fig. 1.View of plasma source.

Keeping discharge is a constricted arc with hollow cathode 1 (fig. 2), intermediate electrode 2 and anode 3. The operating gas is fed into the hollow cathode. Cathode spot exists on the inner surface of the cathode. Electron current flows out of the cavity through the cathode aperture and, further, through the slot of the intermediate electrode, to the mesh-like anode. There is a magnesium film on the inner surface of the copper cathode 1. Arc current threshold for magnesium is about 5 A, and for copper it is higher than the maximum discharge current (20 A). Therefore, copper body of the cathode is not subjected to erosion. It has unlimited lifetime. Erosion of magnesium film is accompanied by its re-deposition onto the opposite wall of the cavity. The loss of magnesium through the cathode aperture and also as a result of its oxidation by residual gas is compensated by erosion of magnesium washer 4. There is a disalignment between the hollow cathode aperture and the slot in the intermediate electrode, for prevention of contamination of plasma by cathode material. To avoid cathode spot formation on the outer surface of the cathode, insulated shield 6 and molybdenum foil 7 is used.

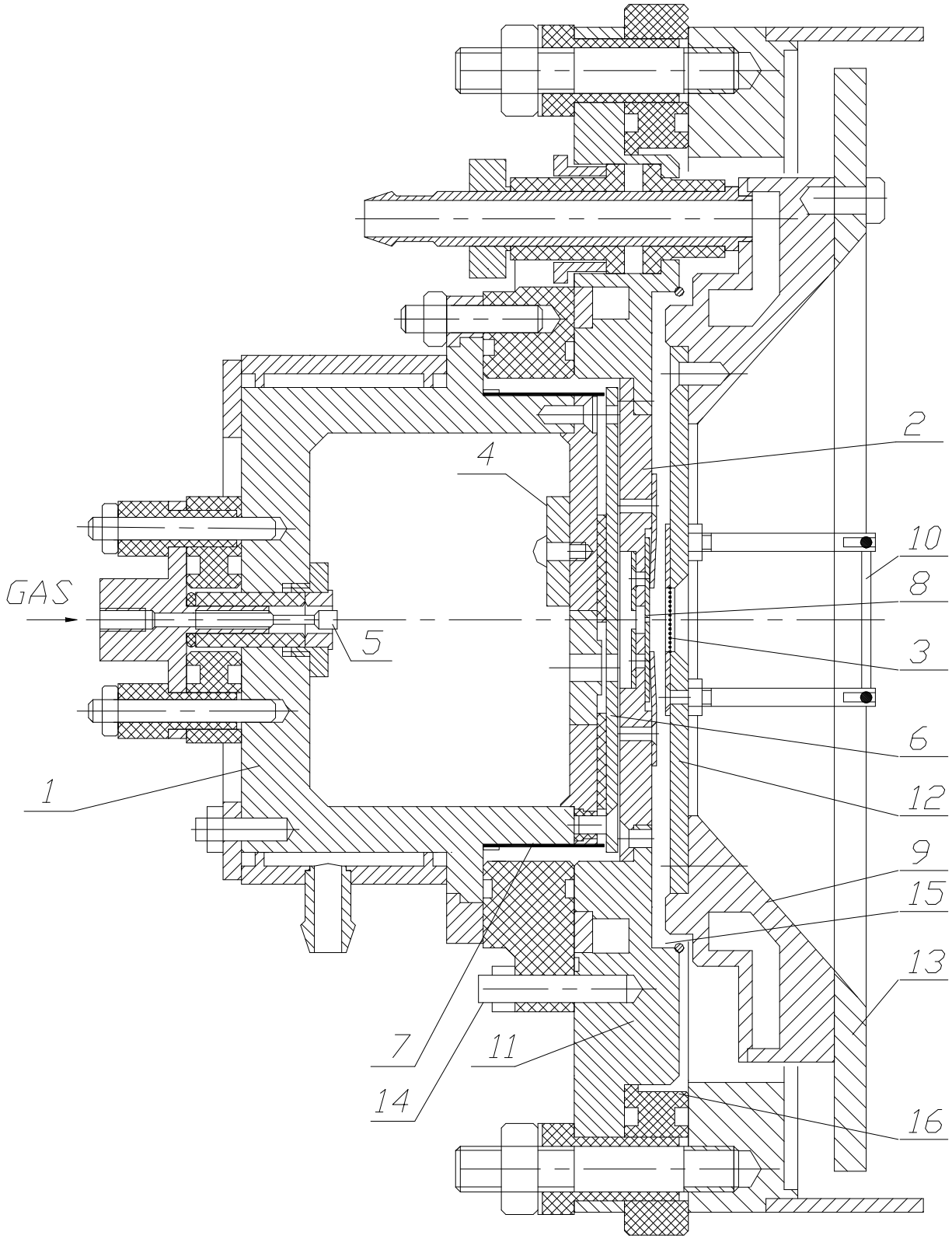

Fig. 2. Sketch of the plasma source. (protective case not shown).

1 – keeping discharge cathode, 2 – intermediate electrode, 3 – mesh-like keeping discharge anode, 4 – Mg washer, 5 – trigger electrode, 6 – arc protection insulated shield, 7 – Mo foil, 8 – changeable Mo plates, 9, 12, 13 – main discharge cathode parts, 10 – mesh-like redistributing electrode, 11 – flange, 14 – pin for mounting on-source block, 15 – delaminated film collector, 16 – insulator.

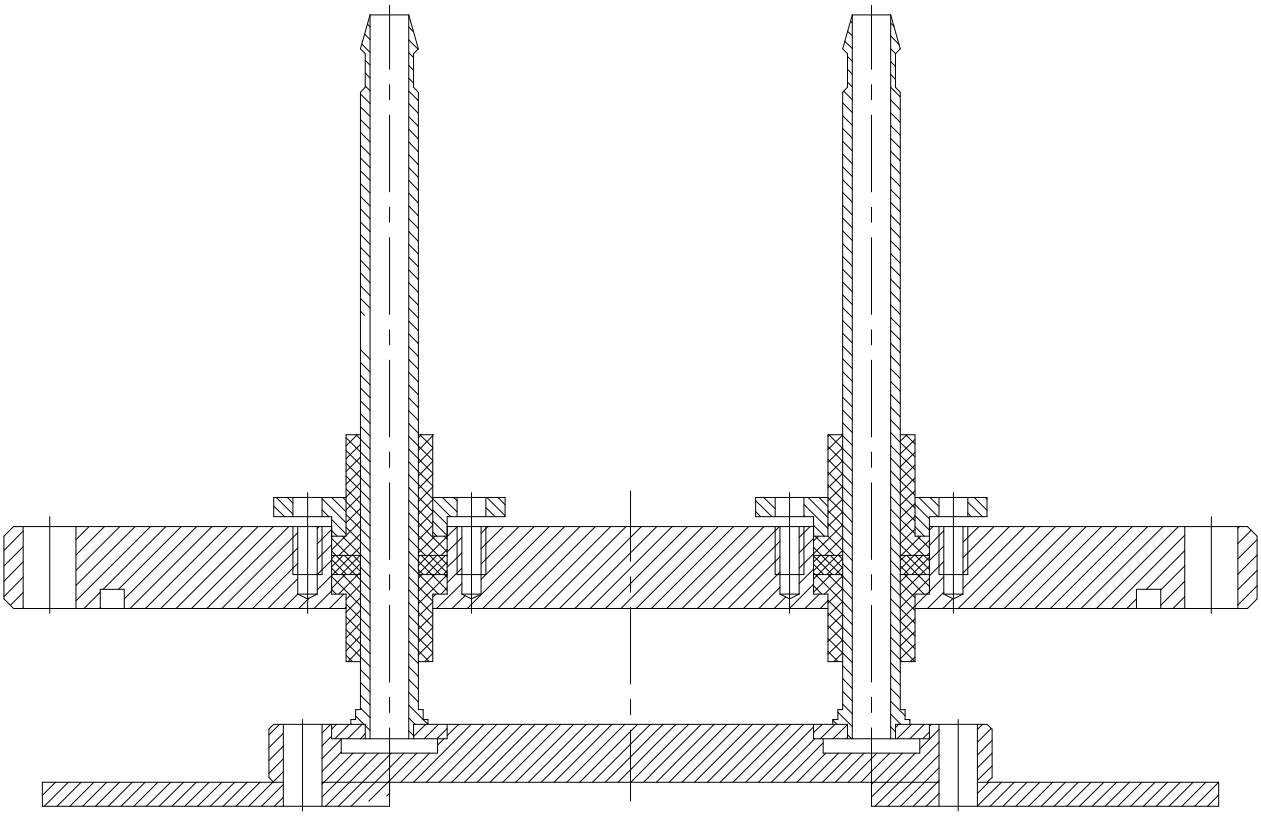

Fig. 3. Sketch of the anode.

Molybdenum insertion pressed in the keeping cathode cover has an aperture aligned with aperture in the shield 6. The insertion also centers the ceramic ring that insulates the cover and the shield.

Keeping discharge is initiated by gas breakdown during the trigger pulse applied between the trigger electrode 5 and cathode 1.

On the copper intermediate electrode 2 wearing molybdenum plates 8 are mounted. The required gap between the plates (0.8÷1,2 mm) can be restored by grinding the working edge of the plates and placing them to required position. The rest parts of the electrode are not subjected to wear.

Keeping discharge power supply provides relatively high open circuit voltage of 800 V needed for stable discharge initiation, but maximum current of the high-voltage part of the power supply is limited by a few mA. In order to reduce the current leak through the cooling water, internal cross-section of hoses connecting different parts of the source is reduced by inserted plastic tubes.

Main discharge with cathode 9 (fig. 2) and anode (fig. 3) installed on other flange of the vessel serves for ionization of gas in the vessel. Most part of electrons produced by keeping discharge pass through the mesh-like anode 3. Injected electrons accelerated within the cathode potential drop ionize gas atoms in the vessel volume. With discharge current higher than 10 A, the effect of compression of the injected

electron beam by intrinsic magnetic field becomes noticeable. Redistributing electrode 10 scatters the electron beam, thus, improving plasma uniformity at high discharge current.

All electrodes of the plasma source are insulated from the ground. The plasma potential sets to a value of +10 - +20 V with respect to the vessel walls. This potential is low for the vessel wall to be sputtered. It is possible to connect the anode of the main discharge to grounded vessel. Installation of anode (fig. 3) on the vessel is not required in this case. However, the plasma density would be 30% lower.

4. Installation and pre-starting procedure

All parts of sources must be assembled according to fig. 2. Partially disassembled plasma source is shown on fig. 4.

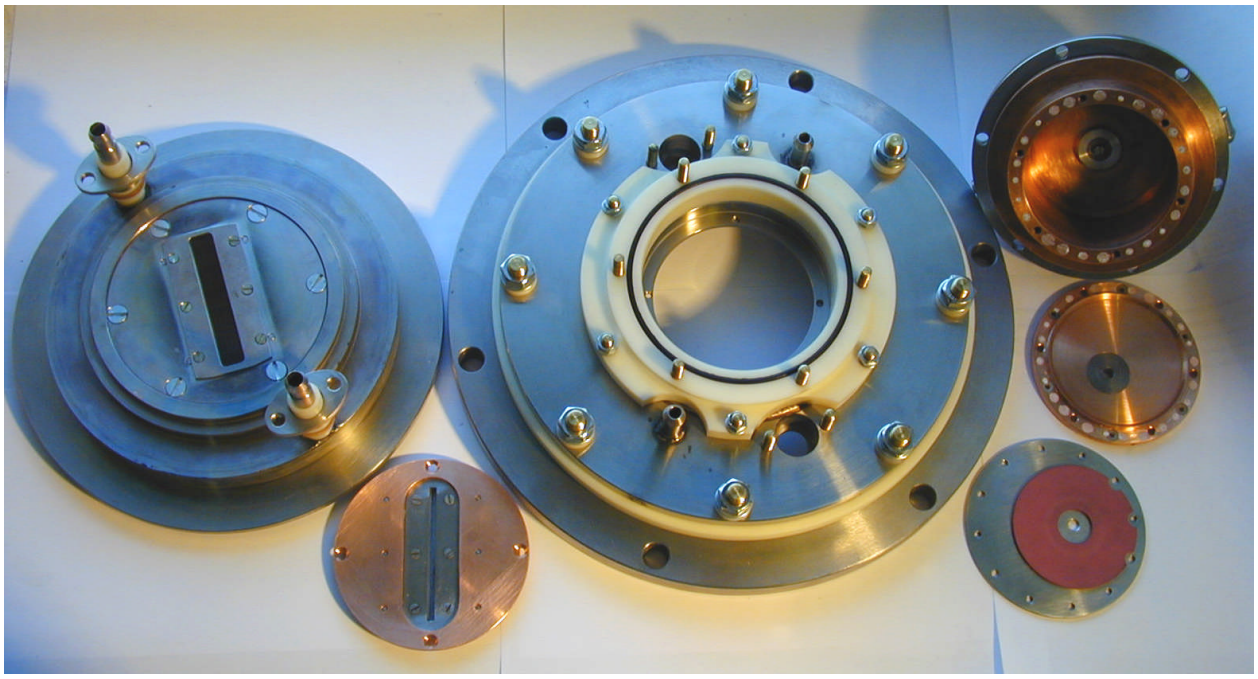

Fig. 4. Partially disassembled plasma source.

Heat sink compound must be used between following parts:

- body of the keeping cathode and cover of the cathode;
- cover of the keeping cathode and ceramic ring placed between the cover and shield 6 (fig. 2);
- ceramic ring and shield 6;
- interfaces of all parts of intermediate electrode 2;
- intermediate electrode and flange 11;
- main discharge cathode parts 12, 9 and 13.

The amount of heat sink compound must be enough to cover at least half of the interface surface. At the same time, it should not be pressed out.

It is necessary to make sure that there is no conductivity between the shield 6 (fig. 2) and keeping discharge cathode. Otherwise, an arc will occur on the shield causing its deformation as a result of heating.

Both vertical and horizontal positions of the plasma source on the vessel are acceptable. In case of horizontal position (the source is on a sidewall of the vessel) the water cooling input must be downward to avoid air bubble formation inside the cooling cavities. The source is cooled with water moving through all electrodes connected in series.

The operating gas is fed into the outlet of trigger electrode holder.

The power supplies must be connected to the plasma sources. There are 5 wires for each plasma source: keeping discharge cathode, main discharge cathode, anode, and two wires of trigger: red end (+) is for trigger electrode and blue end (-) is for keeping discharge cathode. Anode wires of all three sources must be connected to single anode (fig. 3) or to the grounded vessel. A block consisting of 2 capacitors, 2 resistors and a diode, that facilitates discharge ignition and suppresses voltage noise, must be mounted on one of the pins 14 (fig. 2). The connection scheme is shown on fig. 5.

Protective cases must be installed on sources for safety.

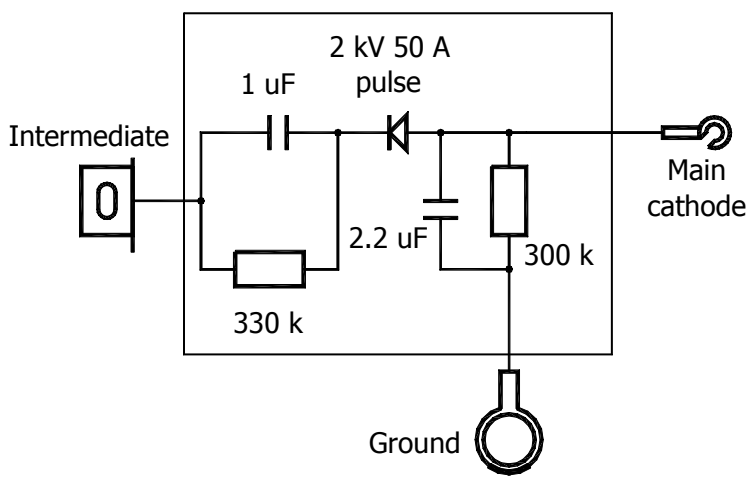

Fig. 5. Connection scheme for on-source block.

5. Order of operation

1. Pump down the vessel. The residual pressure must be lower than $1 \cdot 10^{-4}$ Torr.
2. Open the water cooling system of the plasma source.
3. Set up gas flow rate 40÷80 sccm for each source
4. Switch on the power supply.*
5. Set the required values of keeping discharge current and main discharge voltage for each source.*
6. Turn on plasma sources.*

7. After required time of operation turn off plasma sources and power supply,* close gas feed, close water cooling.

*For more details, see manual of power supply.

6. Technical service and maintenance

#	Operation	Estimated time period between operations	Symptoms for performing operation
1	Cleaning inner surface of keeping cathode and trigger electrode, replacing Mg washer 4 (fig. 2) if necessary	10 - 20 hours	Frequent discharge extinction, poor triggering.
2	Checking resistance between shield 6 and keeping cathode. It must be less than 1 Mohm.*	Every time with operation 1.	Arc on shield 6, its destruction.
3	Changing mesh 3 (fig.2)	10 hours for 0.15 mm W mesh 100 hours for 0.8 mm W mesh	Keeping discharge voltage is lower than 15 V. Main discharge voltage greatly differs from preset value. Power supply turns off automatically with “NE” indication.
4	Cleaning surfaces of electrodes 2 and 12 (fig. 2), removing film flakes from location 15 (Needed if the source axis is horizontal)*	20 - 40 hours	Breakdown between electrode 11 and grounded chamber flange, partial destruction of insulator 16.
5	Cleaning the ceramic tube inner surface in the trigger unit	20 - 40 hours	Poor triggering
6	Restoring the gap between molybdenum plates of intermediate electrode	20 - 40 hours	Increase of minimum operating pressure, nonuniformity of current density along the gap
7	Cleaning anode surface	Depending on oil contamination by pump system and deposition of dielectric	Gradual reduction of plasma density, and, finally, ceasing of main discharge current

* Perform operations before the symptoms appear

Feed system of plasma generator

Introduction

To create plasma in the working volume, plasma generators are used in which an keeping arc discharge is used for the main glow discharge burning. The keeping arc discharge burning voltage weakly depends on discharge current and a constant current power supply is necessary to feed it. In the main (glow) discharge, on the contrary, the discharge current is mainly determined with the keeping discharge current and weakly depends on the discharge burning voltage. A constant-voltage power supply is required to feed the main discharge.

Keeping discharge initiation is realized with a high-voltage pulse supply to the trigger electrode.

The main discharge cathode is connected to the keeping discharge anode. The trigger pulse generator is connected between the trigger electrode and keeping discharge cathode (see Fig. 1).

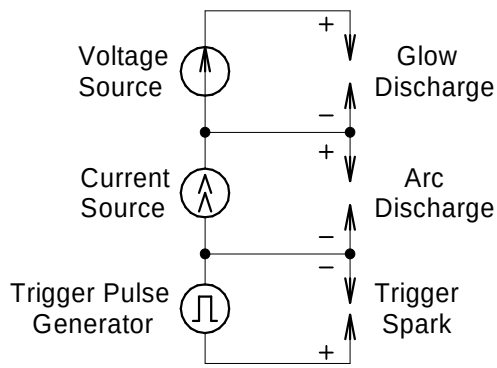

Fig. 1. Feeding of one plasma generator.

1. System destination and structure

The feed system is intended to feed three plasma generators. The system contains four identical supply units. Three of them supply three plasma generators simultaneously. The fourth supply unit is spare.

Each supply unit contains an arc discharge (keeping discharge) power supply, a glow discharge (main discharge) power supply, a trigger pulse generator.

Keeping discharge power supply parameters:

Output current	5-20 A
Current changes at the load voltage change of 30-70 V	5%
Current pulsation, no more than	±10%
Load voltage at discharge burning	30-70 V
Open-circuit voltage	600 V

Main discharge power supply parameters:

Output voltage	60-150 V
Voltage changes at the current change of 5-20 A, no more than	5%
Voltage pulsation, no more than	±10%
Maximum output current	20 A

Trigger pulse generator:

Output voltage	5 kV
Output current	50 A
Pulse repetition rate	1 Hz

Fig. 2 presents the elements of the feeding system, their junction with each other and interaction with the control system.

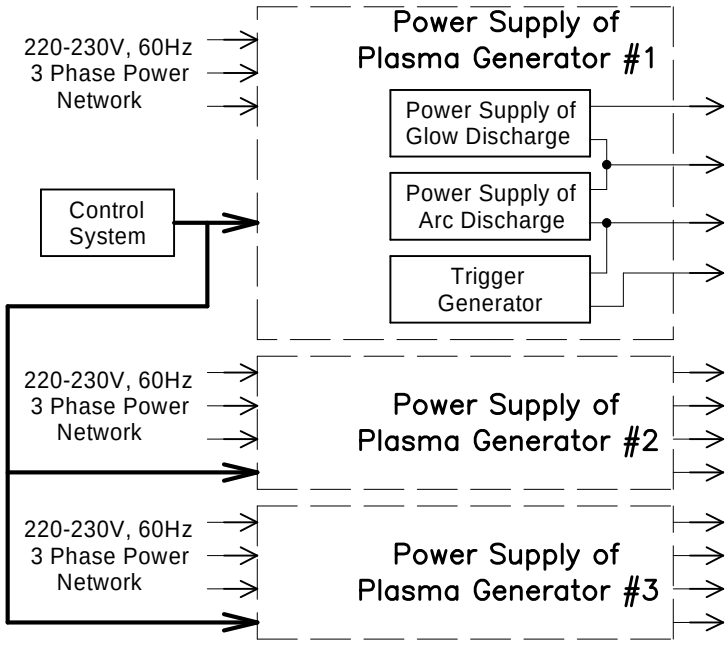

Fig. 2. Feed system structure.

Each power supply is connected to a three-phase alternating current network of 220-230 V, 50 Hz. Power supply outputs are connected to the corresponding plasma generators. All power supplies are controlled by means of a microprocessor control system.

2. Functional schemes of power supplies

2.1. Arc discharge power supply

The arc discharge power supply is an adjustable constant current source of 5-20 A at the load voltage of 30-70 V. Voltage produced by the source at the no-load operation (load current is equal to zero) makes up 600 V.

Fig. 3 presents the power supply functional scheme.

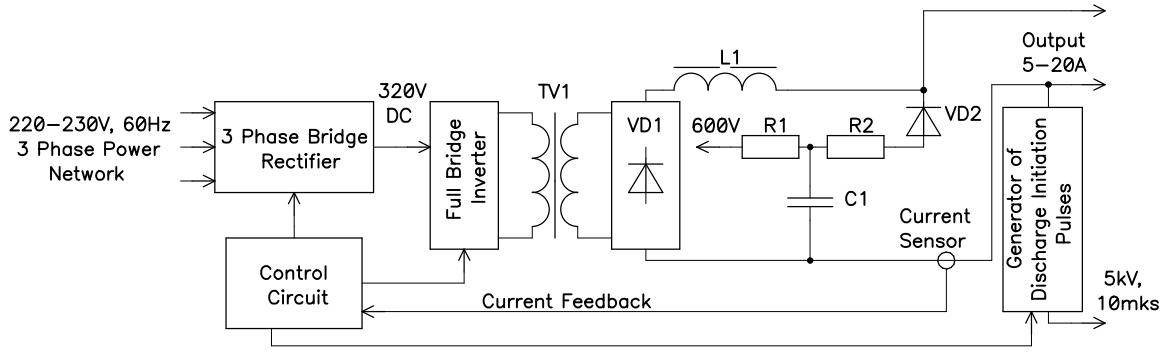

Fig. 3. Functional scheme of the arc discharge power supply.

The device is realized according to the scheme of the switching mode power supply with load current feedback.

Network voltage is rectified with a 3-phase bridge rectifier, filtered with a capacity filter and the obtained constant voltage of 320 V feeds the full bridge inverter. The inverter is assembled at the IGBT-switches and operates at a 20-kHz frequency. The signal is applied from the inverter output to the pulse transformer primary winding. The transformer secondary winding is connected to the bridge rectifier. Maximum voltage at the rectifier output is 70 V, and maximum output current of the power supply is provided. The inductive filter L1 is installed at the rectifier VD1 output. Current sensor installed at the power supply output measures load current and the signal from the sensor output is used as the feed-back coupling by current and is applied to the power supply control circuit. Pulse-length modulation controller regulates the bridge inverter operation according to the feedback signal (changes the conductive state time of the switches) so that constant set current level is maintained at the power supply output.

To provide the open circuit voltage of the power supply of 600 V an keeping low-power source of 800 V is used. Voltage from this source is applied to the arc discharge power supply output through R1, R2, C1.

In the arc discharge power supply there is a trigger pulse generator with the amplitude of 5 kV and length of 10 μs. This generator is operated with the control system and is turned on when there is no current on the load.

The control system provides operation of all assemblies forming the power supply and gives possibility to set a required value of the power supply output current. Besides, the control system verifies the power supply operation regime and generates to the liquid-crystal indicator current values of voltage and current at the supply output and message concerning the power supply state.

2.2. Glow discharge power supply

Glow discharge power supply is a source of constant voltage of 60-150 V at the load current of 5-20 A. A functional scheme of the glow discharge power supply is presented in Fig. 4.

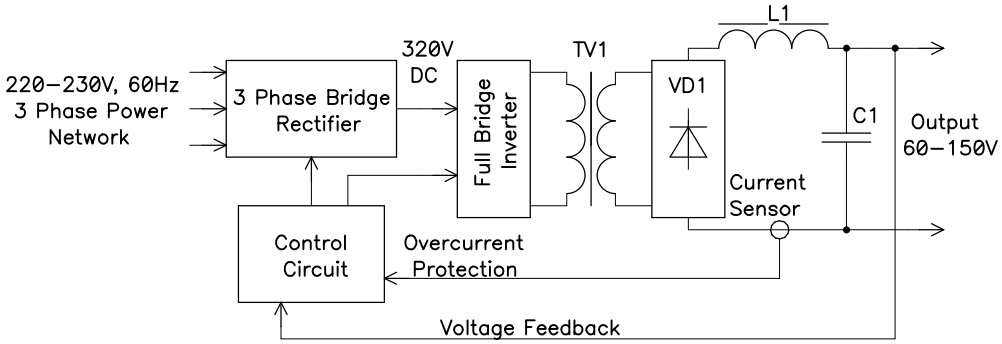

Fig. 4. Functional scheme of the glow discharge power supply.

The glow discharge power supply as well as the arc discharge power supply is mounted according to the pulse power supply topology. Its main difference is that the power supply output voltage is used as the feedback signal governing the bridge inverter operation. Thus, the control system regulates the bridge inverter operation according to the feedback signal maintaining the power supply output voltage at a set level.

At the power supply output the current sensor is installed. The signal is applied from the sensor to the control system and is used to protect the supply from short circuit.

In case of the discharge gap breakdown and the glow discharge transition into the arc one the voltage at the power supply output drops lower than nominal value. The control system follows this fact and disconnects the power supply.

The control system provides possibility to regulate the power supply output voltage and verifies its operation regime.

3. Feed system functional scheme

3.1. Placement of feed system elements in the rack

The feed system is made in the rack with the dimensions of 600x600x180 mm. Four power supplies are installed in the rack. Three power supplies are operating; the fourth supply is the spare, completely functioning device. To use the spare power supply, it is required to disconnect the plasma generator from the failed power supply and to connect to the spare power supply. Each of the four sources is controlled independently.

Each power supply of the plasma generator is mounted at a separate metal panel. The panels are placed inside the rack. In the lower part of the rack there are placed the input and output terminals, four protective automatons (each for the corresponding power supply). The control system is placed at the rack door and is connected to the power supplies with four 40-wire stubs. Operation and control devices (a keyboard and a liquid-crystal display) are disposed at the external side of the rack door.

The rack outward appearance and placement of the elements are shown in Fig. 5.

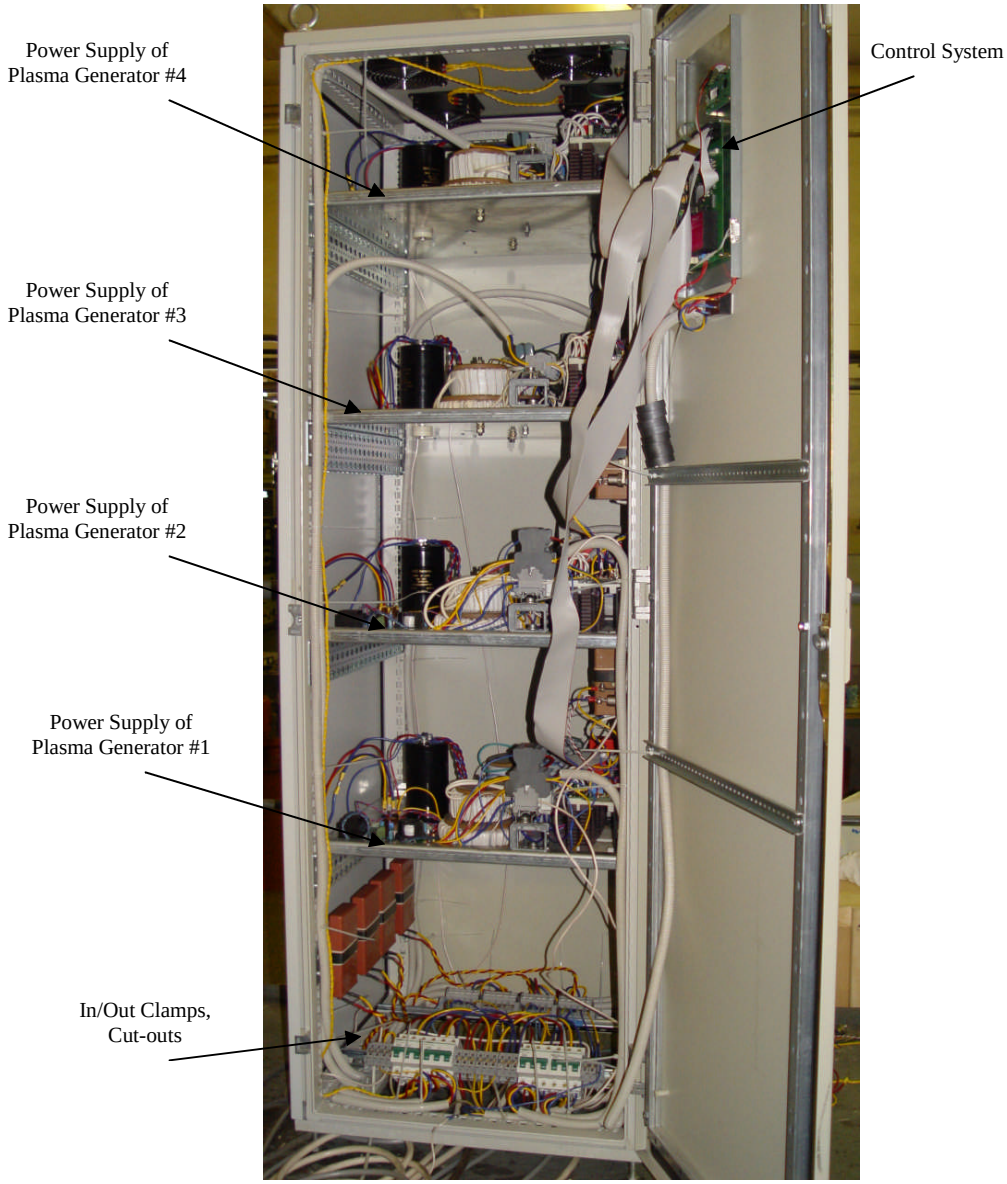

Fig. 5. Placement of the feed system elements inside the rack.

The feed system functional scheme is presented in Fig. 6.

Each of the four power supplies presents a functionally completed module having an identical scheme. Functional scheme presents in detail functional blocks and interblock junctions of the power supply of the plasma generator №1.

3.2. Feed system operation according to functional scheme

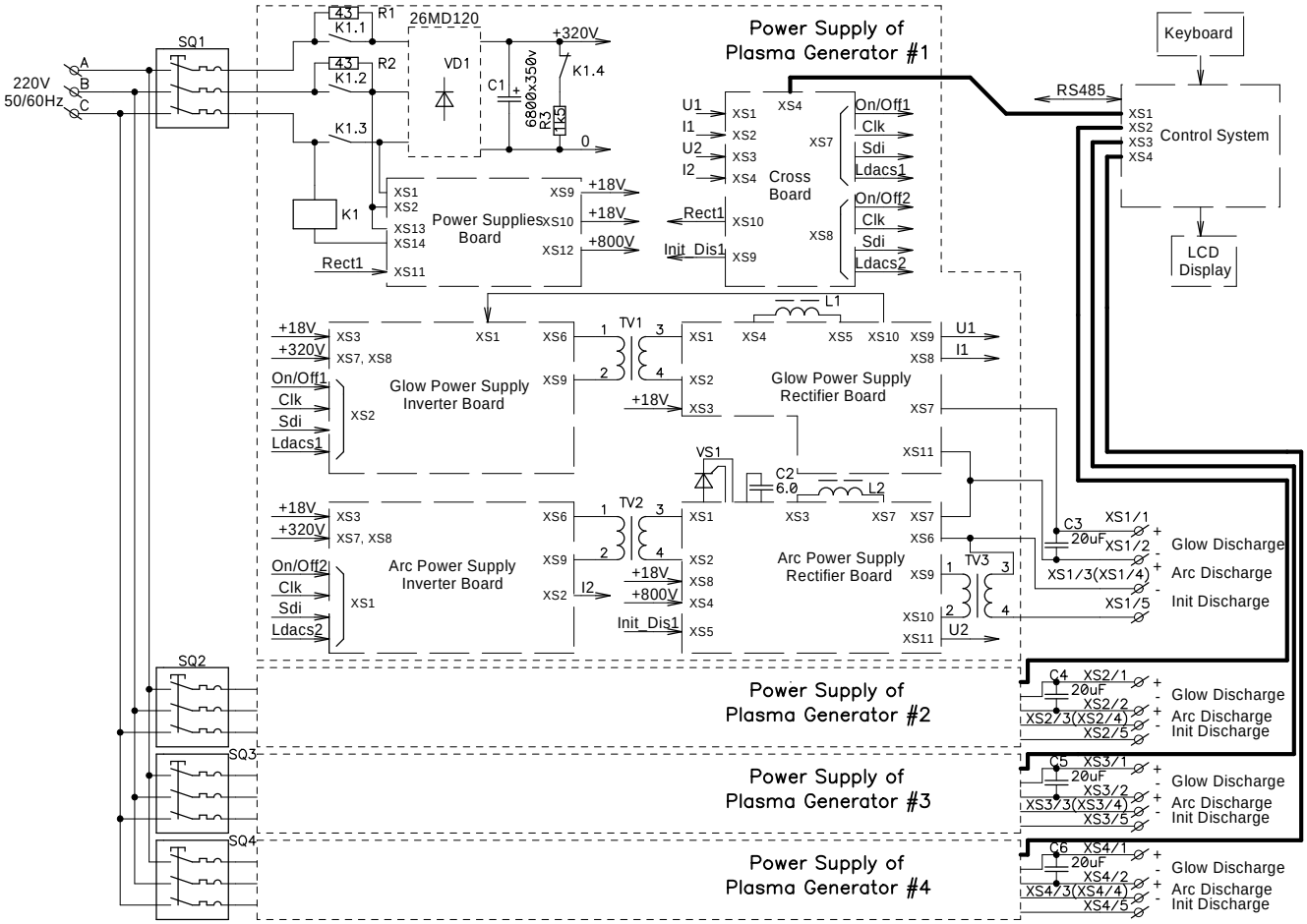

Fig. 6. Feed system functional scheme.

Three-phase voltage of 230 V, 50/60 Hz is applied to the protective automaton SQ1 placed in the lower part of the rack. The supply-line filter C1 begins charging through the resistors R1, R2 and bridge rectifier VD1. The discharge current flowing through the normally closed contacts K1.4 and discharging resistor R3 is much lower than the charging one. A second and a half after the feeding switching on and completion of the capacity C1 charging the control system turns on the contactor switch K1 that connects the bridge rectifier VD1 directly to the network system and simultaneously opens the contact K1.4. After rectifying and filtration, constant voltage of +320 V is present at a capacity filter C1. This voltage is applied to the inverter boards of the arc and glow discharge power supplies.

At the keeping power supply board two power supplies are placed: a power supply of +18 V-voltage applied to the boards of inverters and rectifiers to feed control circuits and a power supply of +800 V-voltage used to form open-circuit voltage of the arc discharge power supply and to feed the trigger pulse generator.

The trigger pulse generator is mounted at the elements of VS1, C1, TV3. The capacitor C1 charged up to 800 V is connected to the primary winding of the set-up transformer TV3 through the thyristor VS1, and a voltage pulse of the 5-kV amplitude is formed at the secondary winding.

Inverter outputs are connected to the primary windings of the transformers TV1, TV2. The secondary windings of these transformers are connected to the bridge rectifiers. The rectifiers are followed with the inductive filter L2 in the arc discharge power supply and LC-filter L1-C3 in the glow discharge power supply.

Keying signals are applied to the interconnect board from the control system to control power supplies. Four 40-wire stubs are used to connect the power supplies to the control system. Control signals diverge to the boards of inverters and rectifiers from the interconnect board.

Fig. 7 presents placement of the feeding module elements at a metal panel. Names and signs of the elements correspond to the functional scheme presented in Fig. 6.

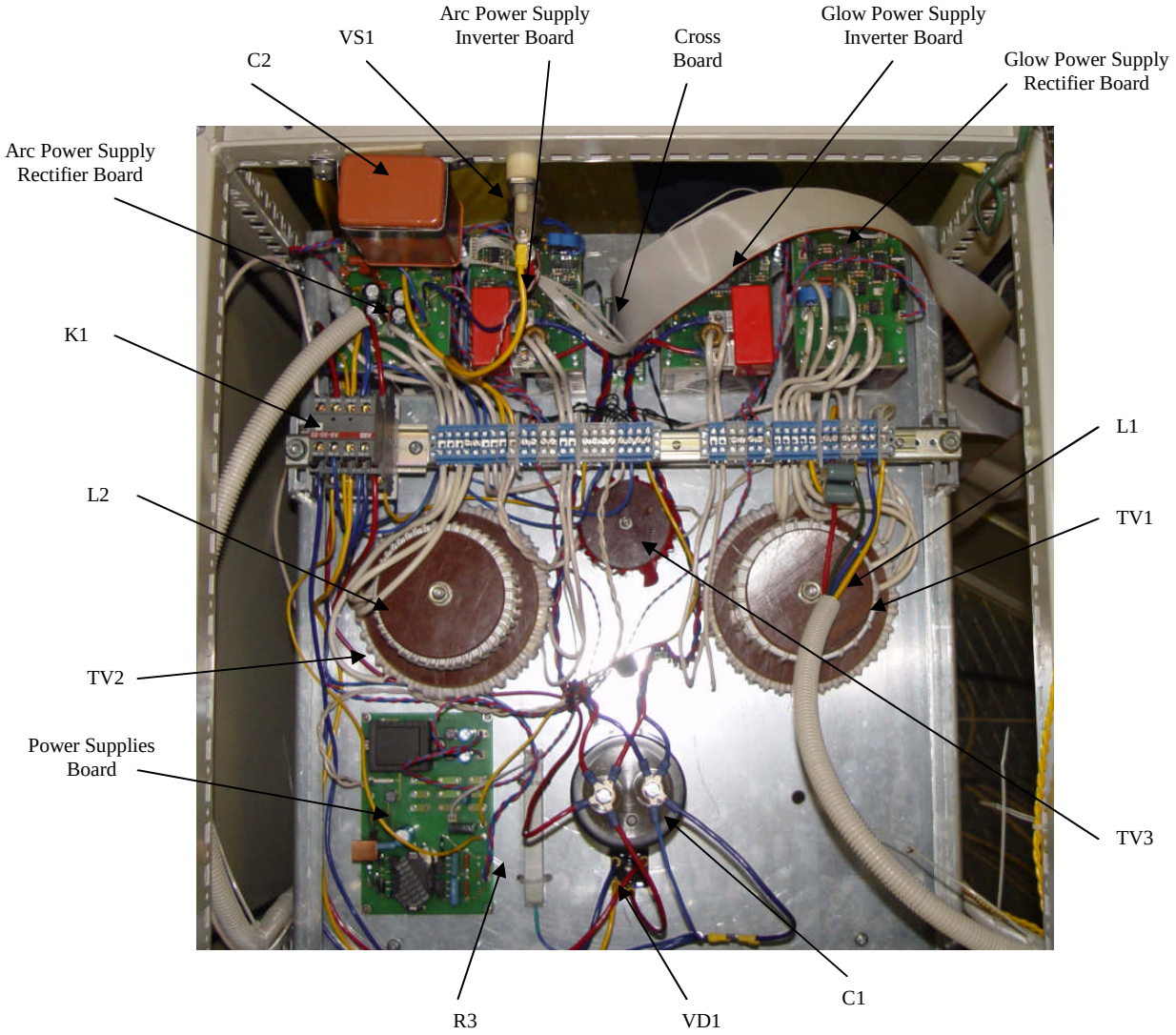

Fig. 7. Placement of feeding module elements.

4. Operation with feed system

4.1. Feed system connection

The feed system connection to the network system is made with a four-wire cable. Three wires are used for connection to the alternating current network system phases. The fourth wire is used to connect protective grounding.

To connect feed modules to the plasma generators, a three-wire cable connected to the terminals XS1/1-XS1/3, XS2/1-XS2/3, XS3/1-XS3/3, XS4/1-XS4/3 is used. To connect the trigger pulse generators to the trigger electrodes, a coaxial cable connected to the terminals XS1/4-XS1/5, XS2/4-XS2/5, XS3/4-XS3/5, XS4/4-XS4/5 is used.

Fig. 8 shows layout of junction terminals, protective automatons and output capacities of the main discharge power supplies.

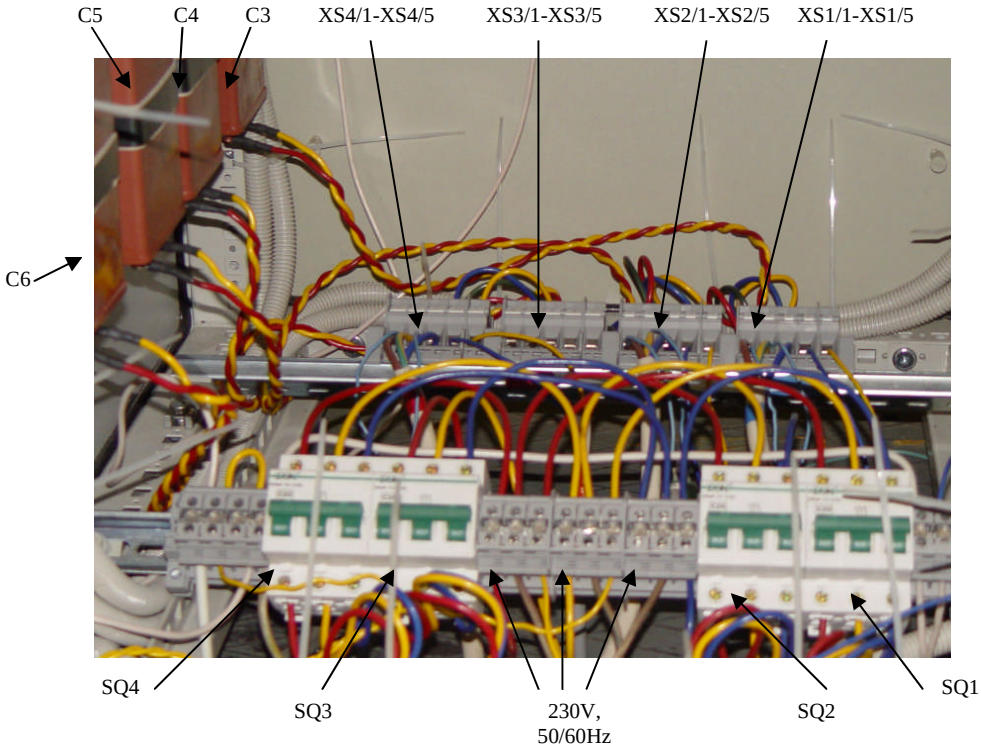

Fig. 8. Layout of junction terminals and protective automatons.

4.2. Power supply control

In order to energize the feed system it is necessary to apply the three-phase voltage of 230 V, 50/60 Hz to the input terminals. After applying the feeding voltage, a liquid-crystal indicator of the control system disposed at the rack door begins to glow. As soon as the preliminary charging of capacity filters is finished (approximately 1.5 sec after the feeding voltage supply) the contactors connecting the input rectifiers to the network system operate.

After switching-on of the feed system the following data are displayed at the control system indicator:

```
U000 I00 Uoc I00 >--
U000 I00 Uoc I00  --
U000 I00 Uoc I00  --
U000 I00 Uoc I00  --
```

Fig. 9. Control system indicator after feeding.

Each line at the indicator corresponds to one of the feed modules (the first line - to the feed module №1, the second – to the feed module № 2, etc.).

The following parameters are displayed in each line (from left to right):

- voltage at the main discharge power supply output;
- current at the main discharge power supply output;
- voltage at the keeping discharge power supply output (the sign Uoc shows availability of the open-circuit voltage of ~600 V at the power supply output);
- keeping discharge current;

- feed module power supply status (value «--» indicates that all modules are disconnected);

The symbol «>» is a cursor showing a feed module being active for control. The choice of the active power supply (cursor update upwards-downwards) is realized with keystroke of the keys «↑» and «↓» at the control system keyboard. For the active feed module it is possible to realize setting of the output parameters (main discharge voltage and keeping discharge current) and to turn on and turn off this feed module as well.

Setting of output parameters:

To set the feed module output parameters, one should make the following:

1. Activate the desired feed module with setting the cursor «>» in the corresponding line and moving it with the keys «↑» and «↓».
2. Press the key «F1»; the inscription «Power Supply N set» should appear at the screen where N is the number of the chosen feed module.
   «U=nnn», where nnn is the current value of the main discharge power supply output voltage.
3. Pressing the keys «↑» and «↓», set the desired output voltage. Pressing the keys «←» and «→» enables the cursor moving to the right and to the left allowing decreasing and increasing voltage values with the keys «↑» and «↓» by a unity, ten or hundred.
4. After exposing the desired voltage, press the key «F3». The following inscription should appear in the next line at the screen: «I=nnn», where nnn is the current value of the keeping discharge output current.
5. Similarly to point 3, set the desired value of the output current.
6. Press «F3» and in the next row the subscription «OK» should appear.
   Verify validity of the introduced parameters and press the key «F3» once more. After this the main screen with current output parameters of power supplies begins to display at the screen.

Fig. 10. Physical configuration and layout of operating controls.

Feed module switching-on:

1. Activate the desired feed module setting the cursor «>» in the corresponding line and moving it with the keys «↑» and «↓».
2. Press the button «Start». The feeding module status should change its value from «--» to «#0». The trigger pulse generator begins operating and the status state symbols display the quantity of the realized initiation trials («#1», «#2» etc.).
3. After the keeping discharge is initiated and the current set by the user begins to flow through it, the main discharge power supply is switched on by means of the control system. The status value is changed to «OK».

Feed module switching-off:

1. Activate the desired feed module setting the cursor «>» in the corresponding line and moving it with the keys «↑» and «↓».
2. Press the button «Stop». The status value should change to «--» that testifies that this feed module is disconnected.

Feed module operation:
During operation of the feed modules, the liquid-crystal indicator displays the values of the output voltages and power supply currents as well as the feeding module status displaying operable condition of the system or possible arising problems.

Possible values of the feed module status:
«--» - the feed module is in the deenergized state;
«OK» - the output parameters of the power supplies of the main and keeping discharges conform to the set values;
«NE» - the output parameters of the power supplies do not conform to the set values.
. The main discharge voltage differs by more than 10 V from the set one or the keeping discharge current differs by 1 A or more from the set one.
«!!» - the keeping discharge failed to be initiated for 10 trials of a trigger pulse supply.
«AP» - too frequent operation of arc protection in the main discharge.

After appearance of the faults «NE», «!!» or «AP» the control system disconnects power supplies of the corresponding module. For the fault reset and appearance of the status «--» at the indicator it is necessary to press the key «Stop».

5. *Feed system control from a personal computer*

The feed system has a possibility of external control from a personal computer. The computer is connected to the feed system via a serial asynchronous interface RS-485. The connector of the interface RS-485 is disposed at the control system panel placed at the internal side of the rack door (see Fig. 11).

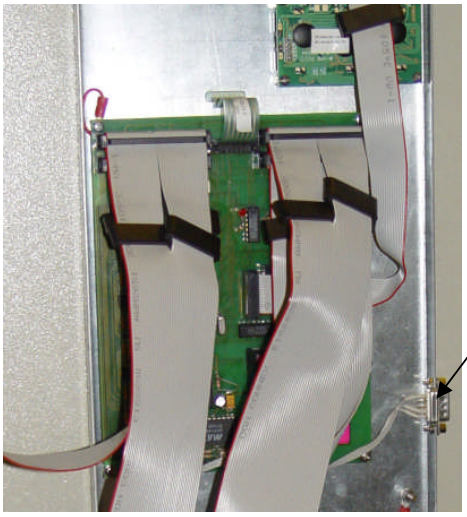

Fig. 11. Connector disposition of RS-485

The DB9 type connector is used. Table 1 presents the connector unsoldering.

Таблица 1. Destination of the connector RS-485 leads-out

Contact number	Destination
1	Data- (A)
2	Data+ (B)
5	GND

Sending commands from the personal computer via the interface RS-485 in accordance with the information interchange protocol and receiving response data it is possible to control entirely the feeding system from the personal computer (changing of the output parameter settings; feed module switching on/off, displaying of output voltages and power supply currents as well as current status at the computer screen).

5.1. Information interchange protocol via serial interface

Serial controller port of the control system is adjusted to the following parameters:
Rate of exchange - 115200;
Bit number of data - 8;
Number of stop bits - 1
Even-odd check - not.

The computer is the master device and the controller of the control system is the slave device. The start of the data communication is always initiated with the master device.

Data packets from the Master Computer enter the controller in the form of ASCII sequences comprising mnemonics of commands and parameters.

Service symbols of protocol:

The following service symbols are used in the ASCII protocol:

Symbol	Description	Dec	Hex
<SOH>	Start of transmission	1	01H
<STX>	Start of text	2	02H
<ETX>	End of text	3	03H
<EOT>	End of transmission	4	04H

Structure of data packets:

The start of the data communication is always initiated with the master computer. The controller continuously receives the data from the serial interface RS-485. After receiving a data packet having proper Device Name in the header of the packet, the controller analyzes the data in the packet, decodes a command, executes it, and responds to the master computer.

Format of a packet sent from the master computer to the controller is:

<SOH><Device Name><STX><DATA><ETX><CRC><EOT>

Here <Device Name> is the identifier of the device when working with several devices on the same line of the serial interface RS-485. The controller has the <Device Name>=”MCU”.

<DATA> is the command and the parameters sent to the controller;

<CRC> is the lower byte of checking sum, calculated from <SOH> to <ETX> inclusive these.

Format of the controller respond is:

<STX><DATA><ETX><CRC><EOT>

Here <DATA> is the respond message or current parameters;

<CRC> is the lower byte of the checking sum calculated from <STX> to <ETX> inclusive these.

All parameters and the checking sum are transmitted in HEX format (each binary byte is presented as two ASCII symbols from 0 to F. IF the received parameters include symbols different from 0-F then

the controller send a respond “ERR BIN”). If the received checking sum and calculated one do not coincide then the controller sends a respond “ERR CRC”.

The Controller responds “UNKNOWN COMMAND” if the command in the received packet is not presented in the command list of the controller.

Commands of the controller

The list of commands of the controller is:

GET - returns current voltages, currents and status of the supplies
DSET - sets the output parameters of the power supplies
DGET - returns current values of the power supply setups
STR - switches on one of the feed modules
STP - switches off one of the feeding modules

Commands for readout of current parameters

Transmitted data: GET
Received data: xxxxxxxxxxxxxxxxxxxxxxxxxxxxxxxxxxxxxxxx

The control system answer to the command GET makes up 40 symbols (2 symbols per a byte) or 20 bytes. 5 bytes of information are transmitted for each feed module including the main discharge voltage, the main discharge current, the keeping discharge voltage, the keeping discharge current, the feed module current status. The data follow in the above-described sequence first for the feed module № 1, then for the feed module № 2, etc. Voltage and current values are given in volts and amperes, respectively, the unity value of the low-order bit being of 1 volt and 1 ampere.

The status byte can assume the following values in the hexadecimal numerical system:

00 feed module is switched off
01 feed module operates in normal mode
02 keeping discharge failed to be initiated after 10 trials
03 trial of initiation №9
04 trial of initiation №8
05 trial of initiation №7
06 trial of initiation №6
07 trial of initiation №5
08 trial of initiation №4
09 trial of initiation №3
0A trial of initiation №2
0B trial of initiation №1
0C mismatch of the set and output power supply parameters
0D frequent operation of the arc protection in the main discharge
0E, 0F keeping discharge has ignited, the main discharge power supply is switched on

Command of setting the output parameters of the power supplies

Transmitted data: DSETxxxxxxxxxxxxxxxx
Received data: OK

8 bytes of data are transmitted with a command as parameters (2 symbols per each) in the following order: the main discharge voltage and the keeping discharge current for the feed module №1, voltage and current for the feed module №2, etc.

Command of reading the set output power supply parameters

Transmitted data: DGET
Received data: xxxxxxxxxxxxxxxx

The control system response to the command DGET makes up 16 symbols (2 symbols per one byte) or 8 bytes of the output parameters set previously. Byte ordering is analogous to the ordering in the command DSET.

Command of the feed module switching-on

Transmitted data: STRxx
Received data: OK

One byte of data (2 hex symbols) is transmitted as a parameter, defining the number of the feed module being switched on.

Number 0 corresponds to the feed module №1, number 1 – to the feed module №2, etc.

Command of the feed module switching-off

Transmitted data: STPxx
Received data: OK

A parameter analogous to the command STR is transmitted.

Electrical schematic diagrams

Schematic diagram and PCB of glow power supply inverter board

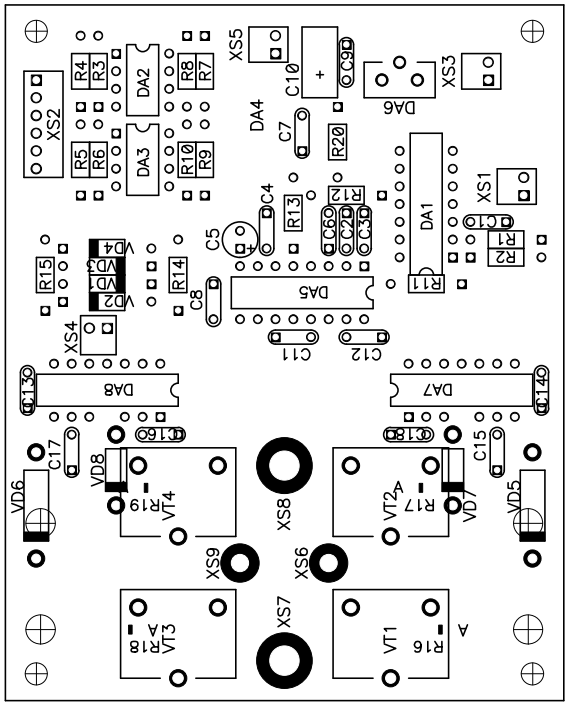

Glow power supply
Inverter circuit

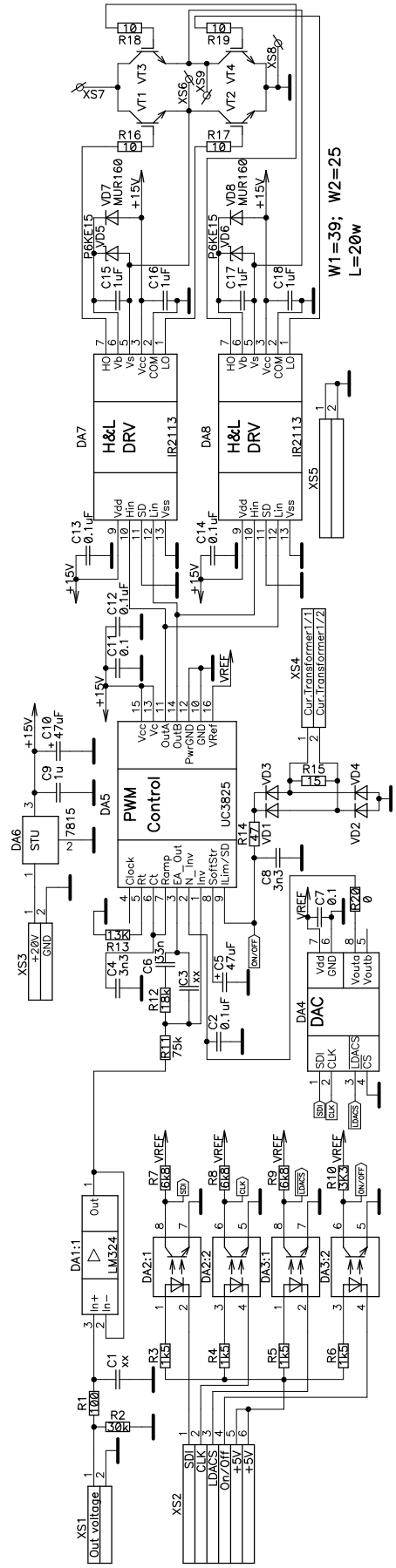

Schematic diagram and PCB of glow power supply rectifier board

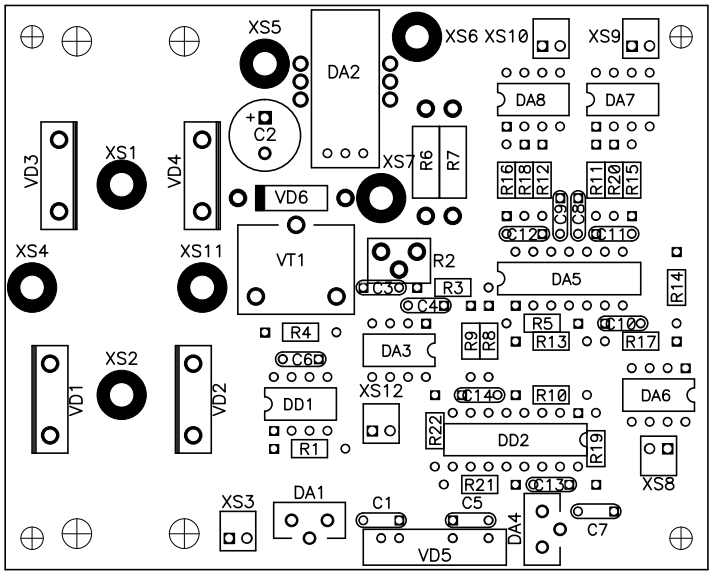

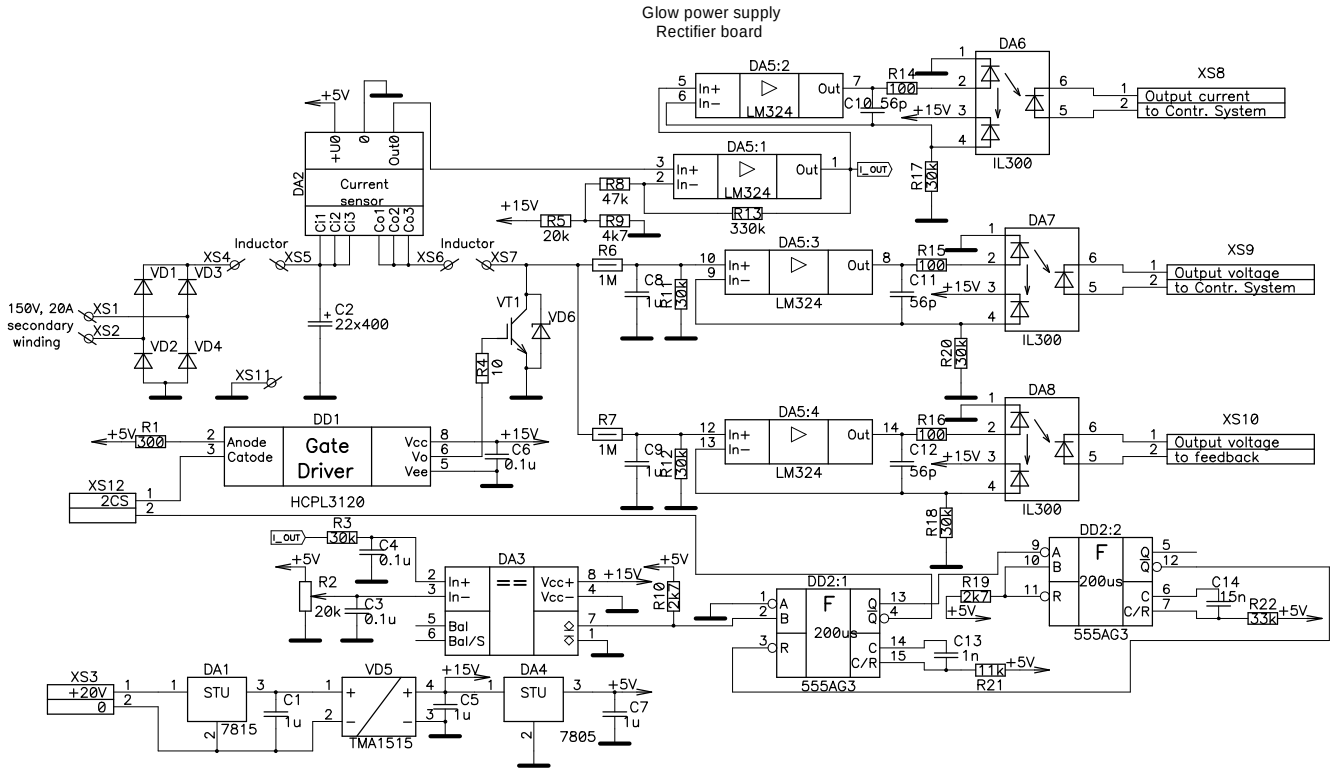

Schematic diagram and PCB of arc power supply inverter board

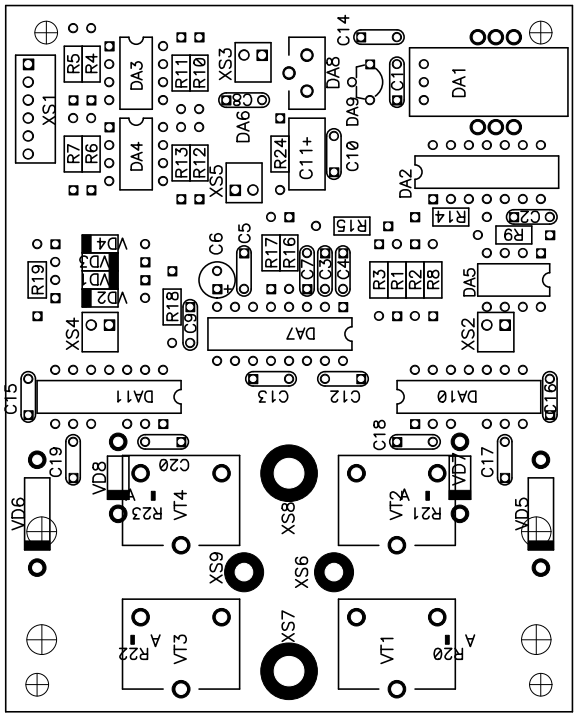

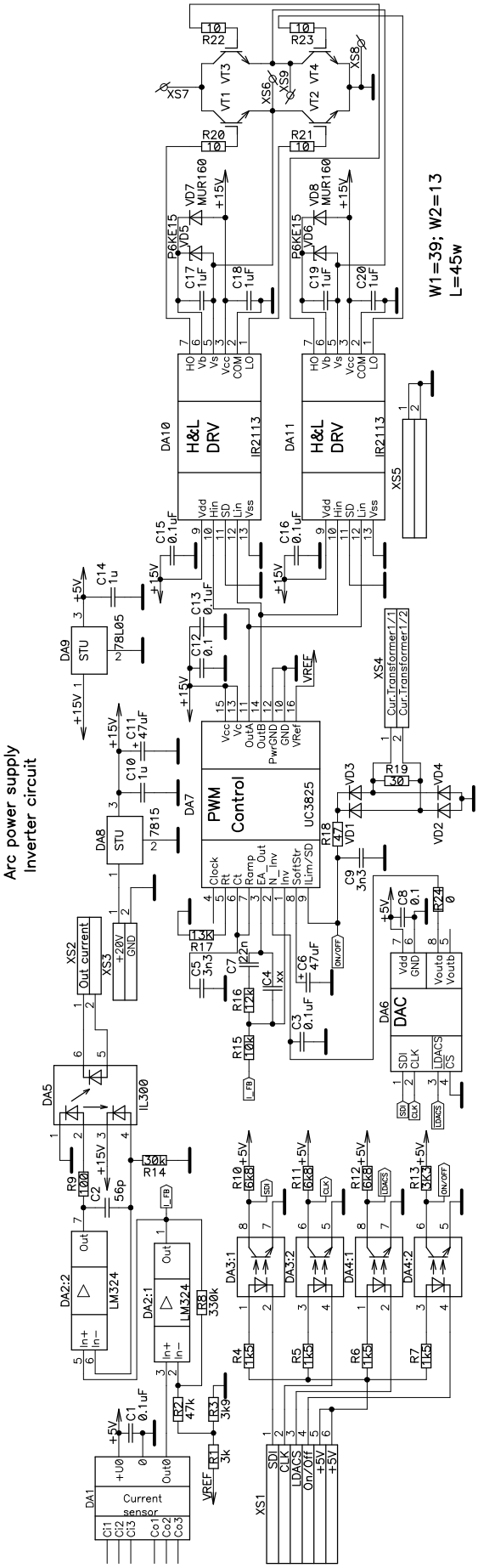

Schematic diagram and PCB of arc power supply rectifier board

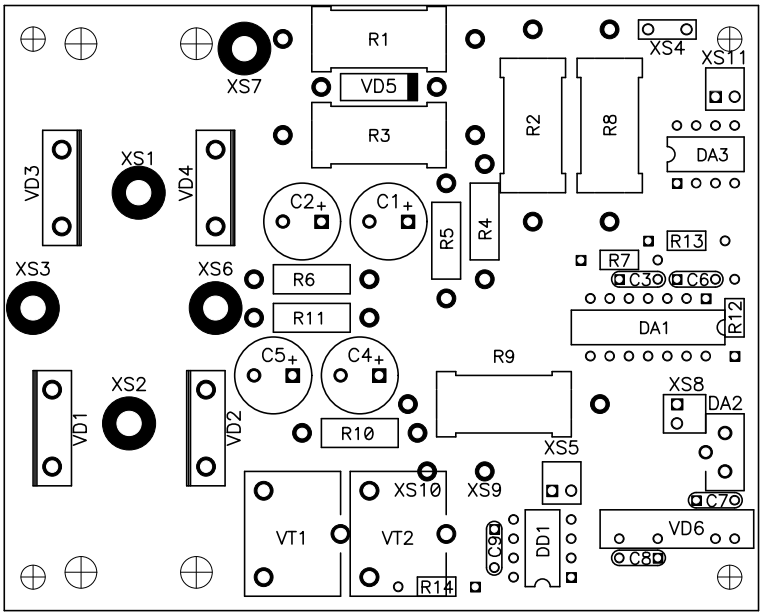

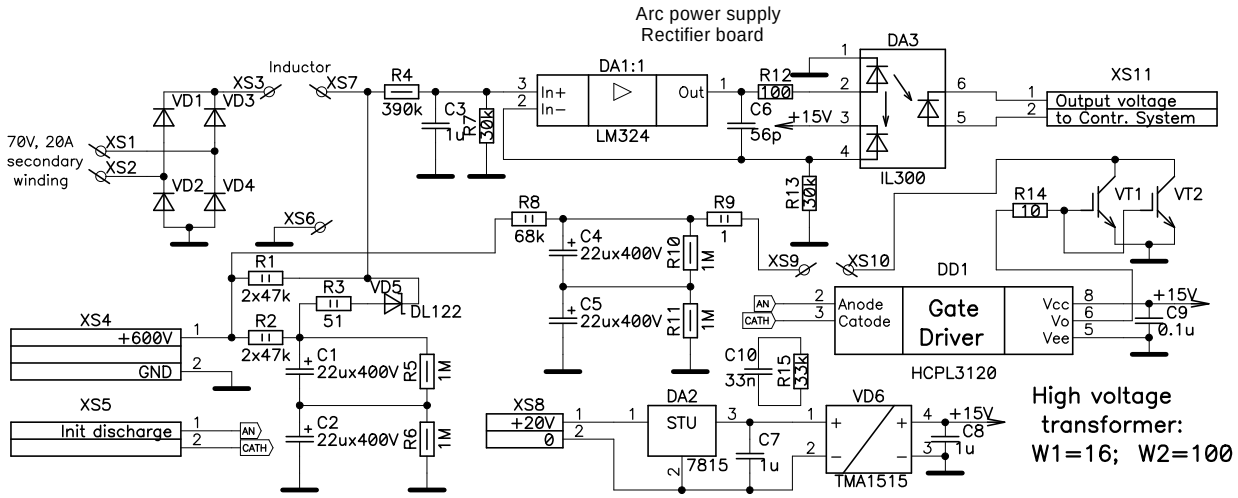

Schematic diagram and PCB of power supplies board

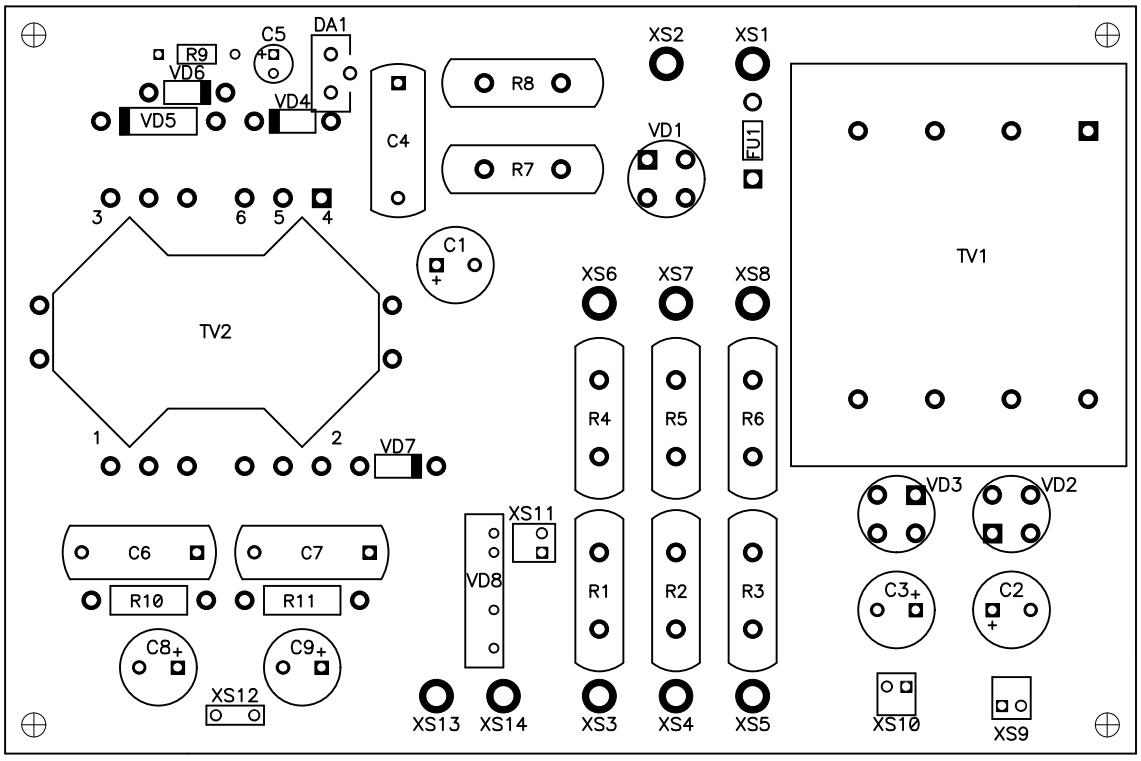

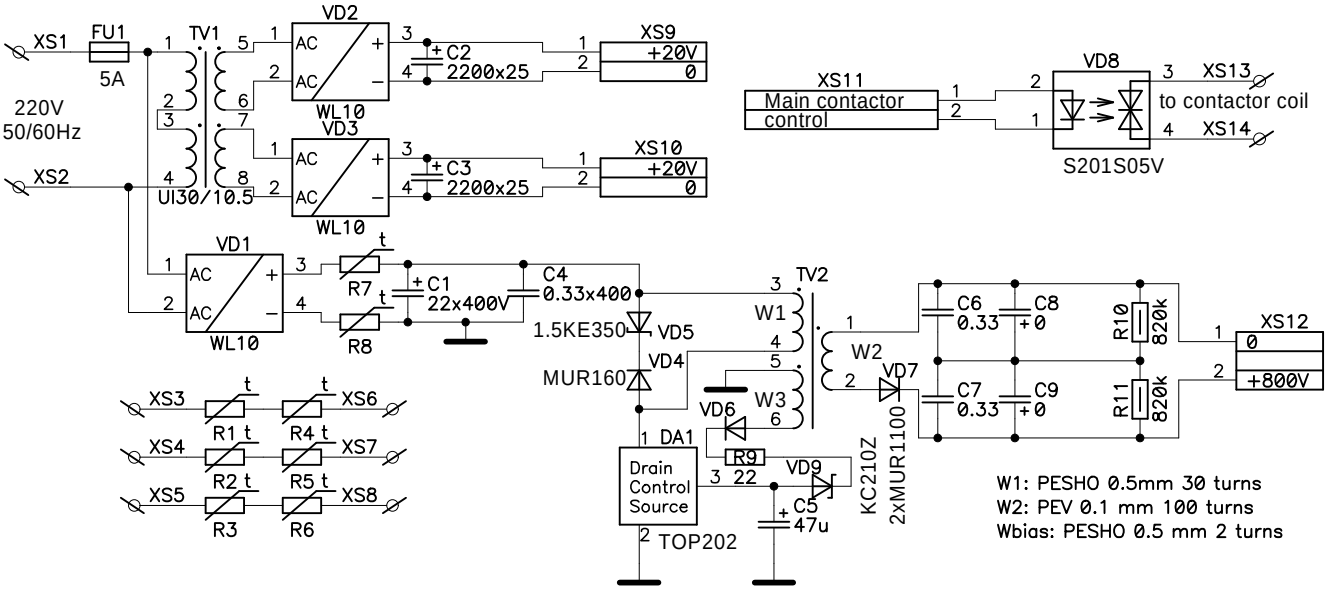

Schematic diagram and PCB of cross board

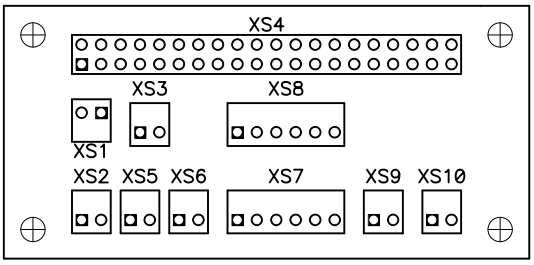

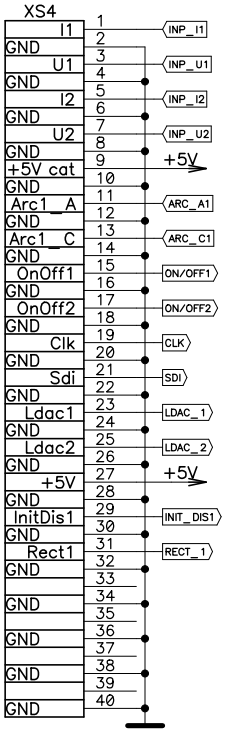

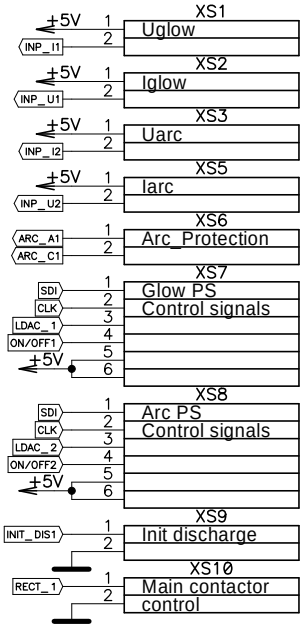

Schematic diagram of control system

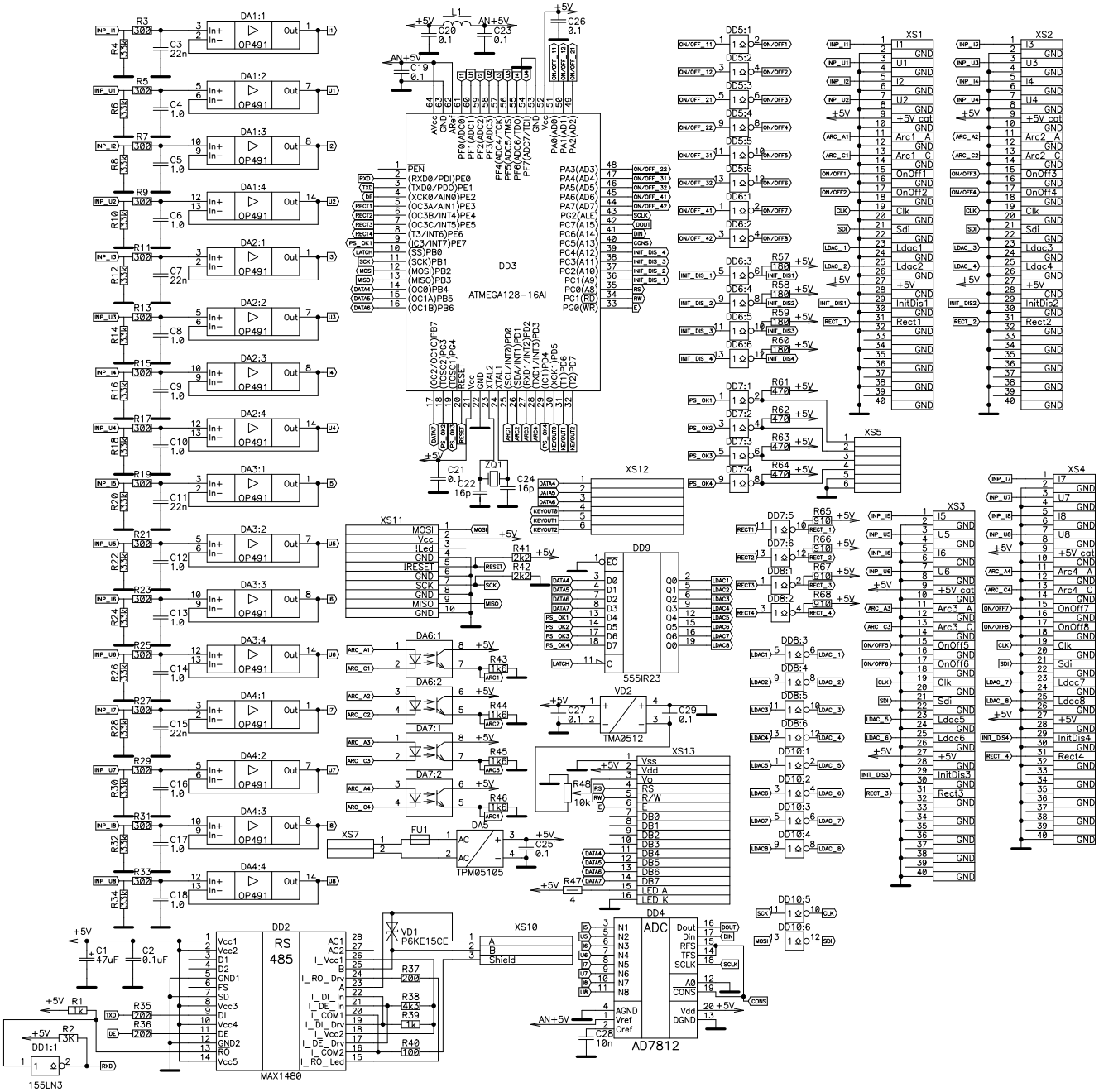

PCB of control system

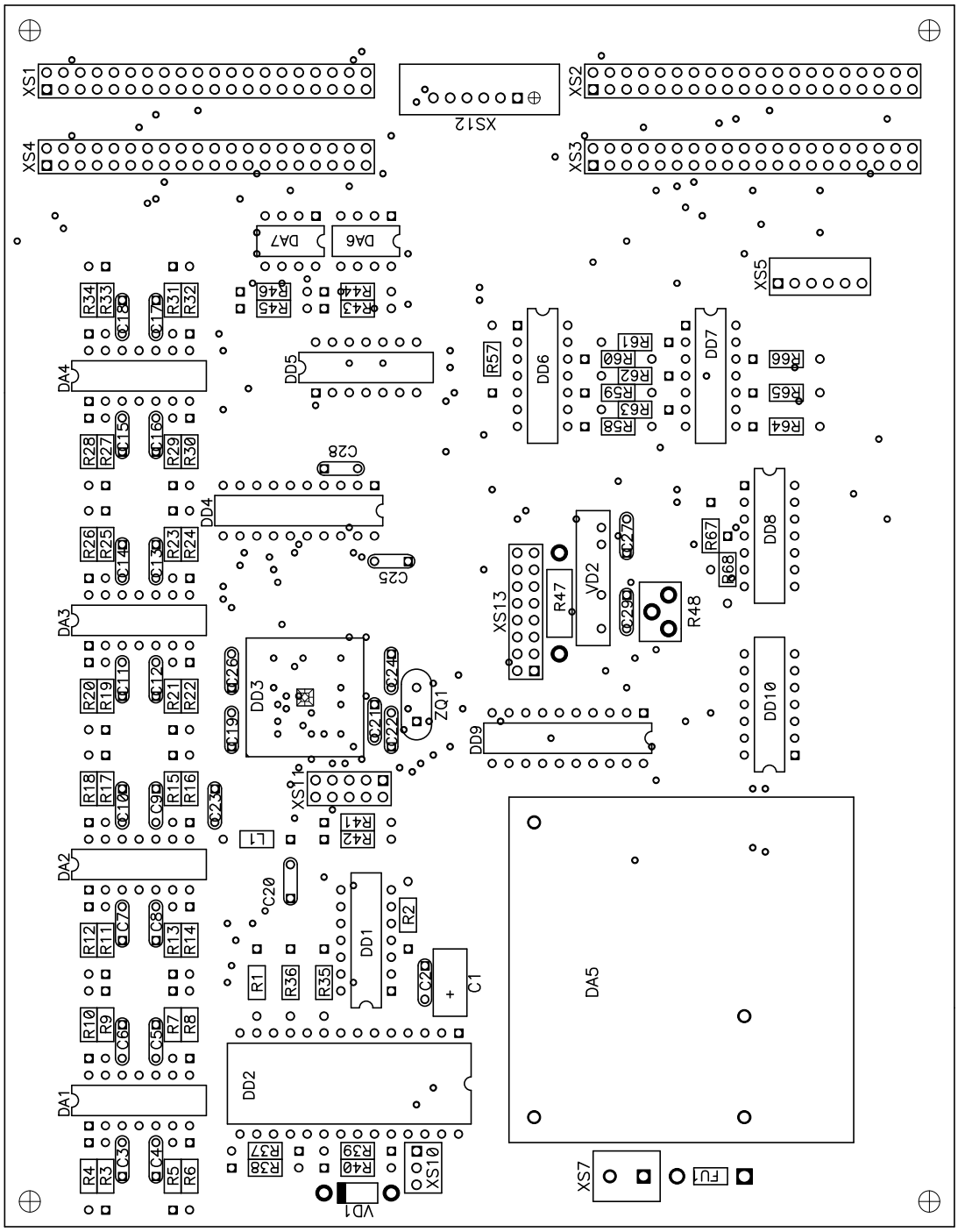

High Energy Ion Technology of Interfacial Thin Film Coatings for Electronic, Optical and Industrial Applications

High Energy Ion Technology of Interfacial Thin Film Coatings for Electronic, Optical and Industrial Applications (Add-On Project)

Material Support Agreement No. 6808686 (Mod 7)

Between

Ernest Orlando Lawrence Berkeley National Laboratory University of California,

Phygen Inc. of Minneapolis, Minnesota

And

High Current Electronics Institute (Tomsk, Russia)

Final report

Principal Investigator

Head of the Plasma

Source Department

Efim Oks, Prof.

RUSSIA-TOMSK-2009

IV. EQUIPMENT SUPPLY AND FINAL REPORT

4.1. Experimental setup (Phygen Inc.)…….74

4.2. Experimental results…….77

4.3. Concluding remarks……..89

References……86

Appendix……...91

I. REVIEW OF PUBLICATIONS AND DETAILED WORK PLAN

1. DLC films: properties and production methods.

1.1. Introduction

At present the term “diamond-like carbon” (DLC) is applied to films of two types: hard coatings based on amorphous diamond-like carbon (a-C films) and hydrogenated amorphous carbon coatings (a-C:H films). "Diamond-like" implies that the films are composed either totally or partly of carbon atoms with sp^3-hybridized electron sheaths with no coarse crystallites (Fig.1); the size of ordered regions is normally no greater than 5 nm. Nevertheless, some physical characteristics of DLC films (hardness, electrical parameters, density) approximate those of a diamond. The properties of a-C films are directly dependent on the ratio between sp^3- and sp^2-hybridized C atoms. In practical terms, DLC films with a large diamond-like (sp^3) component percentage (> 50%) hold the greatest interest. The hardness of these coatings can reach 80 GPa.

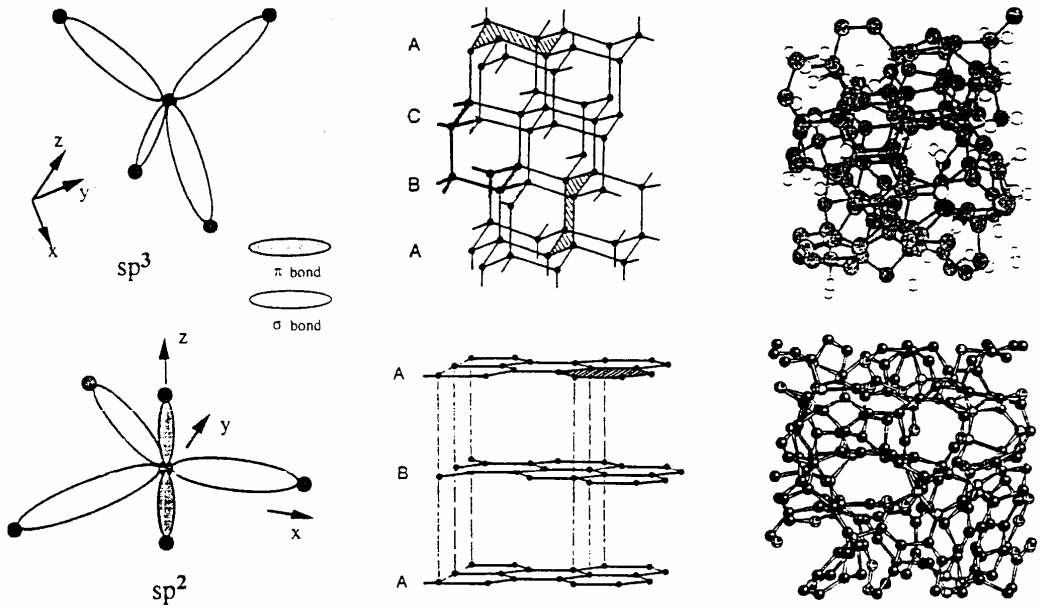

Fig. 1. Types of C-C hybridization (sp^3, sp^2).

Widely used hydrogenated amorphous carbon films are characterized by a large hydrogen percentage (up to 50 %). For this reason the properties of a-C:H

films are variable over a wider range, compared to a-C films, and are dependent on the hydrogen content other than the ratio of sp^3- and sp^2-hybridized hydrogen atoms. The hardness of a-C:H films with ~50% of hydrogen, as a rule, is about 5÷10 GPa. However, this value can be increased considerably (up to 30 GPa) by varying the parameters and composition a-C:H films during deposition.

The peculiar characteristics of DLC films, such as high hardness, high thermal conductivity (five times greater than that of copper), low friction coefficient, good insulating properties, chemical inertness, corrosion resistance, and transparency in the ultraviolet, visible, and infrared spectra [1], dictate their wide use, e.g., for producing hardening coatings of cutting tools (drills, milling cutters) [2], wear-resistant and antifriction layers in friction pairs [3], protective coatings (parts subjected to corrosive media) [4], and biologically compatible antiseptic and thrombo-resistant coatings (medical tools, implants) [5].

1.2. DLC coating production.

There are two main technologies of a-C and a-C:H films production: physical vapor deposition (PVD) and chemical vapor deposition (CVD). The PVD technology (a-C films) includes vacuum arc deposition [6], magnetron sputtering [7], pulsed laser sputtering [8], and ion-beam deposition [9] (in case of a-C films). The CVD technology (a-C:H films) involves plasma-enhanced chemical vapor deposition (PECVD) using RF [10,11], glow [12], or arc [13] gas discharges (in case of a-C:H films). The phase composition of DLC films produced by different methods are depicted in Fig.2 [14].

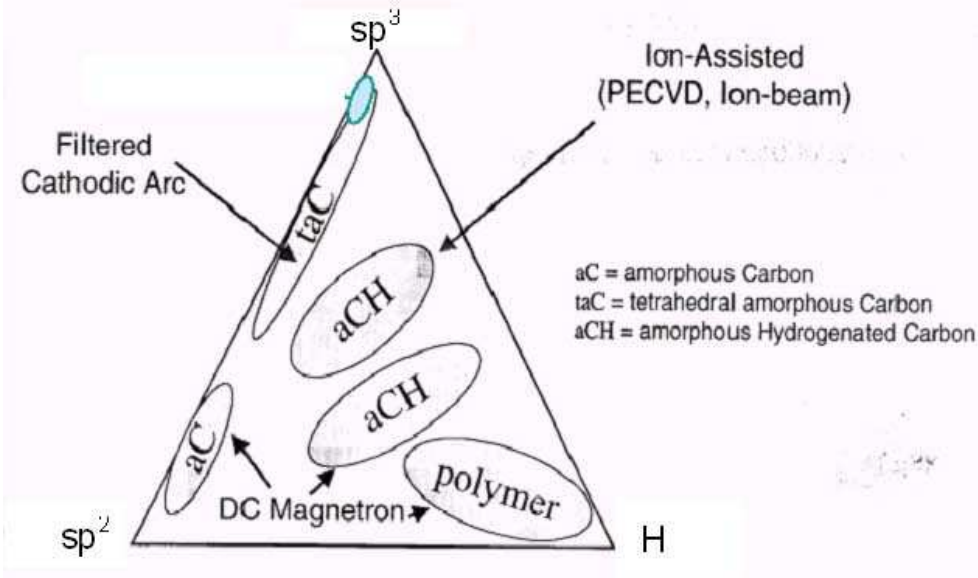

Fig.2. Phase composition of hydrocarbon films [14].

The two technologies, differing in ion-plasma flux production, have one feature in common – the hyperthermal energy (tens and hundreds of electronvolts) of particles which bombard the surface of the growing DLC film. As early as the 50s, theoretical study showed [15] that an energy of ~100 eV is sufficient for a temporal (7×10^{-11} s) local (~ 1 nm) increase in surface temperature and pressure to 3823 K and 1.3×10^{10} Pa, respectively. The required energy can also be transferred to C atoms adsorbed at the a-C film surface in their collisions with accelerated ions of inert gas, e.g., argon [16]. Thus, for a-C or a-C:H films high in diamond-like component to form, the energy per C atom settled on the surface must be ~ 100 eV. According to the data reported in [17], the further increase in particle energy up to 1000÷2000 eV increases the graphite-like C fraction in the coating.

The choice of optimal bias potential in DLC deposition is dictated by many factors (the substrate material, the plasma characteristics) and is a key problem in developing and optimizing the DLC production technology. On application of DC bias potential, the growing dielectric a-C and a-C:H films are charged and broken down. Therefore, in most cases pulsed bias voltage is employed to enable discharging of the film surface during the interpulse interval. On the other hand, it is necessary to provide the required energy (≈100 eV) per deposited C atoms. This

means that increasing the DLC deposition efficiency requires not only an increase in gas supply to the substrate and in treated surface area, but also the previous degree of the energy action (ion bombardment) on the formed C coating surface. Evidently this condition can be met only with sufficient plasma ionization near the substrate.

In the PVD and CVD methods, the rate of growth of a-C and a-C:H films, as a rule, is no greater than 1÷3 μm/h and depends on the treated surface area which is normally several tens of square centimeters [6-13].

A separate problem arising in DLC deposition is the film – substrate adhesion which is attainable either by making chemical bonds between the coating and the substrate or by forming a transition layer through ion mixing [18,19]. A contribution to adhesion can also be the internal stress relaxation in the film under the action of ion bombardment [20]. Therefore, allowance should be made for variation in both the plasma parameters and the bias voltage to provide the formation of the transition layer and the growth of the DLC film in one vacuum cycle.

In technological terms, the methods of DLC films production from nonequilibrium plasmas are most attractive and widespread. First, this is due to the fact that the initial gas need not be heated to high temperatures to be dissociated, as in the case of pyrolysis of hydrocarbons by the hot-filament method [21] or in the flame of a gas burner [22]. Thus, the substrate escapes heating responsible for sp^3-hydrogen graphitization. Second, the nonequilibrium plasma is a flexible instrument for the initiation of different chemical reactions, and variations in the plasma parameters may provide the desired composition and deposition rate.

Taking into account the equipment delivered to Phygen Inc., this review will consider the methods of DLC films production with a special emphasis on the a-C:H films formation by Plasma-Enhanced Chemical Vapor Deposition method.

1.3. DLC films production by physical vapor deposition.

In 1971 S. Aisenberg and R. Chabot were first to report on the DLC synthesis by the vacuum-plasma method, i.e., low-energy ion beam deposition [23]. Schematic of the setup used in this experiment is shown in Fig. 3.

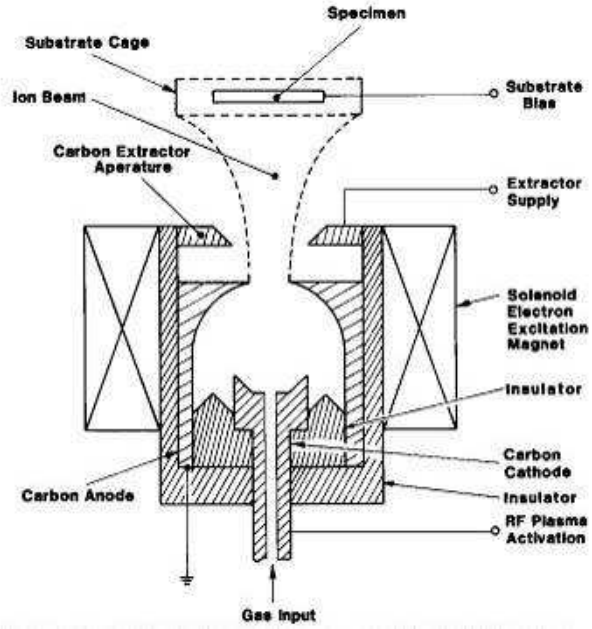

Fig.3. Cross-sectional view of the cylindrical ion deposition source [23].

The ion beam was extracted from the plasma formed in arc sputtering of graphite electrodes at 0.27÷6.7 Pa. Differential pumping made it possible to hold low pressure (~ 10^{-4} Pa) in the chamber. The energy of ions settled on the substrate was controlled by applying pulse or RF bias potential and was 40 eV. The rate of film growth was 5 nm/s. Certain of the film properties were found to approximate the characteristics of natural diamonds and hence these films got the name DLC or a-C films. The best-quality coatings were shown to develop in the energy range 30÷150 eV [24]. Thus, this method allowed the production of high-quality a-C films on different substrate, but the area of uniform film deposition was no greater than 2÷3 cm in diameter.

An attempt to enlarge the deposition area was made by using ion-beam sputtering of a graphite target [9]. Schematic of the ion-beam sputtering system is shown in Fig. 4.

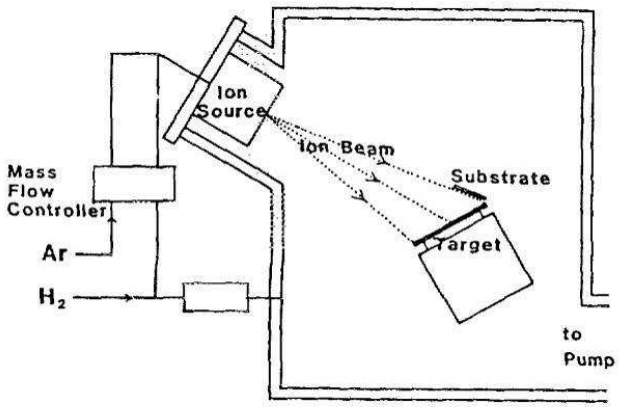

Fig. 4. Schematic of the ion-beam sputtering system.

A ∅10-cm graphite disk was sputtered by a ∅25-mm Ar ion beam. The angle of beam incidence on the target was 30^0. The ion current and energy were 60 mA and 1200 eV, respectively. The pressure in the chamber was kept at a level of 7×10^{-3} Pa. The substrate was located near the target and was near-parallel to the beam such that the growing film surface was bombarded by ions at a varying angle, deriving only part of the ion energy. The ion current densities to the target and to the substrate were 1 and 0.04 mA/cm^2, respectively. The hardness of the a-C film developed was greater than 30 GPa. The shortcomings of the method are the low rate of film growth and the as yet small substrate area. Moreover, the energy of sputtered atoms, in this case, is (~0.1÷1 eV) which necessitates additional ion assistance of the a-C film growth.

The most-used method of DLC films production is vacuum arc sputtering of graphite (vacuum arc deposition) [6], which is primarily due to high rate of film growth and high film hardness. Another feature of vacuum arc deposition is higher average power (~ 1 kW), compared to pulsed laser sputtering (~ 1 W). Although vacuum arc deposition and pulsed laser sputtering provide near-similar a-C films properties and plasma characteristics, the vacuum arc deposition method makes possible larger deposition surfaces and higher rate of film growth, and it is therefore more competitive, than pulsed laser sputtering.

Experiments on a-C films vacuum arc deposition were pioneered in the Soviet Union in the 70s [25,26]. A characteristic feature of the vacuum arc is a large droplet fraction in the initiated ion flux. Though this problem is solved to advantage through magnetic filtration (Fig.5) suggested for the first time in [27], the use of the filter decreases the rate of film growth to less than hundreds of nm/h.

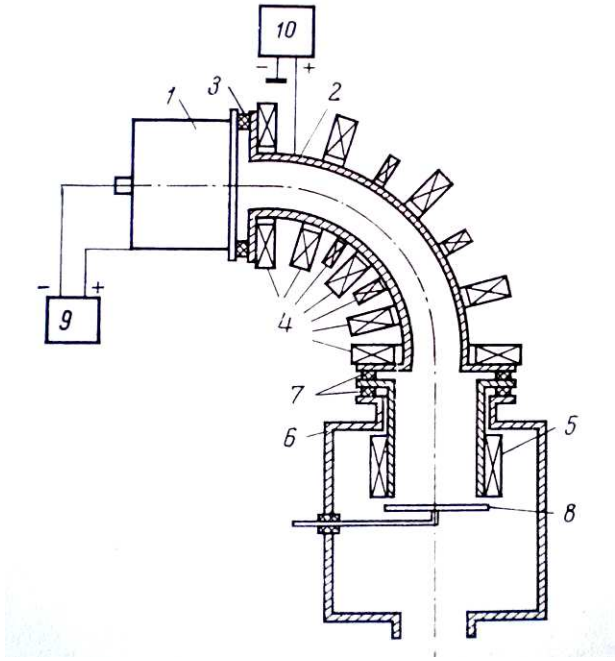

Fig. 5. Vacuum arc filtration: 1 – plasma source, 2 – plasma filter, 3, 7 – insulators, 4, 5 – magnetic solenoids, 6 – vacuum chamber, 8 – substrate.

1.4. DLC films production by chemical vapor deposition.

In most CVD methods of a-C:H films production, the ion-plasma fluxes initiated in various ways from the hydrocarbon gas discharge plasma are condensed on the substrate, and the films properties are governed by both the plasma characteristics and the conditions on the substrate. Bulk hydrocarbon plasmas are mainly produced using glow [12] and RF [11, 28-30] discharges and their versions. The plasma-forming gases are typically methane and acetylene. Compared to methane, acetylene has lower ionization potential, which provides higher plasma densities and higher rates of DLC deposition.

It was the DC glow discharge that was first to be proposed for hydrocarbon decomposition and a-C:H films deposition. The a-C:H films production by CVD

with the use of this discharge type is described rather thoroughly in [12]. Flat conducting substrates were arranged on a ∅55-cm rotating platform. The platform served as a cathode and the vacuum chamber as an anode. A DC voltage of 1 kV was applied between the electrodes. The methane pressure in the chamber and the discharge power were varied in the ranges 5.3÷16 Pa and 100÷250 W, respectively. Tests were performed with various substrate materials, including Al, Cu, W, Ni, Mo, Au, Si, GaAs, Ti, TiN, steel, stainless steel, Pyrex glass, quartz, ceramics, and Lexan. The rate of a-C:H film growth was 12 nm/min, the film hardness reached 25 GPa, and the ratio between H and C atoms (H/C) and that between of C atoms with tetragonal and trigonal bounds (sp^3/ sp^2) were 0.4 and 0.6, respectively. Despite the small content of diamond-like carbon, these coatings displayed good tribological characteristics, which made them usable in friction pairs.

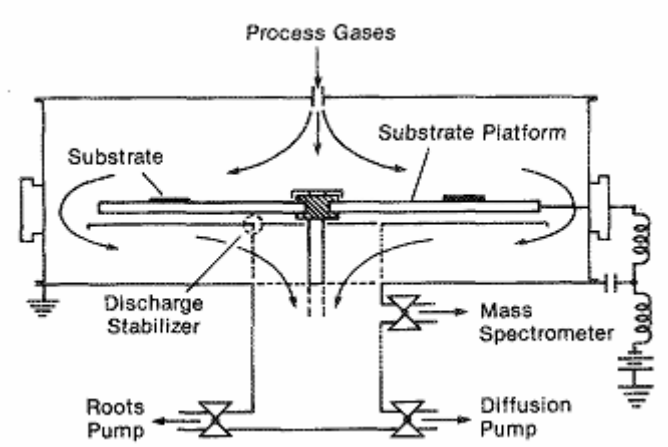

Fig.6. Simplified schematic of the DC plasma reactor [12].

The DC glow discharge is attractive primarily due to its simple realization. However, some peculiarities of this discharge considerably limit its application in a-C:H films deposition. The main shortcoming of this deposition method is that the substrate on the cathode is at negative DC potential of ~1 kV and the film surface, because of good insulating properties of diamond-like a-C:H films, is charged by the discharge current. This leads to a decrease in efficiency and, with a certain coating thickness, to cessation of surface bombardment by ions. Charging of the surface may also cause an electrical breakdown of the a-C:H film. All these factors impair

the coating quality and make impossible the formation of thick films. Other shortcomings of this method are the high pressure (1.3÷40 Pa), the low plasma density (about 10^9 cm^{-3}), and the moderate current density on the substrate (0.1÷0.2 mA/cm^2). As a result, the ion percentage in the ion-plasma flux condensed on the substrate is found to be no greater than 3÷5%, with most of the ion energy expended in gas phase collisions. The thus obtained a-C:H films are reach in polymer- and graphite-like phases due to the insufficient energy per carbon atom (10÷20 eV). Besides methane, methane-hydrogen mixtures, butane, and benzol vapors were used as the working gas. It was shown that dilution of methane with hydrogen does not affect the a-C:H film characteristics, and the glow discharge instability in butane and benzol vapors makes these gases unacceptable.

The next step in developing the PECVD technology was the use of RF discharges. In [28] DLC coatings were formed using an inductive RF discharge initiated in a cylindrical chamber of diameter 44 cm and height 55 cm (Fig.7). The RF discharge power supply provided a peak power of 50 kW and an average power of 1 kW at a frequency of 100-500 Hz. A pulsed bias voltage of amplitude up to 40 kV, pulse duration 2-300 μs, and maximum current up to 6 A was applied to a chamber-insulated disk on which a target was located. The operating pressure was 0.8-1.2 Pa. The substrate material was silicon. The plasma-forming gases were methane (CH_4) and toluene (C_7H_8).

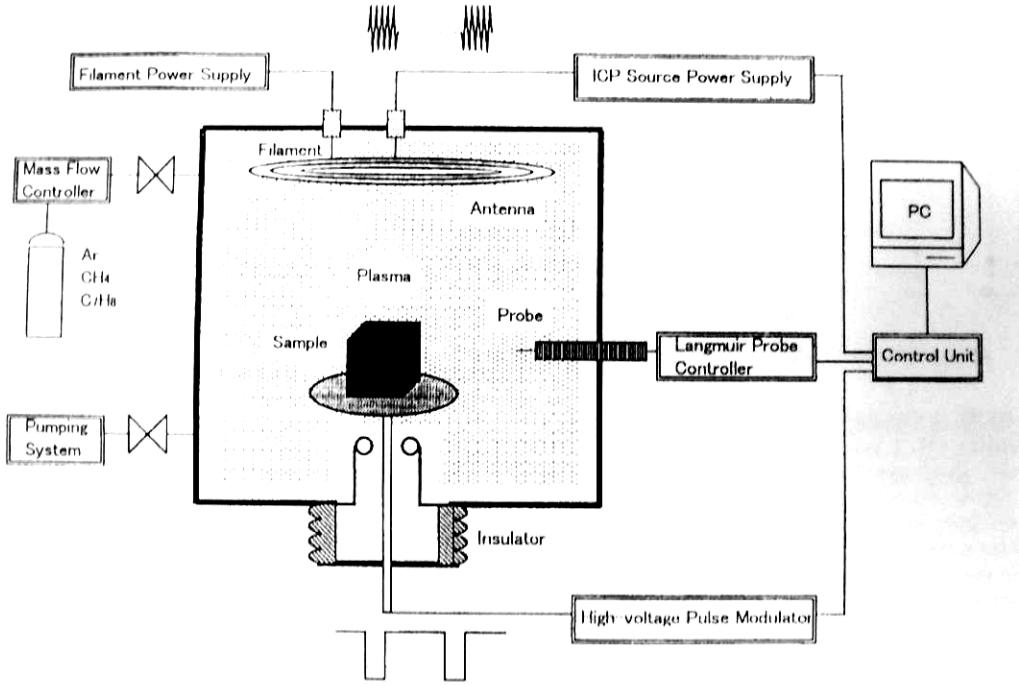

Fig. 7. Schematic of the pulsed PSII apparatus [28].

The parameters of DLC film deposition were the following: the CH_4 and C_7H_8 flow rate 10 sccm, the pressure during the deposition 1 Pa, the peak power of pulsed plasma 15 kW, the implantation voltages 20 and 5-20 kV for CH_4 and for C_7H_8, respectively, the high voltage pulsewidth 5 μs, and the pulse frequency 200 Hz. The implantation times for CH_4 and C_7H_8 plasma treatment were 5 and 60 m, respectively. The sp^3 to sp^2 bond ratio was 0.28. The film hardness was up to 28 GPa.

In [29] a 13.56-MHz capacitive RF discharge was used to produce a-C:H films from the methane plasma on silicon and stainless steel (440C) substrates (Fig.8). Negative bias high-voltage pulses (normally, –20 kV, 100 Hz, 50 μs) were applied to the substrate holder. Methane was supplied into the chamber with a constant flow rate of 20 sccm. The operating pressure was $2.5 \cdot 10^{-1}$ Pa. The deposition time was 2 h. The DLC coatings obtained on the stainless steel substrates displayed a good adhesion and a low frication coefficient (0.006, compared to 0.6 of untreated specimens).

At Los Alamos National Lab. (USA), a capacitive RF discharge was used to generate bulk hydrocarbon plasma in a cylindrical chamber of diameter 1.5 m and height 4.6 m (Fig. 9) [18,30,31].

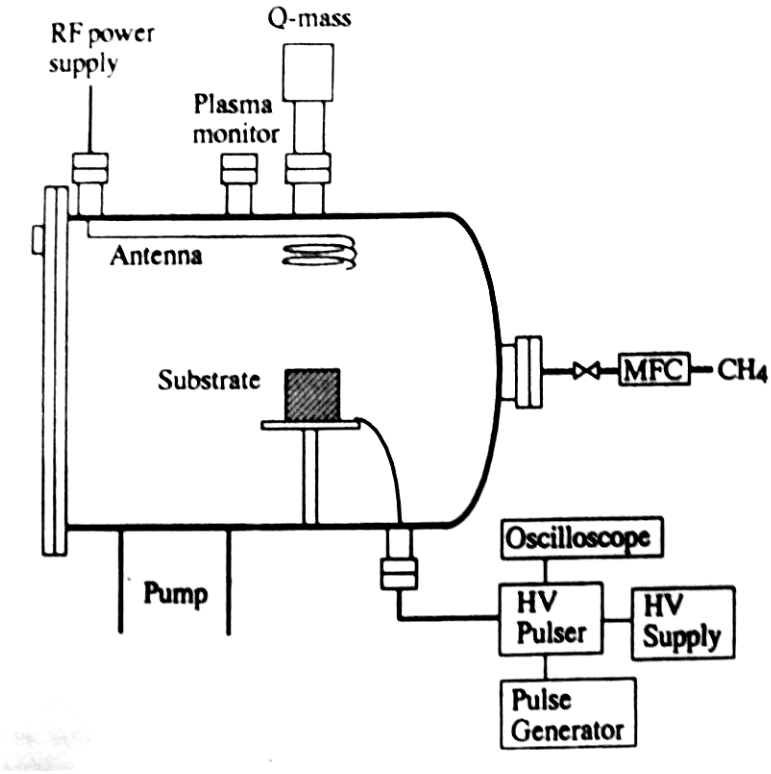

Fig. 8. Schematic of the PSII system [29].

Fig.9. Plasma cleaning, ion implantation, and DLC deposition of 1000 automotive pistons in the former OFES facility (Los Alamos National Lab.)

The working gas was acetylene. The pressure in the chamber ranged between 0.07 and 0.33 Pa. A discharge of power 100÷1000 W was excited in the chamber using an RF antenna (13.56 MHz), with the plasma density variable between $10^8 \div 10^9$ cm^{-3}. The antenna served as a cathode and the grounded chamber as an anode. The substrates were placed in a separate holder at the center of the chamber. The area of the treated surface reached 3 m^2. Due to the large free path length (15÷20 cm), the plasma filed uniformly (with an accuracy of ± 10%) the entire working volume. As this took place, no shadow effect occurred that made it possible to treat bulky parts. Rectangular bias voltage pulses of amplitude from –200 to –4000 V, duration 20 s, and frequency ~12 kHz were applied to the substrate holder. The highest-quality hydrogenated amorphous diamond-like films were obtained at a pressure of 0.07 Pa and a bias voltage amplitude of –600 V. The film hardness reached 26 GPa, the percentage of sp^3-fixed carbon was 50÷70%, and the hydrogen

percentage was about 20%. However, the coating deposition rate in this mode was only 150 nm/h due to the low operating pressure and the low plasma density. The use of an inductive-type RF discharge allows an increase in plasma density to 10^{10} cm^{-3} and thus a better-quality of a-C:H films, as shown in [28] and demonstrated by researchers of Los-Alamos National Lab. [32].

The above review of the existing a-C:H films deposition methods suggests that the low rates of film growth in a RF discharge and hence the low technological efficiency are primarily associated with the low plasma density and with the small degree of plasma ionization which in turn owes to the low energy transfer coefficient from the RF generator to the plasma.

This parameters can be increased essentially by use of microwave ECR plasma [33-35] for a-C:H films deposition. In [33] hard amorphous hydrogenated diamond-like carbon films was deposited using an electron cyclotron resonance microwave plasma with a separate radio frequency power bias applied to a substrate stage (Fig.10). Approximately 360 watts from 1 kilowatts of microwave power at approximately 2.45 GHz was transmitted through waveguide and quartz window into the plasma chamber 12. The tube 32 was used to transfer a plasma generation gas, such as hydrogen (H_2). The circular gas ring 54 was used to transfer a reaction gas (such as methane , acetylene, and propane) into the deposition chamber 30. The summarized pressure in the plasma chamber was 10 – 1 Pa. 13.56 MHz RF external power bias was applied to the sample holder 42.

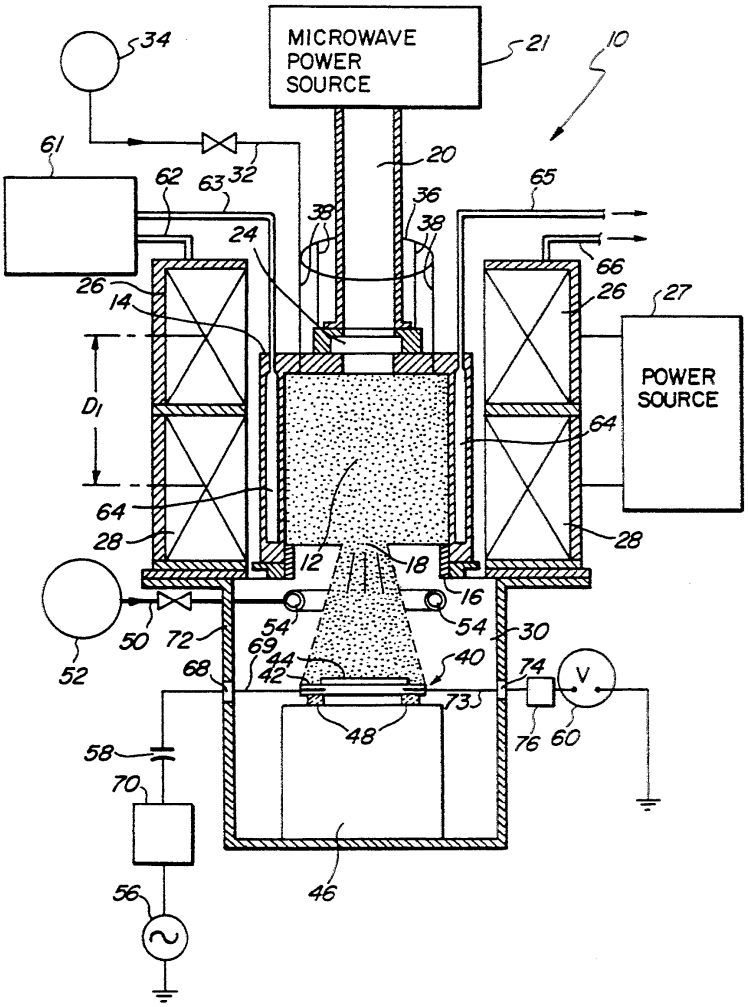

Рис. 10 - ECR microwave reactor for deposition of DLC films [33].

The deposition rate was approximately 1.5 μm/h at a pressure of 0.5 Pa, ratio of CH_4 to H_2 concentration 50%, and 0.5 μm/h at a pressure of 1.7 Pa, ratio of CH_4 to H_2 concentration 17%. The lower deposition rate, in opinion of the authors, was caused by increased hydrogen ion etching, given the negative bias voltage, and the higher hydrogen fraction of the plasma.

Dense plasmas provide efficient hydrocarbon gas dissociation and ionization in the discharge which, in tern, ensures a high-quality of a-C:H coatings and a high rate of their growth. In the case in question, the rate of film deposition depended on the ion current density to the substrate surface (i.e., on the microwave ECR discharge power) and was 1.5 nm/s at j=1.5 mA/cm^2 (P=400 W). The thus obtained coatings had a hardness of 60 GPa and a density of 2.85 g/cm^3 and contained 70% of sp^3-fixed carbon.

Despite the fact that the plasma of RF and microwave ECR discharges make possible high-quality a-C:H films and high rates of film growth, their use in technological processes is a problem. The fact is that at present no method exists of producing extended or bulk microwave ECR plasma, and hence scale application of this method is impossible. Moreover, the equipment needed to realize a microwave ECR discharge is expensive and is difficult to fabricate and maintain. The plasma of a low-pressure arc gas discharge is much more attractive for a-C:H films deposition [11,83]. Due to the relatively high discharge current (1÷100 A), the plasma density (10^{10}÷10^{11} см$^{-3}$) in this case is greater than that characteristic of DC glow and RF discharges, including all their modifications.

Represented in [36] plasma gun 1 was formed by a cathode 2, an intermediate electrodes 3,4 and anode 19, located in the vacuum chamber 8. A high-frequency power source 18 (13.56 MHz, 11 W) with maximum output of 500 watts was connected to the substrate holder 17. Argon was introduced into the vacuum chamber from discharge gas inlet 12 up to the pressure of $4 \cdot 10^{-2}$ Pa. A voltage of about 80V was applied to plasma gun. Methane (CH_4) gas was introduced into the vacuum chamber from the reaction gas inlet 13 up to the pressure of $1 \cdot 10^{-1}$ Pa.

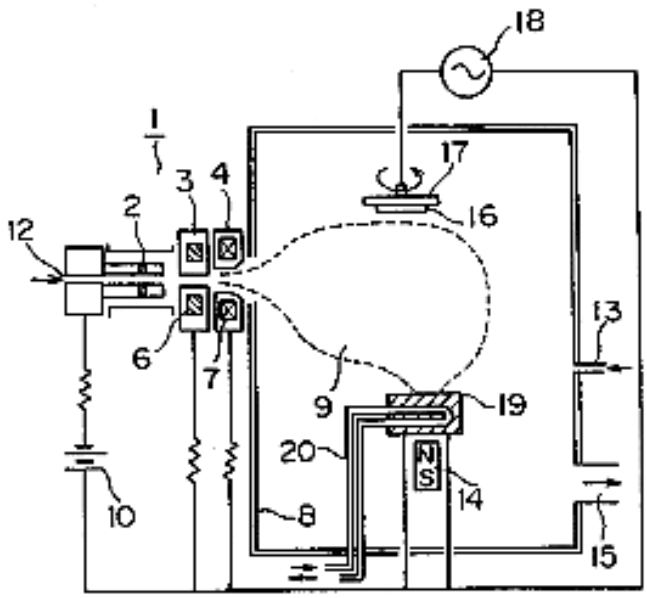

Fig. 11 – Schematic of the system on the basis of arc discharge [36].

Ni, Si, glass and Al_2O_3-TiC substrates was employed. The process duration was about 20 minutes, for forming a DLC films of 300 nm in thickness on the substrate 16. The DLC films hardness form 20 to 30 GPa was obtained.

Unfortunately, is not specified in the patent, what the volume of plasma allows to generate such discharge system. However, it is obvious, that the energy of electrons low than 80 eV insufficiently for dense plasma formation in the large volumes. Furthermore, there are no any filters in the design of this system, therefore the contamination of generated gaseous bulk plasma by cathode erosion products is possible.

1.5. Conclusion.

Thus, successful DLC film formation from hydrocarbon-containing plasma requires the following:

1. For producing a metastable diamond-like carbon phase, the deposited energy per carbon atom must be ~100 eV. (This is most commonly attained by maximizing the plasma density near the substrate and by applying the required bias potential to the substrate).

2. For achieving the acceptable technological efficiency of the process, the rate of film growth and/or the treated surface area per vacuum cycle must be maximized. (This is attainable, e.g., by increasing the operating pressure and the power deposited to a discharge and also by forming reasonably homogeneous plasma bulks).

3. The adhesion between the DLC film and the substrate must be satisfactory. (A possible way of solving this problem is preliminary plasma treatment of the substrate surface and the formation of a carbon-containing transition layer between the film and the substrate with the use of plasma-immersion ion implantation).

Three SPACE-2 plasma generators delivered to Phygen Inc. allow the production of reasonably homogeneous plasmas in large vacuum volumes (up to 1 m^3), with the maximum plasma density up to 10^{11} cm^{-3}. A plasma generator of this

type is well suited for successful generation of hydrocarbon-containing gas plasmas (methane, acetylene etc.). Obviously the high plasma density and the high discharge current (compared to RF-discharge systems) must provide higher rates of a-C:H film growth and/or a possibility to treat a larger surface area per cycle, and this is a very promising trend. At the same time, a review of the literature shows that up to now there has been no experiment performed to synthesize DLC coatings from bulk dense plasmas produced by constricted arc discharge systems with electron injection.

1.6. Detailed work plan.

Milestone 1.” Detailed work plan ”

Duration: 1 month

1. Prepare a literature survey (scientific journals and relevant patents) in the area having to do with plasma deposition of diamond-like carbon (DLC).
2. Purchase required materials for fabrication of HCEI plasma hardware.
3. Set up Tomsk analogous experimental facility.
4. Submit survey and detailed work plan to Phygen and LBNL.

Milestone 2. ”Hydrocarbon plasma source operation ”

Duration: 4 months

1. Operation of plasma source with hydrocarbon gas. Research of hydrocarbon plasma influence on operating parameters and maintenance period.
2. Maintenance of high efficiency of hydrocarbon gas utilization.
3. Insertion of necessary changes into the plasma generator design.
4. Design and manufacture of gas equipment.
5. Design and manufacture of low-voltage (LV) pulse bias power supply (up to 600 V).
6. Design and manufacture of high-voltage (HV) pulse bias power supply (up to 20 kV).

7. Participate in three-way conferencing about specifics of hydrocarbon plasma discharge and DLC deposition processing.
8. Submit a brief progress report to Phygen and LBNL.

Milestone 3.”Experimental research on DLC deposition”.

Duration: 5 months

1. Finding of operating parameters (plasma density, hydrocarbon and argon flow rate, substrate pulse bias parameters, surface temperature) for DLC deposition on silicon samples. Measurement of hardness and thickness of obtained coatings.
2. Carry out a DLC deposition on metal samples (Stainless Steel, HSS).
3. Use of different hydrocarbon gases (methane, acetylene, propane) for DLC deposition.
4. Carry out a DLC deposition on previously nitrated surface.
5. Carry out a DLC deposition on previously implanted surface.
6. Perform optimization of operating regimes for DLC deposition. Detailed description of process rules for optimum DLC synthesis.
7. Ship pulse bias power supply to Phygen.
8. Participate jointly in conferencing about specifics of experiments, based on the literature survey and the existing Phygen system and about requirements dictated by the specific application of DLC formation.
9. Submit a final report to Phygen and LBNL.

Milestone 4.”Equipment commissioning and final report”.

Duration: 2 months

1. Install equipment at Phygen Corp.
2. Assist the collaboration in assessing the results of Phygen laboratory tests.
3. Submit a final report to Phygen and LBNL.

II. HYDROCARBON PLASMA SOURCE OPERATION

2.1. Experimental test stand (IHCE, SB, RAS, Tomsk).

The design of the plasma generator arranged on a test stand at Plasma Source Department (IHCE SB RAS, Tomsk) is shown in Fig.12. The physical principle of plasma generation is that the electrons emitted from the constricted arc discharge region and accelerated in the cathode layer of the main discharge ionize the gas in the chamber volume. All generator electrodes are insulated from each other and from the grounded vacuum chamber by ring kaprolon insulators and are cooled by running water. Hollow cathode 1 of the emitter discharge is made of copper and has an inner diameter of 82 mm and a height of 57 mm. The emitter discharge is initiated by a gas breakdown on application of a high-voltage pulse between trigger electrode 5 and the cathode 1. The working gas is supplied into the cavity of the cathode 1 through a hole in which the trigger electrode 5 is located. Magnesium ring 4 is placed on the cathode cover near an outlet of diameter 6 mm. The axis of the cathode cavity outlet is displaced with respect to the constriction channel in intermediate electrode 2.

For more efficient heat removal, the cover and the cathode contact through a heat-conducting paste. In order to decrease the outlet erosion, molybdenum insert is pressed into the cover of the cathode 1. The cathode face is covered with an insulating stainless steel shield 6 to preclude arcing. The anode of the emitter discharge is a tungsten grid located on the electrode 12 and connected to the cathode of the main discharge. The geometrical transparency of the grid is 75 %. The emission windows in the intermediate electrode 2 and in the main discharge cathode 12 are rectangular in shape, which provides injection of a ribbon electron beam into the working volume. For the plasma density to be more uniform at the maximum discharge current, flat distributing grid electrode 10 is used. For increasing the lifetime of the electrode 2, the constriction channel is diaphragmed by two movable molybdenum plates 8. For more efficient heat removal from the cathode of the main

discharge, the intermediate electrode, and the demountable element to the water-cooled parts of the generator, use is made of heat-conducting paste. The anode of the main discharge is a separate unit and is a stainless steel disk of diameter 100 mm.

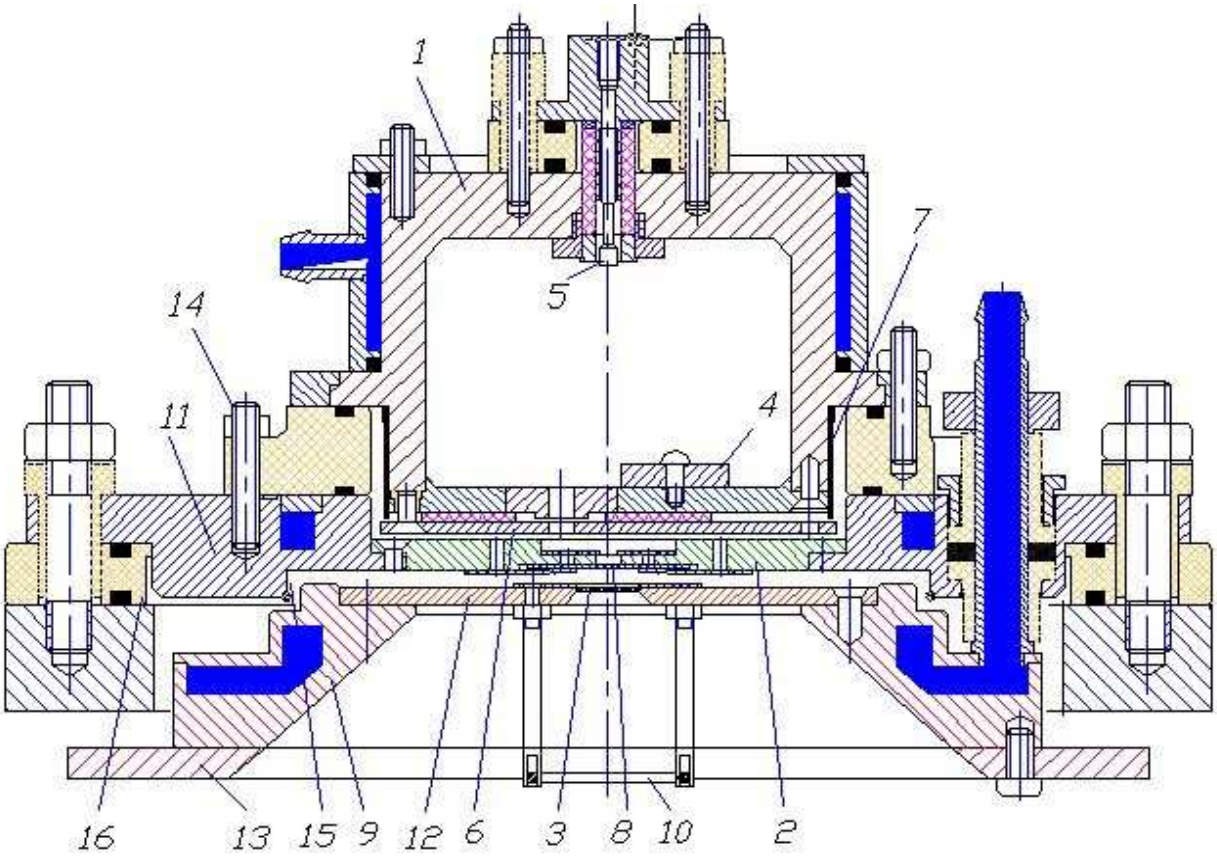

Fig. 12 - Sketch of the plasma source discharge system.

1 – keeping discharge cathode, 2 – intermediate electrode, 3 – mesh-like keeping discharge anode, 4 – Mg washer, 5 – trigger electrode, 6 – arc protection insulated shield, 7 – Mo foil, 8 – changeable Mo plates, 9, 12, 13 – main discharge cathode parts, 10 – mesh-like redistributing electrode, 11 – flange, 14 – pin for mounting on-source block, 15 – delaminated film collector, 16 – insulator.

The plasma generator is mounted on the face of the vacuum chamber of volume 1 m^3 (Fig.13), pumped by a diffusion pump with a pumping rate of 2000 liter/min. The anode of the main discharge is placed at the bottom of the vacuum chamber. The main parameters of the plasma generator are cited below.

Emitter discharge current	3 – 20 A
Main discharge voltage	10 – 130 V
Main discharge current	0.5 – 20 A
Working gas	Ar
Operating pressure	$(4 \div 10) \cdot 10^{-2}$ Pa
Maximum plasma density at the center of the 1 m^3 volume	$3 \cdot 10^{10}$ cm^{-3}

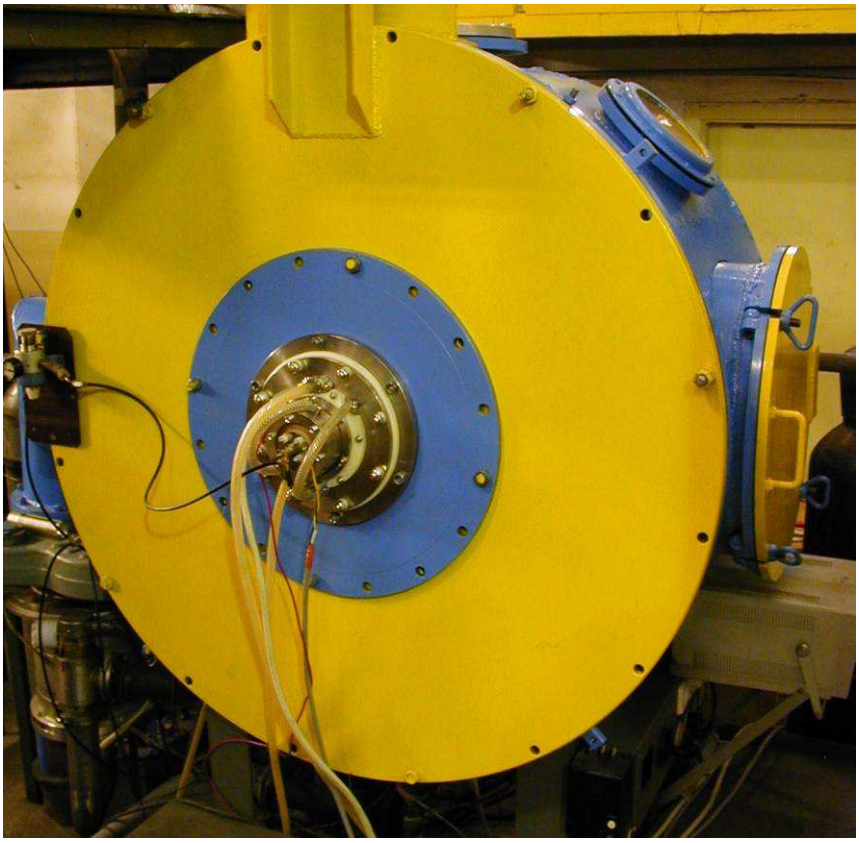

Fig. 13. Photo of the SPACE-2 plasma generator installed at the Plasma Source Department (Tomsk, IHCE, SB, RAS).

A plasma source identical to that delivered to the Phygen Inc. On the upper flange of the vacuum chamber, there is a vacuum lock for quick specimen replacement. The anode of the main discharge is at the bottom of the vacuum chamber. The plasma density is measured with a flat Langmuir probe located at the center of the chamber.

Argon is supplied directly to the cathode cavity of the emitter discharge. It is highly undesirable to supply hydrocarbon to the cathode of the emitter discharge, since this involves contamination of the surface at which cathode spots operate and deposition of hydrocarbon-combustion products on the electrode insulators. Hence, hydrocarbon should be supplied directly to the vacuum chamber. In experiments, hydrocarbon was supplied from the side of the plasma source with a 20 cm displacement from the discharge system axis (Fig. 14).

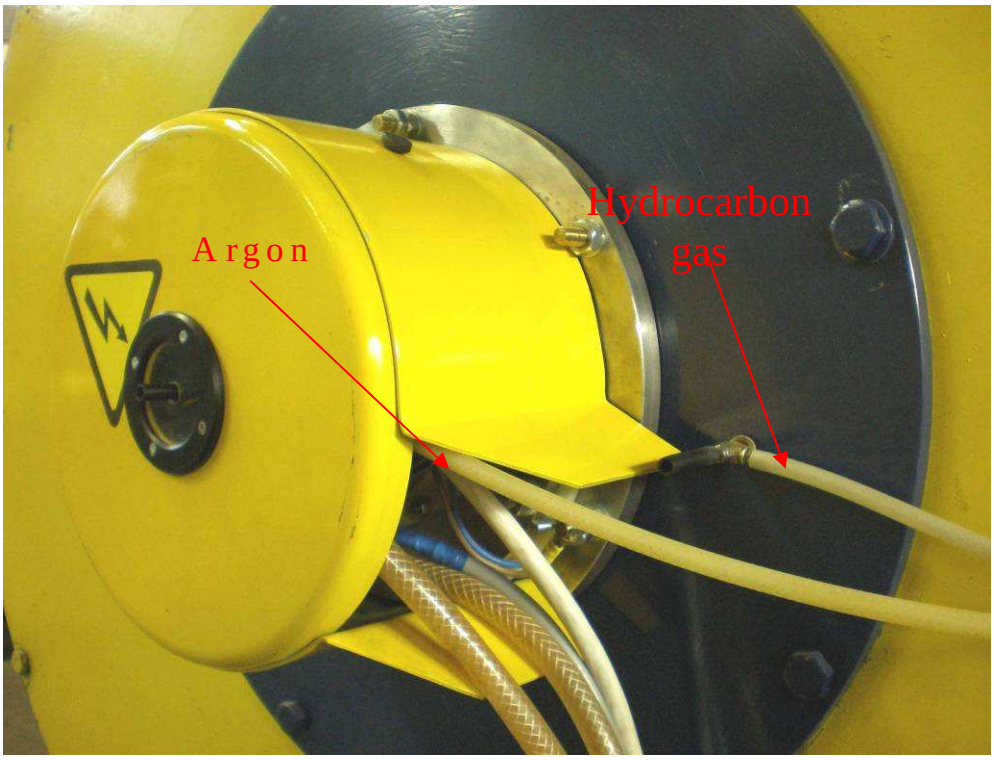

Fig. 14. Arrangement of the gas supply tubes.

The gas supply is controlled by two flowmeters operable in corrosive media (Fig. 15). The flowmeters are calibrated against nitrogen. The actual flow rates are determined using correction factors for a certain type of the working gas.

Fig. 15. Flowmeters.

Experiments show that the position of additional hydrocarbon feeding to the vacuum chamber (the displacement from the discharge system axis) is of great importance. For 20 cm displacement from the discharge system axis, gas supply with a flow rate of 20-30 sccm increases the plasma density in the volume only slightly (Fig. 15). Similar results were obtained for argon and nitrogen. This effect can be explained as follows. The degree to which the gas is ionized in the plasma of the main discharge is no greater than 5 % (weakly ionized plasma), and hence the ionization degree of the gas supplied to the chamber in this way cannot exceed the above value and change considerably the plasma density in the volume.

At the same time, increasing the feeding of gas (e.g., argon) directly to the discharge chamber by this value causes a proportional increase in plasma density in the volume (the upper curve in Fig. 15a). Thus, in further experiments, additional gas feeding in the vacuum chamber was directed at the center of the emission hole in the cathode of the main discharge. The gas was filled with the use of a special tube, as shown in Fig. 16. Thus, the degree to which the additional gas supplied to the vacuum chamber was ionized was increased by 30-40 % (Fig, 15b).

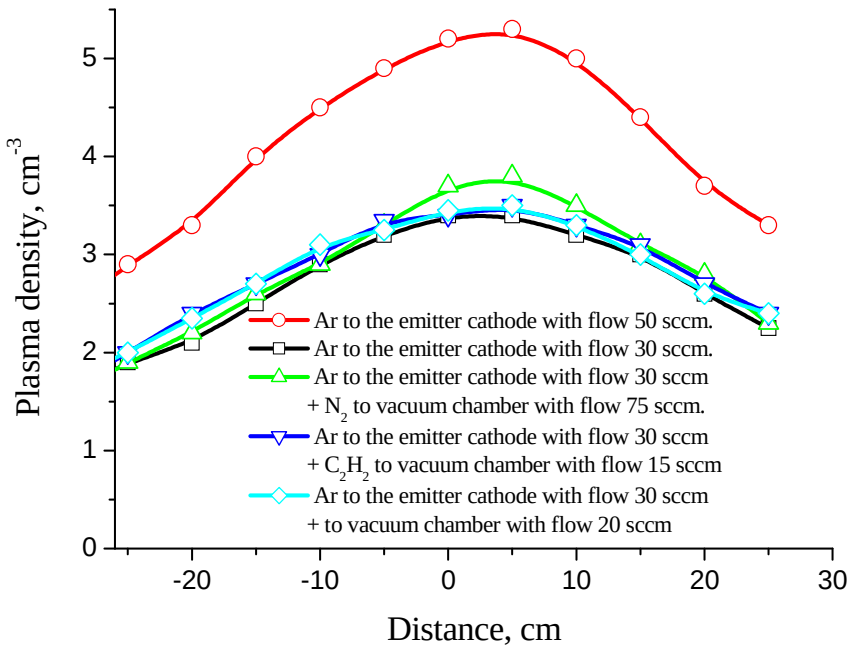

a

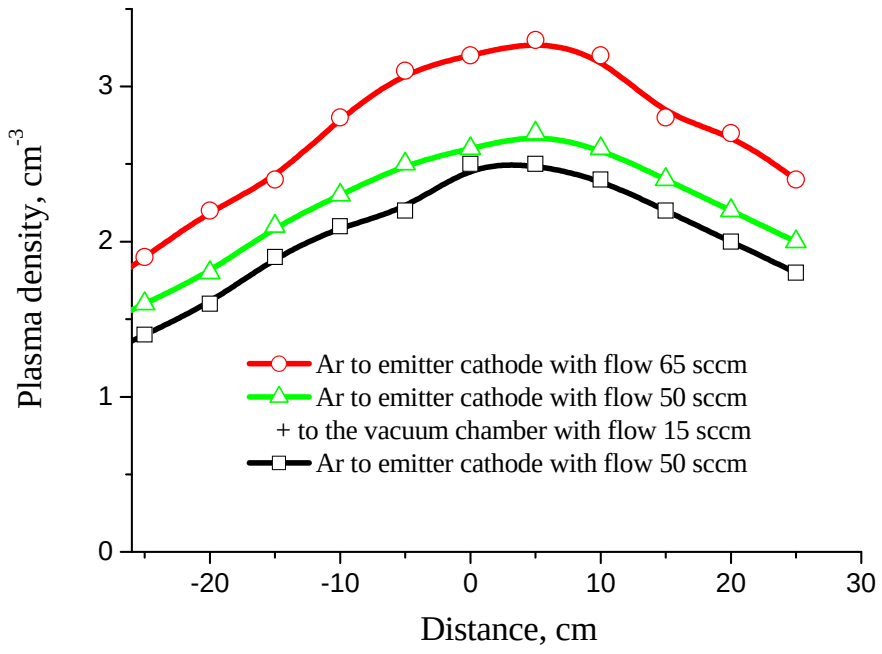

b

Fig. 15. Spatial plasma density distribution at the center of the chamber (0-center of the chamber): additional gas feeding with a 20 cm displacement from the discharge chamber axis (a); additional gas feeding toward the center of the emission aperture (b).

Fig. 16. Hydrocarbon supply to the center of the emission hole in the cathode of the main discharge.

The operation of the main discharge in a carbonaceous atmosphere results in so-called “soot” settled on the electrodes of the discharge system and on the walls of the vacuum chamber. This causes a change in the plasma parameters (the discharge current, the plasma density) and reduces the time between routine maintenances of the discharge system. As indicated earlier, for the effect to be weakened, it is preferable to fill inert gas (argon) to the cathode cavity of the emitter discharge and hydrocarbon directly to the vacuum chamber. In this case, the hydrocarbon combustion products affect only the electrodes of the main discharge, while not affecting the ignition and operation of the emitter discharge.

Life tests with pure argon and without additional hydrocarbon (acetylene) feeding show that the parameters of the main discharge during the operation remain nearly constant (Fig. 17).

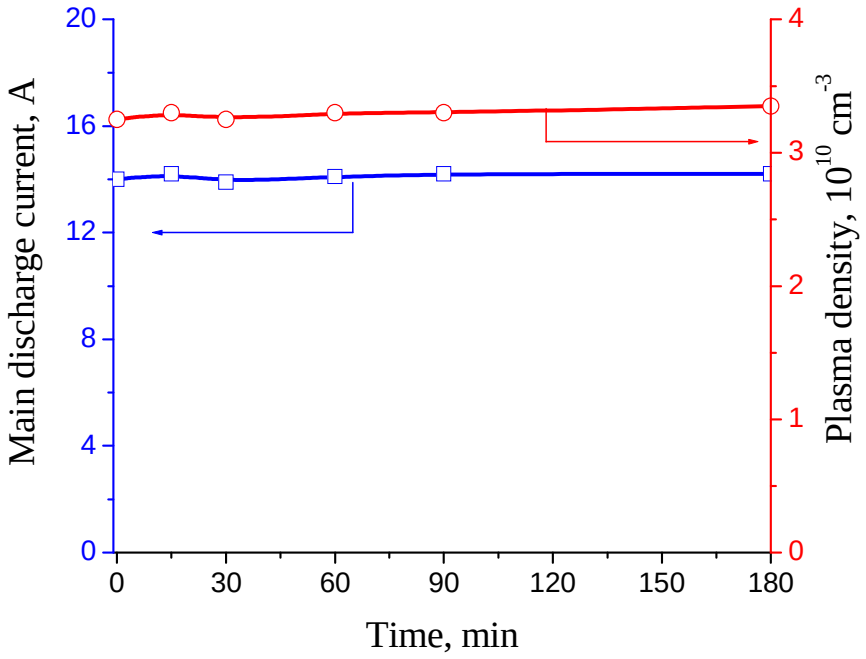

Fig. 17. Variation in the plasma density and in the main discharge current for pure argon. The emitter discharge current is 15 A, the main discharge voltage is 100 V, and the flow rate is 35 sccm.

When acetylene is filled to the vacuum chamber with a flow rate of 35 sccm, a jump-like decrease in plasma density is observed (Fig. 18). This can be due to the electron affinity of carbon and hydrogen, which is responsible for capture of free electrons by atoms with the production of negative ions. The further decrease in plasma density and main discharge current is associated with the processes occurring directly on the electrodes of the main discharge. After 3 h operation, the plasma density and the main discharge current decrease by 25 % and 35 %, respectively.

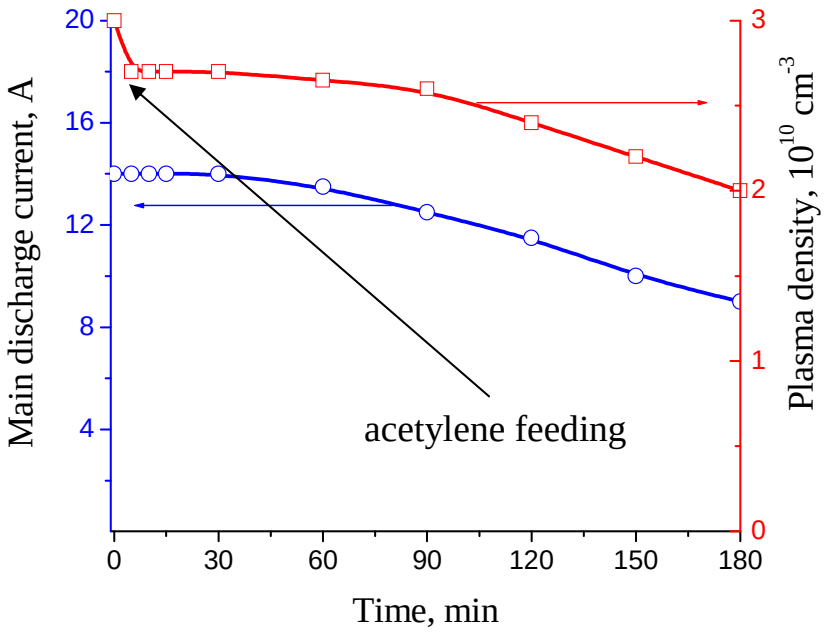

Fig. 18. Variation in plasma density and main discharge current for argon-acetylene mixture. The emitter discharge current is 15 A, the main discharge voltage is 100 V, the argon and acetylene flow rates are 35 sccm.

Mechanical cleaning of the anode surface has but a minor effect on the discharge parameters. The main discharge current increases by 10 % and the plasma density only by 5 %.

Cleaning of the cathode surface and replacement of the tungsten grid causes the main discharge current and the plasma density to regain their initial values. Since the cathode of the main discharge has a negative potential with respect to the plasma, its surface is partially cleaned during the operation due to ion bombardment. However, for the acetylene flow rates in question, the deposition rate of combustion products is more than an order of magnitude greater than the rate of ion sputtering. Moreover, soot settling reduces the cathode grid lifetime. The high temperature at the centre of the grid provides cleaning of this part of the grid, while at the periphery soot settling prevails. As a result, the contribution of the peripheral part of the grid to the current transport decreases, while that of the central part increases. Thus, the temperature at the center of the grid continues to elevate. Life tests show that after 5 h operation with acetylene supply, only 50 % of the cathode grid remains

conductive (Fig. 19,a). For the emitter discharge current above 10 A, this part of the grid is intensively heated and is destructed within less than 10 h of operation.

This problem can be solved by using tungsten wires 0.8 mm thick instead of the fine tungsten grid (Fig. 19,b). In so doing, the wire separation must be shorter than the cathode layer thickness. Thus, in response to the decrease in geometrical transparency, the main discharge current decreases by 10-20 %, while the grid lifetime increases about two times.

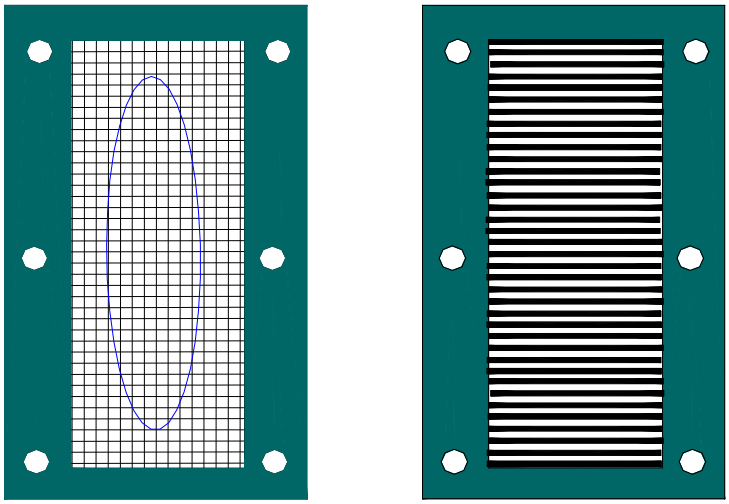

а б

Fig. 19. Versions of the cathode grid of the main discharge: fine tungsten grid (a); tungsten wires (b).

Contamination of the anode surface with dielectric films can be precluded by increasing the temperature of the anode surface. For this purpose, a stainless steel plate of area 100 cm^2 is used as the anode of the main discharge (Fig. 20). The power released during the discharge operation elevates the plate temperature to 600 ^oC, which provides evaporation and graphitization of dielectric films settled on the anode surface. A trouble with this method is that the temperature required for evaporation is attainable only at relatively high currents of the main discharge (15-20 A), otherwise the dielectric films do settle on the anode surface. However, this condition is rather easily provided with the use of three plasma sources operating into one common anode.

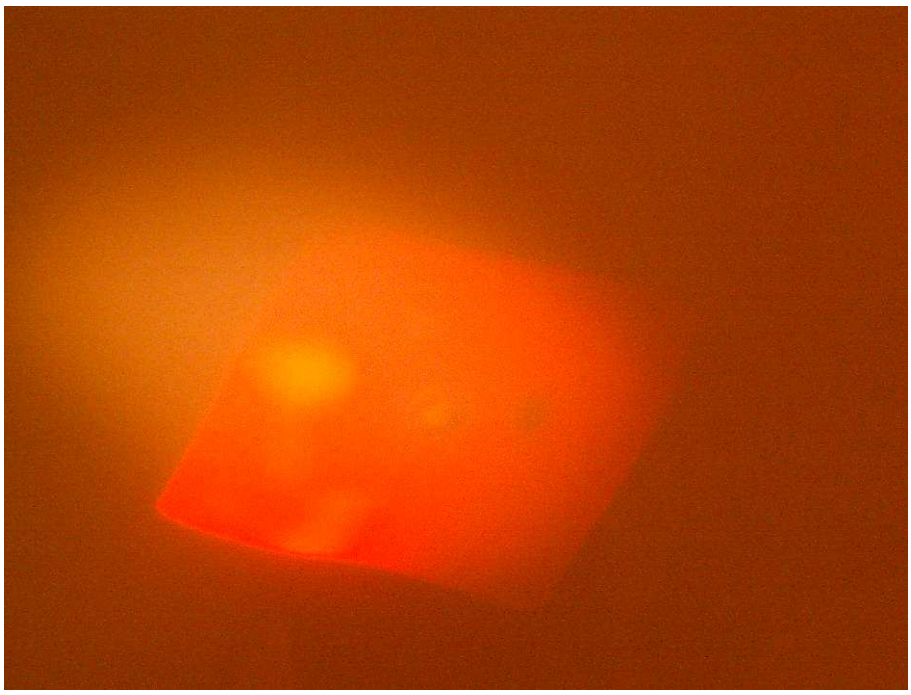

Fig. 20. Heating of the anode plate of the main discharge during the operation.

It should be noted that the life tests did not reveal any electrode breakdown over the insulator surfaces. This is due to the hydrocarbon feeding directly to the vacuum chamber and to the design of the discharge system, which precludes contamination of the insulators during the operation of the main discharge.

For specimen bias in the plasma, a prototype of the bias power supply with low-voltage (down to -700 V) and high-voltage (up to -20 kV) circuits was designed and tested. The design makes it possible to apply both negative and positive voltages to a specimen. It also provides protection from short-circuits and arcs in all operating modes (at a load current greater than 2 A, the control circuit deenergizes the source output for 5 μs). The prototype is powered by a 220 V single-phase voltage. A photo of the control panel and prototype elements is shown in Fig. 21.

Fig. 21. Photo of the prototype of the bias voltage source.

In the implantation mode, pulsed voltage is applied from the output of the control circuit to an air-cooled step-up transformer located in the immediate vicinity of the input connector of the vacuum chamber (Fig. 22). The overall dimensions of the transformer case is 35×30×22 cm. The maximum output voltage of the transformer is 30 kV. The maximum operating current of the transformer is 1 A at a pulse duration of 50 μs and a pulse repetition frequency of 500 Hz.

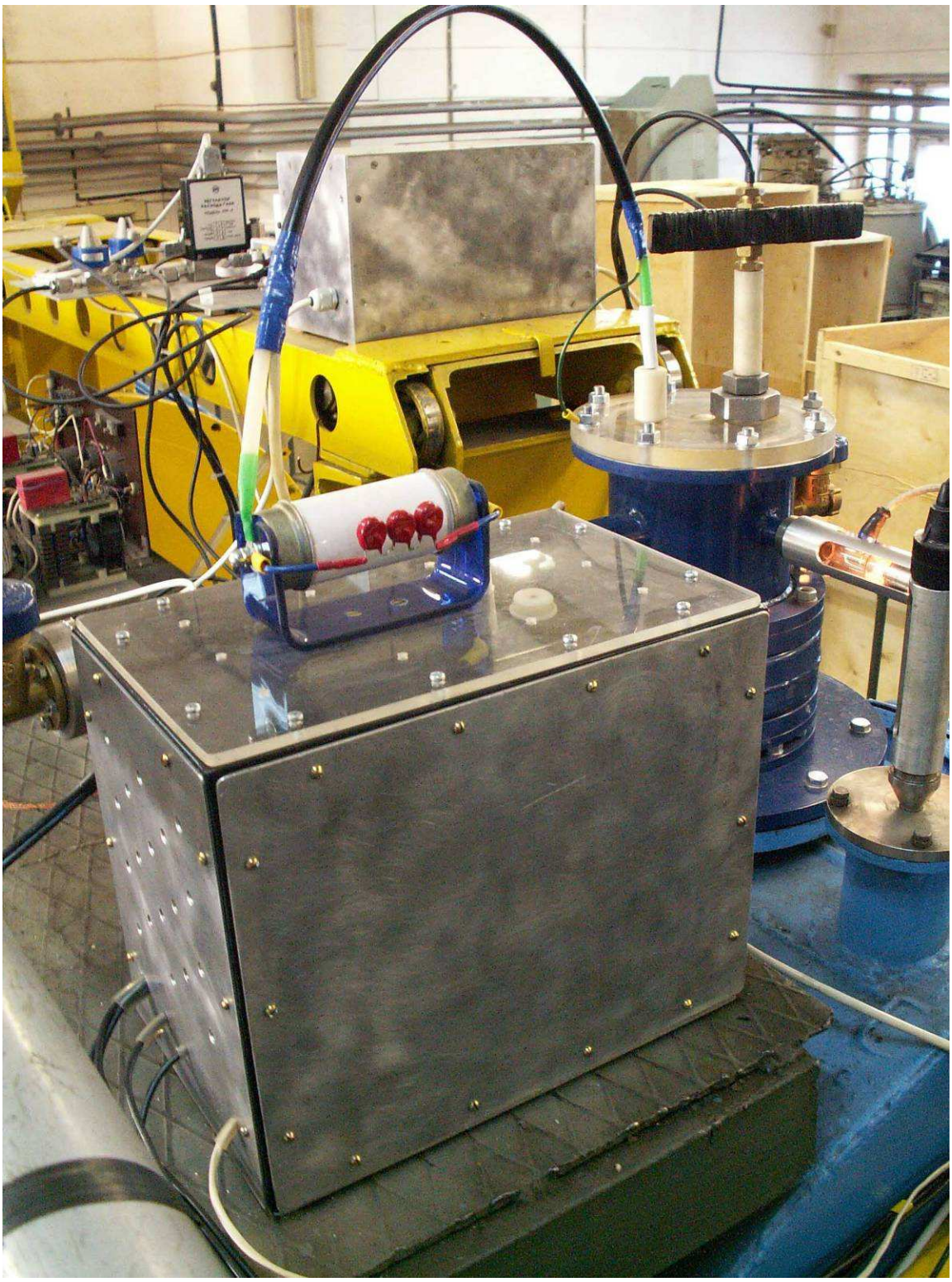

Fig.22. Photo of the high-voltage transformer.

The bias voltage source allows the following operating modes:

a. Ion cleaning.

In this mode, the source produces a negative dc voltage down to -700 V with a current up to 2 A and allows gradual adjustment of the voltage amplitude.

b. Nitriding.

In this mode, the source produces a pulsed bipolar bias voltage with negative and positive amplitudes up to 700 V and 20 V, respectively. In this mode, the ion and electron currents can reach 2 A and 10 A, respectively. The pulse repetition frequency is varied discretely in the range from 7 to 43 kHz. The source allows gradual adjustment of the voltage amplitude, pulse duration and duty factor. Figure 23 shows a typical waveform of the bias voltage on the plasma load (100 cm^2 specimen area).

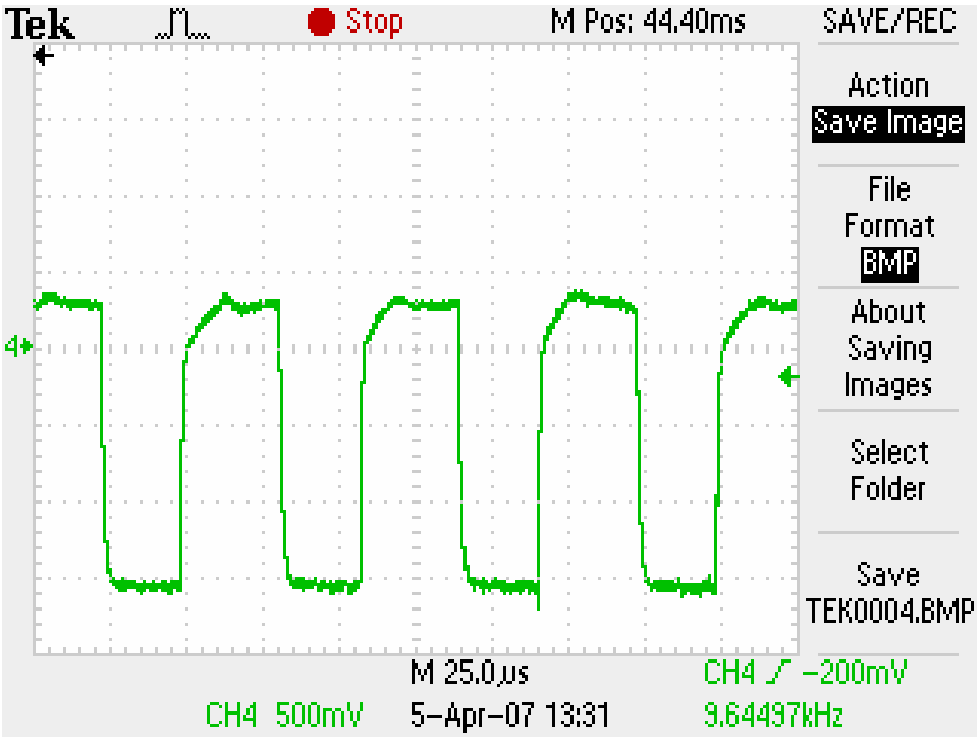

Fig. 23. Waveform of the bipolar bias voltage in the nitriding mode (50 V/div).

c. DLC film deposition.

In this mode, the source produces negative pulsed bias voltage with amplitude up to 500 V. The pulse repetition frequency is varied discretely in the range from 7 to 43 kHz. The source allows gradual adjustment of the voltage amplitude, pulse duration, and duty factor. Figure 24 shows a waveform of the bias voltage on the plasma load.

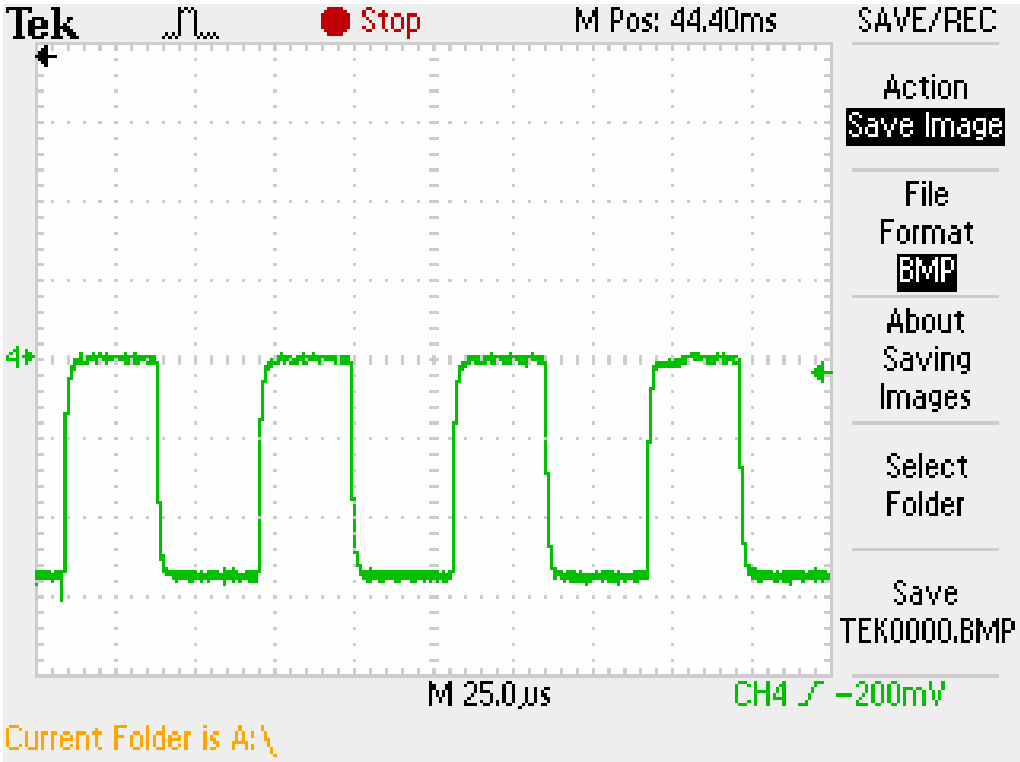

Fig.24. Waveform of the negative pulsed bias voltage in the DLC deposition mode (50 V/div).

d. Implantation.

In this mode, the source produces negative pulsed bias voltage with amplitude up to minus 20 kV and maximum current up to 1 A. The pulse repetition frequency is varied discretely in the range from 100 to 500 Hz. The pulse duration is variable between 5 and 40 µs. The source allows gradual adjustment of the voltage amplitude. Figure 25 shows waveforms of the bias voltage and ion current during the operation into the plasma load.

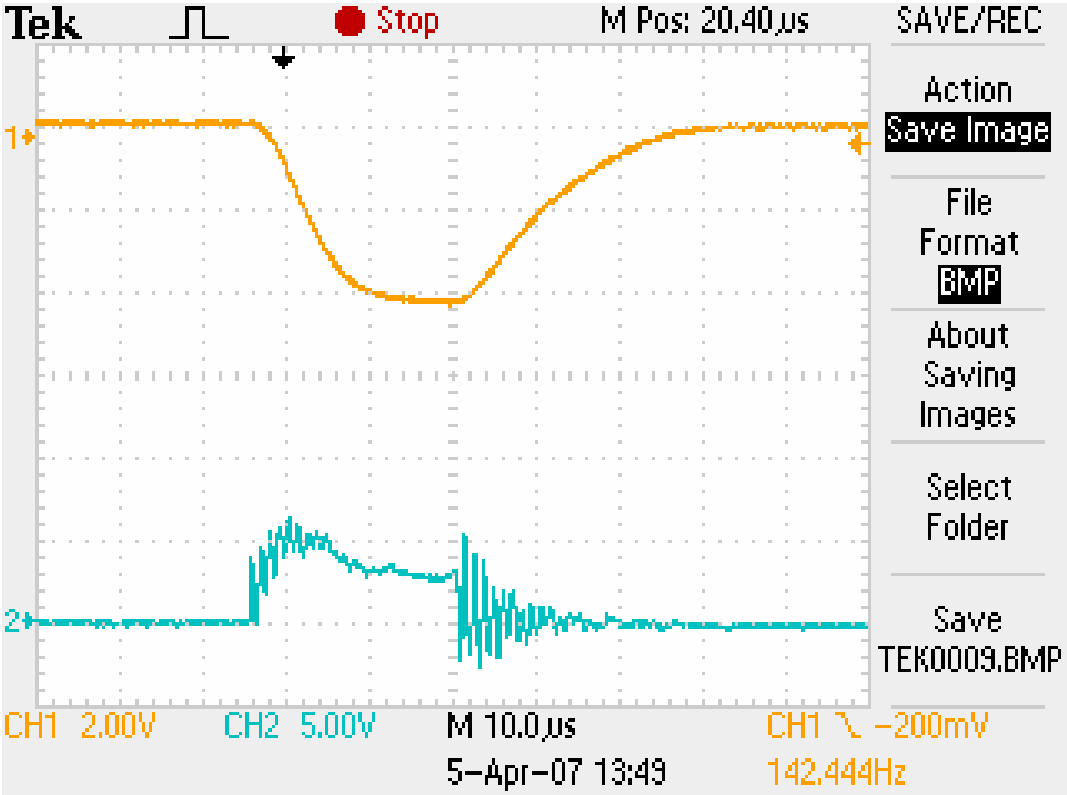

Fig.25. Waveforms of the bias voltage (the upper trace, 10 kV/div) and ion current (the lower trace, 1 A/div) in the implantation mode.

2.2. Conclusion.

In order that the lifetime of the discharge system is maintained, inert gas (argon) should be filled to the cathode cavity of the emitter discharge (the first discharge cell) and hydrocarbon directly to the vacuum chamber. Thus, the presence of hydrocarbon (e.g., acetylene) changes the parameters of the main discharge only (the discharge current, the plasma density). For the ionization degree to be increased, the additional gas feeding must takes place in the immediate vicinity of the emission aperture in the cathode of the main discharge.

Life tests of the plasma source operated with acetylene show that soot settled on the anode of the main discharge decreases the main discharge current and the plasma density by 10 % and 5 %, respectively. This problem is solvable in part by using an insulated anode plate heated by the electron current to high temperature. It

should be noted that this method is inapplicable to the cathode of the main discharge, since the required power at the cathode surface proves to be unattainable at the ion current density in question. At the same time, cleaning of the cathode surface through Ar-ion bombardment is ineffective, because the deposition rate of dielectric films is more than two times greater than the sputtering rate. Apparently, the time between routine maintenances of the main discharge cathode, in this case, is reduced and will be determined by the hydrocarbon flow rates during the DLC film disposition, which is one of the objectives of the next stage of research.

The designed prototype of the bias voltage source will make it possible to realize the scheduled experimental research at milestone 3. The preliminary experiments allowed us to determine the parameters and the circuit of the new bias source to be delivered to Phygen Inc.

III. EXPERIMENTAL RESEARCH ON DLC DEPOSITION

3.1. Experimental setup and procedure.

The experimental setup for DLC film deposition is shown schematically in Fig. 26.

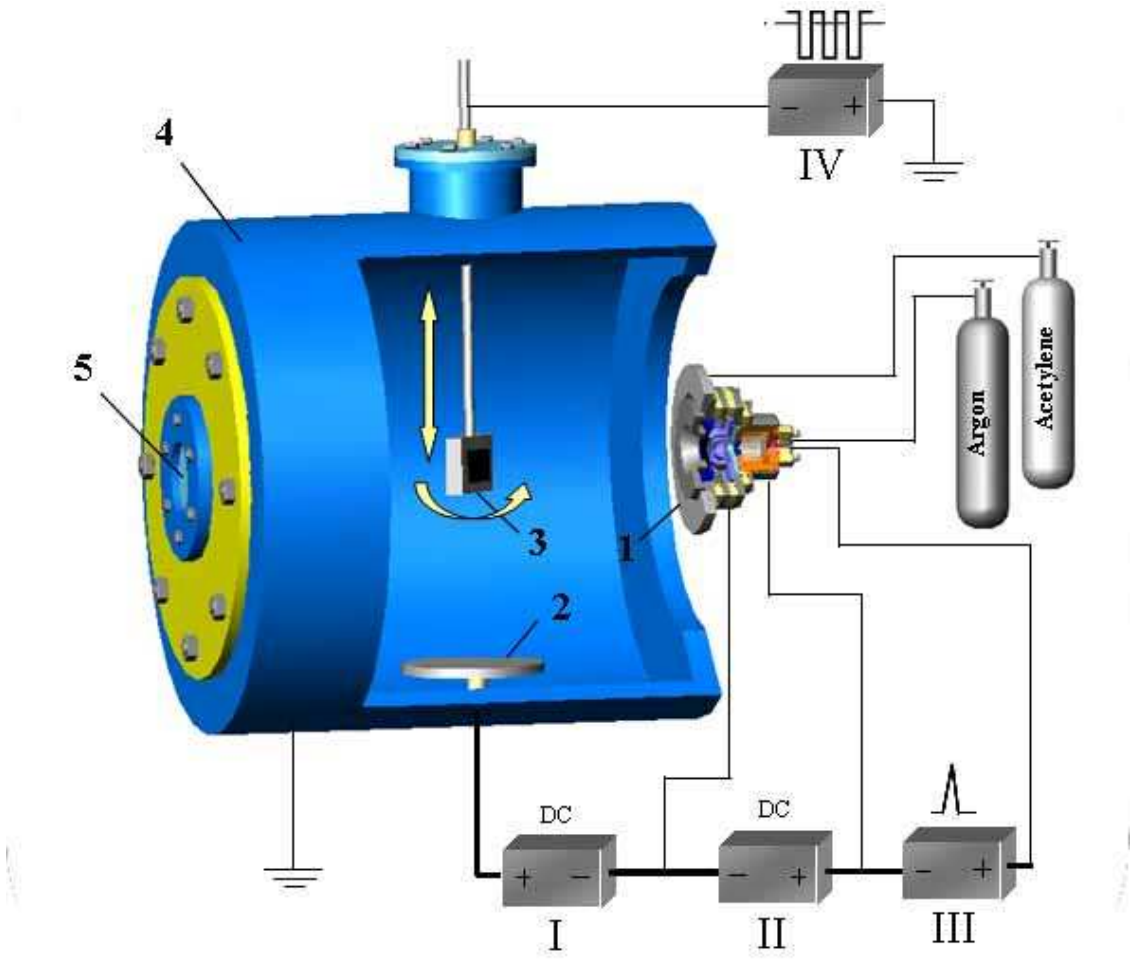

Fig.26. Scheme of experimental setup.

Plasma generator *1* was located on the face of vacuum chamber *4* of volume 1 m^3. At the bottom of the vacuum chamber, there was stainless steel anode *2* of the main discharge. The area of the anode *2* was 150 cm^2. Window *5* was used for visual observation and infrared measurement of the specimen temperature. DLC films were deposited on structural black steel, stainless steel, and high-speed steel. Before deposition, the specimen surface was mechanically polished with diamond paste and wiped with ethyl alcohol. The specimens were placed on movable holder

3 at the center of the chamber. The area of the specimens was 2÷4 cm^2 and that of the holder was ~100 cm^2. Voltage from power supply IV was applied to the specimens. Power supplies I-III were used to power the discharges. The plasma density was measured using a plane Langmuir probe with a guard ring and a collecting surface of area 5 cm^2. The probe was arranged 10 cm away from the specimen holder.

For increasing the lifetime of the cathode grid of the main discharge, the operating current of the emitter discharge was decreased down to 10÷15 A. The voltage of the main discharge was 100 V. The flow rate of argon to the cathode cavity of the plasma generator was 30÷35 sccm. The flow rate of acetylene to the chamber was varied between 10 and 30 sccm. Methane and a propane-butane mixture were also used as hydrocarbon gases, but preference was given to acetylene because it provides higher deposition rate, compared to that of the above gases.

The hardness and the elastic modulus of the DLC film surface layer were studied with a NanoTest 600 nanoindenter (MicroMaterials, Great Britain). The maximum load on the Berkowich diamond indenter (a trihedral pyramid) was 200 mN. The final hardness and elastic modulus were found by averaging the results of ten measurements. The penetration depth of the indenter into the coating versus the applied force was analyzed by the Oliver and Phar method [37].

The hardness H was calculated from the expression:

$$H = P_{max} / A \qquad (1)$$

where P_{max} is the maximum applied load and A is the indenter – specimen contact area.

The indenter – specimen contact area was calculated form the expression:

$$A = 24.5h_c^2 + C_1 h_c \qquad (2)$$

where C_1 = 1.65 10-6 and is a constant descriptive of deviation from the ideal geometry of the Berkowich pyramid due to rounding edges.

The value of h_c was determined from the expression:

$$h_c = h_{max} - 0.75\, P_{max}/S \qquad (3)$$

where h_c is the penetration depth of the indenter into a specimen, h_{max} is the maximum penetration depth of the indenter, and S is the contact stiffness of the material.

Before film deposition, the specimen surface was subjected to ion cleaning in the Ar plasma. In so doing, a negative dc bias voltage of -200÷500 V was applied to the specimen for 5÷15 min.

The experiments show that the use of only low negative pulsed bias voltage (to -600 V, 5÷50 kHz) precludes the formation of amorphous DLC films on the metal surface. Within a few minute after deposition, the DLC films were fully separated from the specimen surface (Fig. 27).

Fig. 27. Films deposited on the SS surface in the low-voltage mode.

Our previous review of relevant publications suggests that the formation of hard adhesive DLC films on the metal surface requires application of high negative bias voltage of -(10÷20) kV [38-40].

However, our experiments on DLC film deposition with high negative bias voltage repeatedly revealed clear-cut regions where the film thickness was much smaller than that on the rest of the surface or was entirely absent (Fig. 28). The effect was observed no matter what the holder temperature and spatial orientation and the specimen temperature and material.

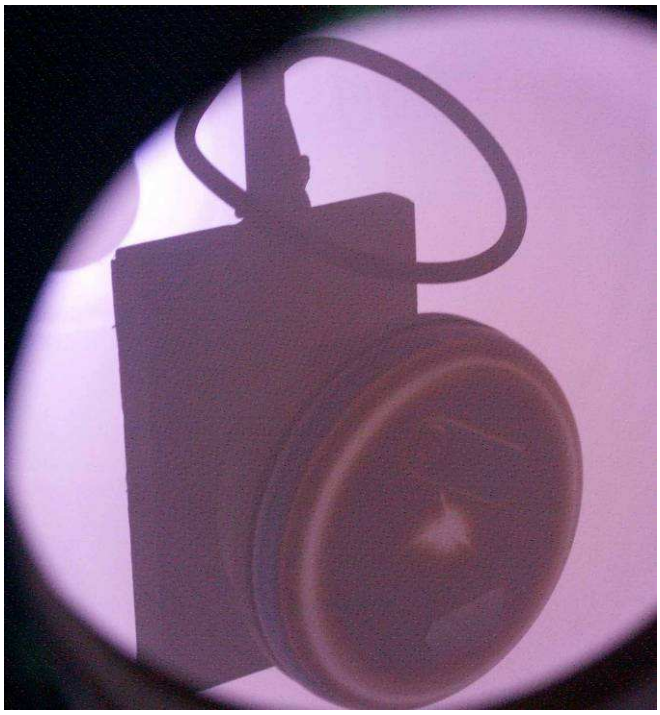

Fig. 28. Surface nonuniformity of the films deposited in the high-voltage mode.

The surface irregularity is attributable to sputtering of the films due to ion focusing in the near-electrode layer. Actually, with a negative bias voltage of -(200÷500) V, the ion layer thickness for the above plasma density is no greater than 1 cm, i.e., much smaller than the holder diameter, whereas with negative bias voltage of –(10÷20) kV, the layer thickness becomes comparable with the diameter of the specimen holder. Since the expanding layer tends to assume a spherical shape and, at $1 \cdot 10^{-1}$ Pa, the layer can be considered collisionless, regions of more intense ion bombardment where sputtering dominates over deposition appear at the holder center and rounding edges (Fig. 29,a). This supposition is indirectly supported by the distinct diminution of the inhomogeneous region with increasing the operating pressure, e.g., to $5 \cdot 10^{-1}$ Pa. In this case, the free path of ions (~2÷3 cm) becomes smaller than the near-electrode layer thickness (~7÷12 cm).

To eliminate the effect, a ring protruding 2 cm above the holder level was arranged at the holder periphery (Fig. 29,b).

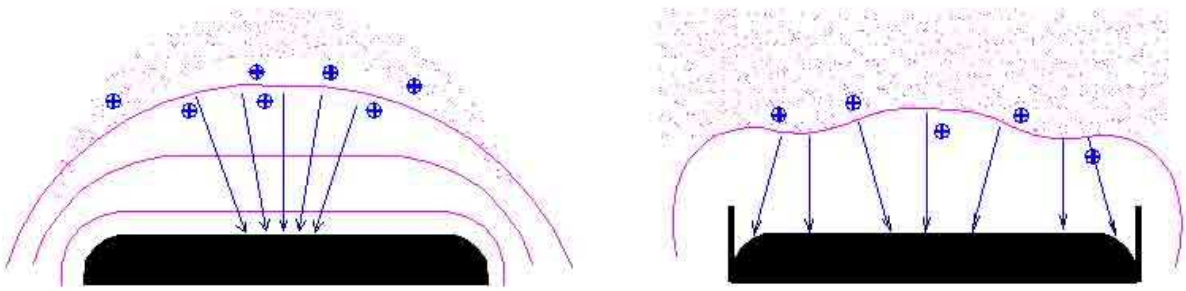

а б

Fig. 29. Influence of the specimen shape on the near-electrode layer.

In further experiments, such design of the holder allowed uniform DLC film deposition on the specimens region.

3.2. Deposition of DLC films on stainless steel specimens.

3.2.1. Friction coefficient of DLC films.

The parameters of DLC film deposition on SS specimens are indicated in Table 1.

Table 1. Parameters of DLC film deposition on SS specimens.

Current of the emitter discharge	12 A
Voltage of the main discharge	100 V
Current of the main discharge	8 A
Plasma density	$1.6 \cdot 10^{10}$ cm^{-3}
Flow rate of argon	35 sccm
Flow rate of acetylene	25 sccm
Amplitude of negative bias voltage	-10, -15, -20 kV
Full pulsewidth	50 μs
Pulse repetition frequency	500 Hz
Deposition time	15 min.

Photos of the specimens with DLC coatings are shown in Fig. 30. The friction coefficient of the DLC films was measured with a high-temperature tribometer (CSEM Instruments, Switzerland). Since high-speed steel is difficult to shape for tribological tests, SS specimens were used to measure the friction coefficients of the films. The surface of all specimens was polished in one cycle. A ∅3 mm tribological WC-8 (tungsten carbide) ball traveled around a circle of radius 5 mm with a linear velocity of 10 cm/s under 1 N load. The total track was 100 m long. First, we measured the friction coefficient of the initial specimens (without DLC films). Figure 31 shows the measured friction coefficients for the initial specimens. The friction coefficient was about 0.92. The friction coefficients measured for the specimens with DLC films are shown in Figs. 32-34.

Fig. 30. Specimens for tribological measurements:
without film (1), U_{bias} = -10 kV (2), U_{bias} = -15 kV (3), U_{bias} = -20 kV (4).

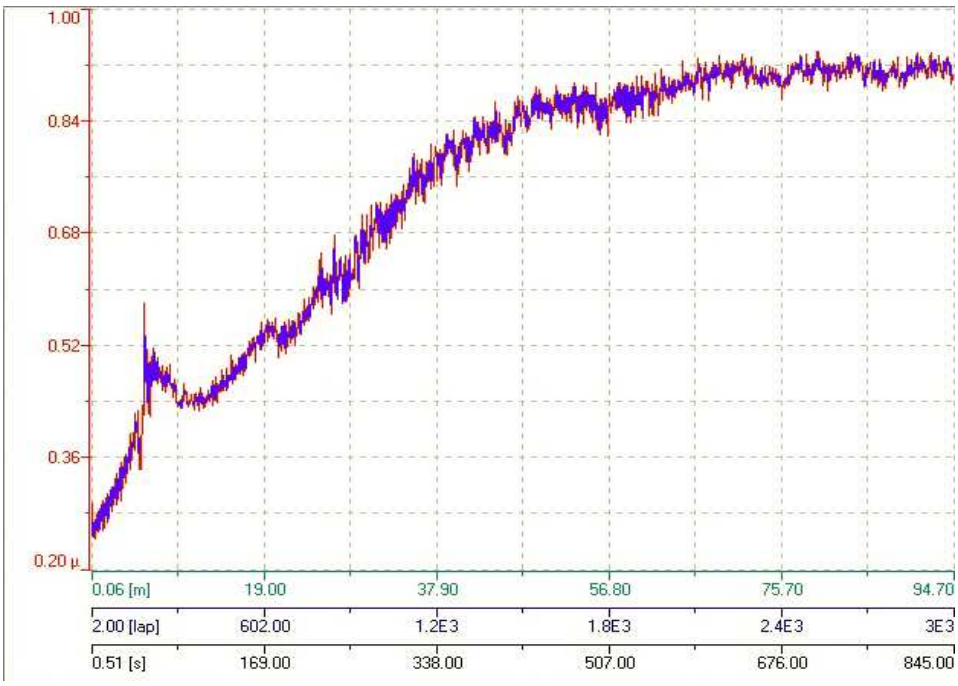

Fig. 31. Friction coefficient of the initial SS specimen without DLC film.

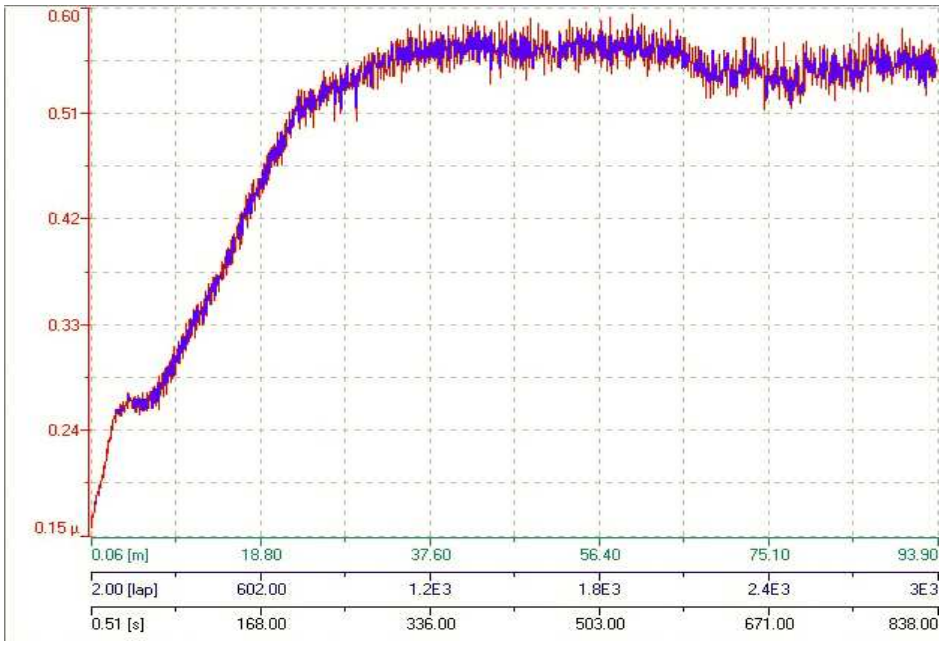

Fig. 32. Friction coefficient of the SS specimen with DLC film.

U_{bias} = -10 kV.

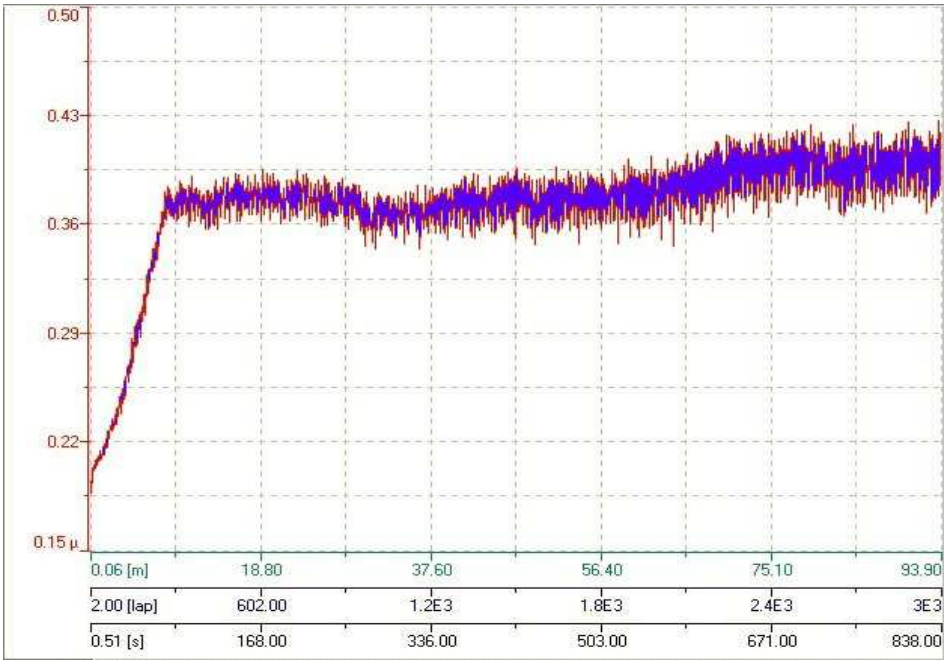

Fig. 33. Friction coefficient of the SS specimen with DLC film.

U_{bias} = -15 kV.

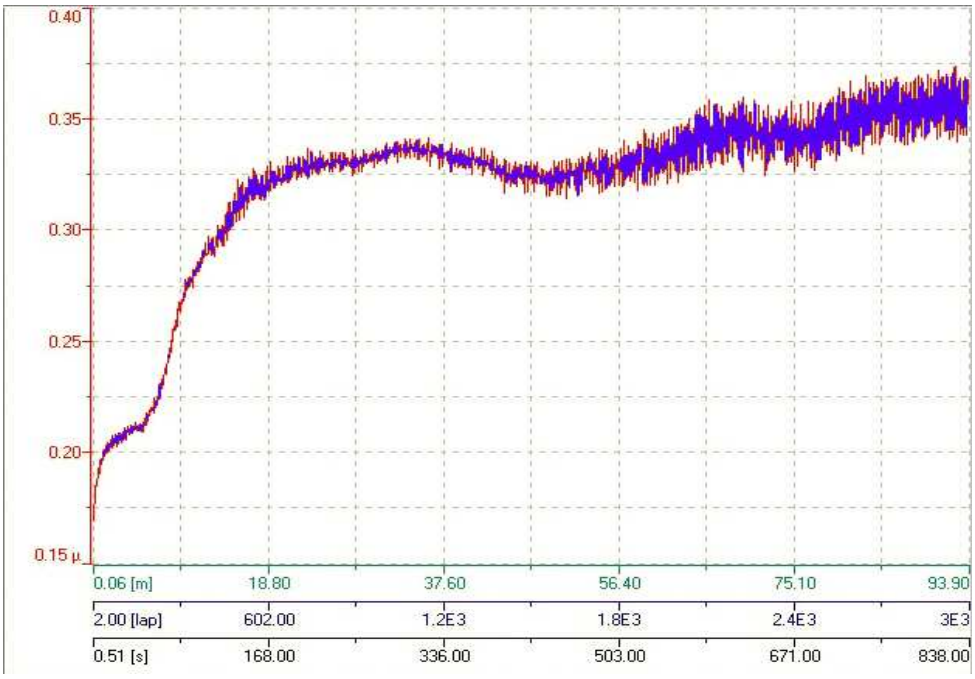

Fig. 34. Friction coefficient of the SS specimen with DLC film.

U_{bias} = -20 kV.

The plots suggest that the DLC film deposition leads to at least a double decrease in the friction coefficient of the SS specimen. Increasing the amplitude of negative bias voltage decreases the friction coefficient. However, it should be noted that the difference in friction coefficient for amplitudes of bias voltage -15 and -20 kV is insignificant.

3.2.2. Microrelief of DLC film surfaces.

The microrelief of DLC film surfaces was examined using a Solver P47 atomic-force microscope (NT-MDT, Russia). Images of the surfaces were taken in the contact mode with the use of a CSC12 silicon cantilever (NT-MDT). We examined the SS specimens obtained with the parameters indicated in Table 1. The results of examination are shown in Figs. 35-38.

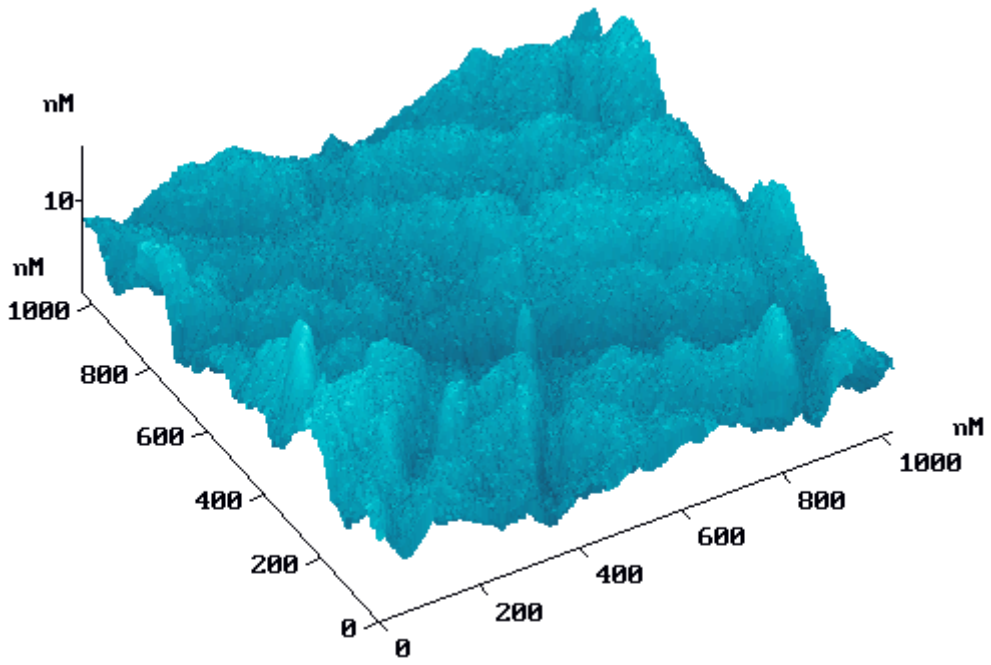

Fig. 35. AFM image of the SS surface without DLC film (Ra=1.9 nm, Rq = 2.4 nm).

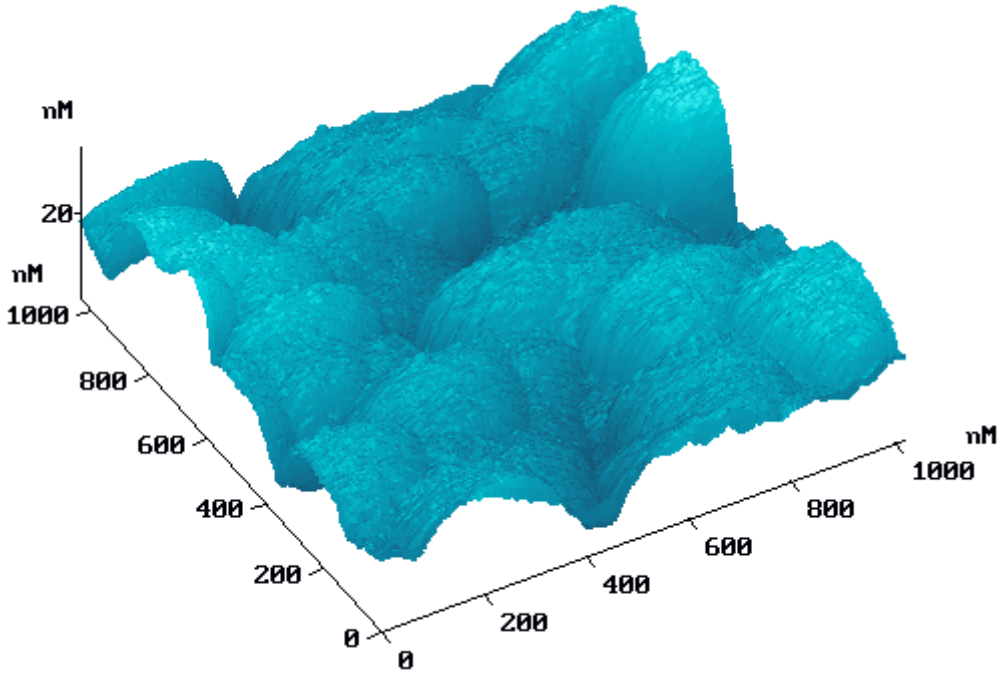

Fig. 36. AFM image of the SS surface with DLC film (U_{bias} = -10 kV). (Ra=4.8 nm, Rq = 6.2 nm).

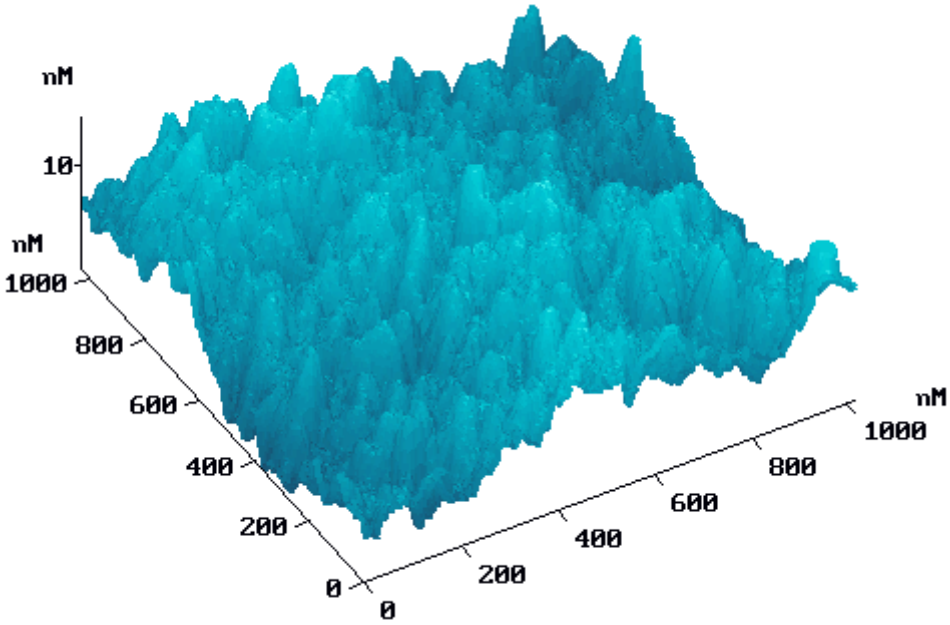

Fig. 37. AFM image of the SS surface with DLC film (U_{bias} = -15 kV). (Ra=2.0 nm, Rq = 2.5 nm).

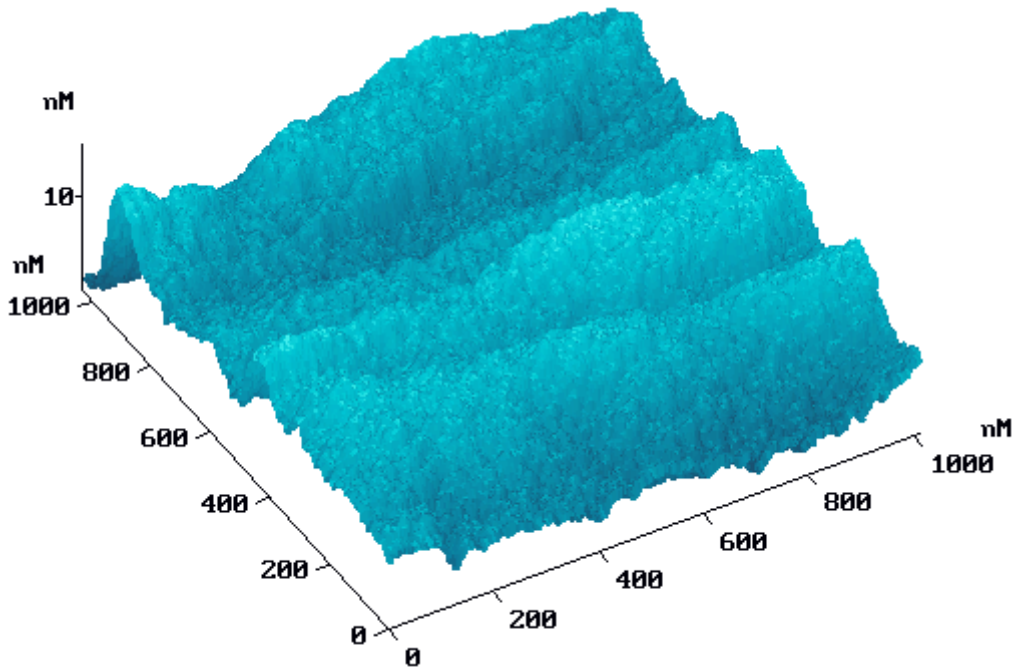

Fig. 38. AFM image of the SS surface with DLC film (U_{bias} = -20 kV). (Ra=2.1 nm, Rq = 2.6 nm).

The examination shows that the root-mean-square values of surface roughness for -15 and -20 kV (2.5 and 2.6 nm, respectively) are only moderately greater than those for the initial specimen (2.4 nm). At the same time, the specimens display lower friction coefficients due to the presence of the DLC film on the surface. Comparison of three specimens with DLC films shows that the coating obtained at U_{bias} = -10 kV features not only the greatest roughness (6.2), but also the highest friction coefficient (0.55).

3.2.3. Hardness of DLC films.

Figure 39 shows the measured hardness of the specimens shown in Fig. 30.

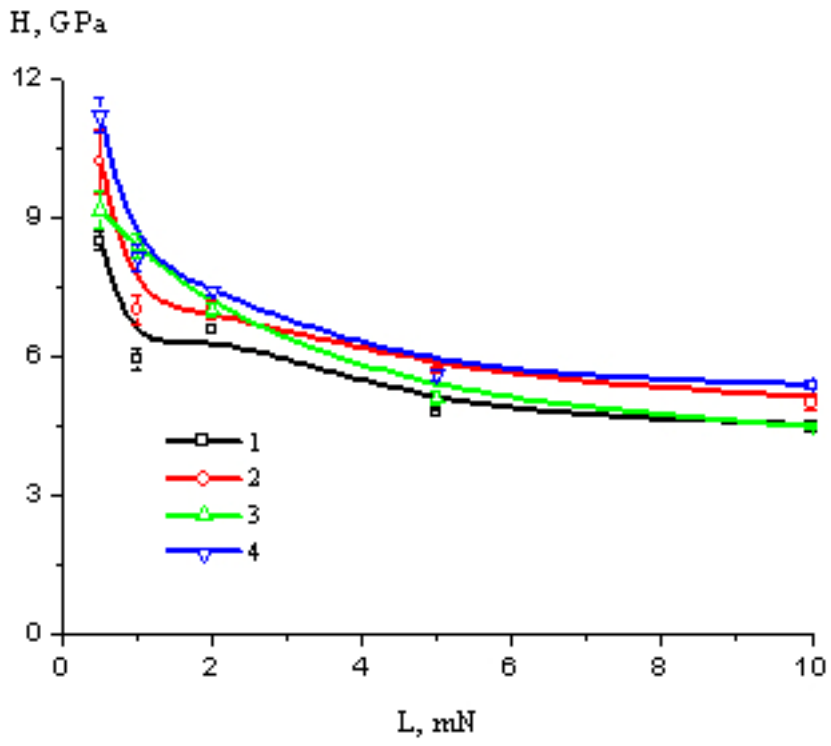

Fig. 39. Specimen hardness versus the applied load for SS specimens: without DLC film (1), U_{bias} = -10 kV (2), U_{bias} = -15 kV (3), U_{bias} = -20 kV (4).

Note that the typical SS steel hardness is 4÷5 GPa. The relatively high surface hardness (6÷8 GPa) of the initial SS specimen obtained in our experiments at small loads (0.5÷2 mN) are presumably associated with hardening of the specimen surface on polishing, but the actual specimen hardness shows up at loads greater than 5 mN. Thus, it can be concluded that DLC film deposition allows an increase in SS surface hardness by 5÷6 GPa. The elastic modulus of the deposited DLC film is 140÷180 GPa. It should be noted that the ratio of the hardness H to the elastic modulus E is about 0.1, which is typical of diamond-like films [41]. At the same time, attempts to find correlation between the coating hardness and the friction coefficient have not met with success. In [42], specimens of higher hardness display higher friction coefficients, whereas in [43] the situation is the reverse. Apparently,

peculiar properties of the coatings, e.g., the contents of sp^2 and sp^3 hybridization, are important in this case. .

Despite the relatively small hardness, these coatings can be used as wear-resistant coatings under low and average loads. Moreover, because of the sp^2 phase, the films feature low friction coefficients.

At high loads, “indentation” of the films may occur. From this standpoint, it makes sense to preliminary increase the surface hardness of metal, before deposition of DLC films. The surface hardness, e.g., of stainless steel, can be increased by plasma nitriding.

In experiments, the specimens were preliminary nitrided in two modes: with negative dc bias voltage (-800÷1000 V) and with low bipolar pulsed bias voltage (10÷30 kHz). In the bipolar mode, the amplitude of positive bias voltage was determined reasoning from the condition that provides the specimen temperature required for nitriding, by closing the electron current (up to 10 A) of the main discharge on the specimen. Negative bias voltage must preclude the formation of oxide film, which is an obstacle to nitrogen diffusion, on the specimen surface while precluding intense ion sputtering of the surface. Nitrogen was supplied to the vacuum chamber with a flow rate of 65 sccm. The flow rate of argon was 25 sccm. The pressure in the vacuum chamber was $(1\div7)\cdot10^{-1}$ Pa. The plasma density was about $2\cdot10^{10}$ cm^{-3}. The specimens were nitrided for 5 h and cooled in vacuum with nitrogen supply for 60 min.

The experiments show that both negative dc bias voltage and bipolar pulsed bias voltage (10÷30 kHz, +15/-250 V) provide the specimen temperature sufficient for nitriding (400÷500 °C). However, with bipolar bias voltage, ion sputtering of the surface was insignificant, and hence this mode is more attractive for technological applications. After nitriding in this mode, the surface hardness of the SS specimens reached 15÷17 GPa, whereas the initial hardness of these specimens was about 4÷5 GPa. The high hardness of the nitrided specimens, compared to the initial values, is presumably associated with a high Cr content (up to 18 %) of the steel and hence with a large fraction of hard CrN particles formed in the near-surface layer

during nitriding. The surface hardness and the elastic modulus of the DLC film on the SS specimen in relation to the load are shown in Fig. 40.

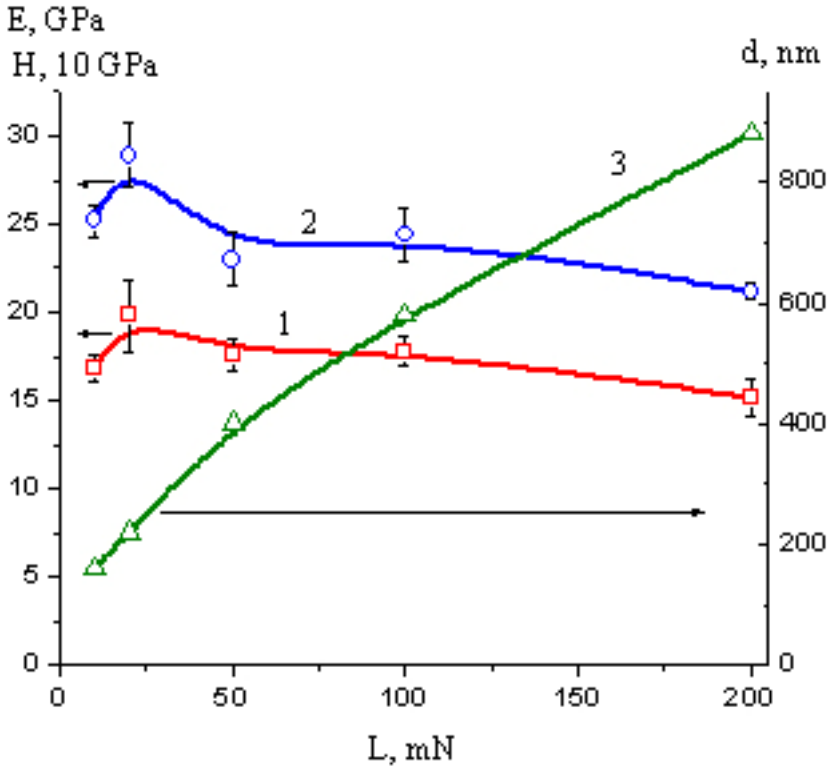

Fig. 40. Hardness (1), elastic modulus (2), and nanoindenter penetration depth (3) versus the load for the SS specimen after bipolar nitriding.

After bipolar nitriding, DLC film was deposited on the specimen. The main parameters of DLC film deposition are indicated in Table 2.

Table 2. Parameters of DLC film deposition on the SS specimen.

Current of the emitter discharge	15 A
Voltage of the main discharge	100 V
Current of the main discharge	12 A
Plasma density	$1.3 \cdot 10^{10}$ cm^{-3}
Flow rate of argon	30 sccm
Flow rate of acetylene	15 sccm

Amplitude of negative bias voltage	10 kV
Full pulsewidth Pulse repetition frequency	30 μs 400 Hz
Deposition time	30 min

Figure 41 shows the specimen after deposition of DLC film. The hardness and the elastic modulus measured after deposition are shown in Fig. 42. The plots in Figs. 40 and 42 suggest that the hardness of the deposited DLC film is comparable, within the measurement error, with that of the nitrided layer and is about 15÷17 GPa.

Fig. 41. DLC film on the nitrided SS surface. (During the deposition, the upper corner of the specimen was shielded).

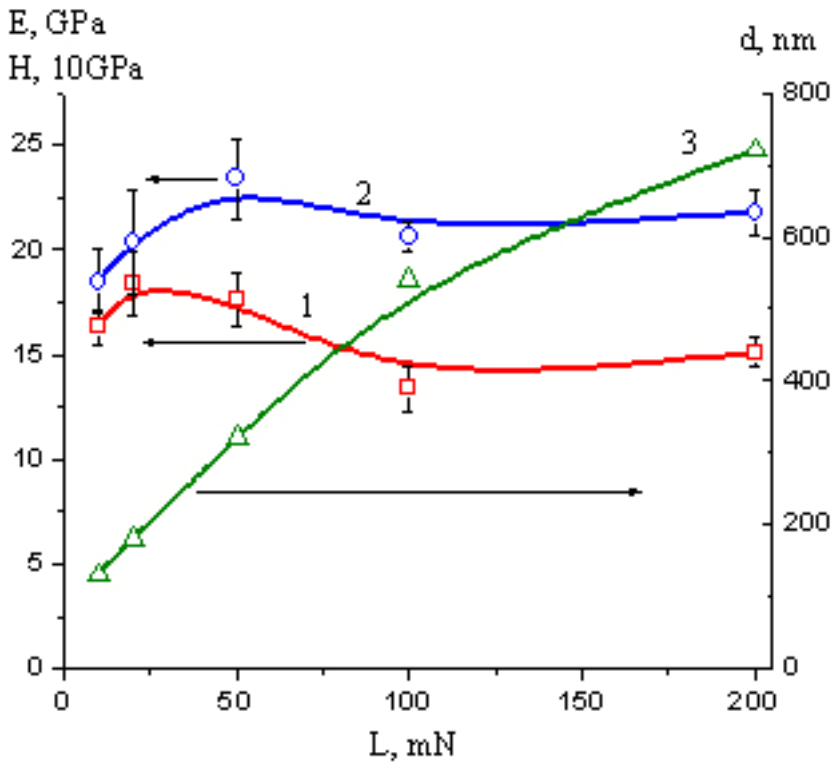

Fig. 42. Hardness (1), elastic modulus (2), and nanoindenter penetration depth (3) versus the load for the nitrided SS specimen after DLC film deposition.

Despite the significant increase in surface layer hardness, compared to the initial value, this mode of nitriding has the shortcoming of a long time it takes for the specimen to be heated to ensure efficient nitrogen diffusion deep into the material. A possible alternative way of increasing the SS surface hardness and reducing the process time is implantation from the surrounding N_2-containing plasma. The main parameters of implantation are indicated in Table 3.

Table 3. Parameters of implantation for the SS specimen.

Current of the emitter discharge	15 A
Voltage of the main discharge	100 V
Current of the main discharge	12 A
Plasma density	$2 \cdot 10^{10}$ cm^{-3}
Flow rate of argon	30 sccm
Flow rate of nitrogen	30 sccm
Amplitude of negative bias voltage	15 kV
Full pulse width	40 μs
Pulse repetition frequency	400 Hz
Implantation time	60 min

The specimen was cooled in vacuum with nitrogen supply for 60 min. The measured hardness and elastic modulus of the obtained specimen are shown in Fig. 43.

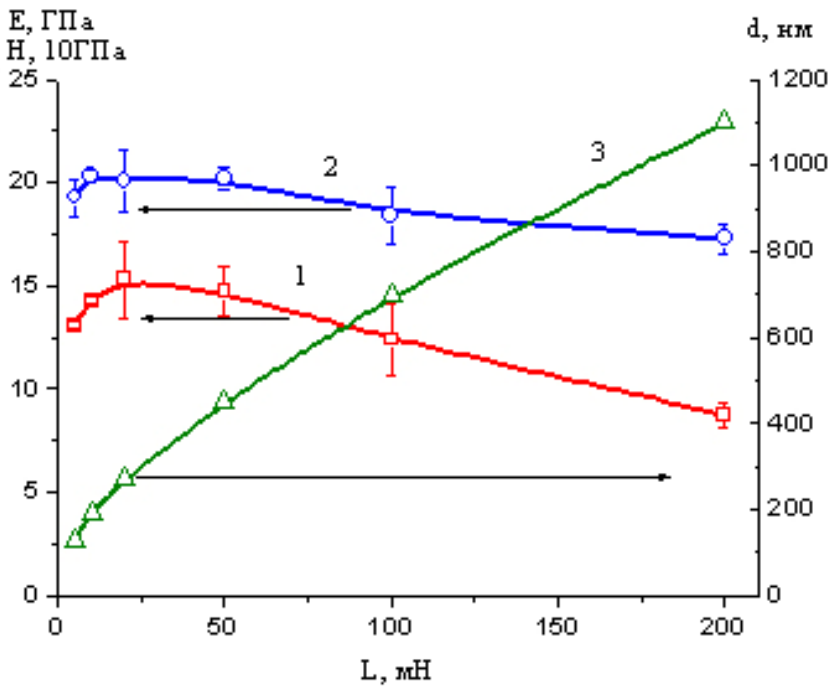

Fig. 43. Hardness (1), elastic modulus (2), and nanoindenter penetration depth (3) versus the load for the N^+-implanted SS specimen.

Although the hardness in this case is smaller than that in nitriding, this mode is quite applicable for increasing the surface hardness of SS-type steel before deposition of DLC film. The unquestionable advantage of the process is that the implantation time is only 1 h, as opposed to low-voltage nitriding that takes about 5 h.

3.3. Deposition of DLC film on high-speed steel specimens.

3.3.1. Hardness of DLC films.

The next series of experiments was performed on russian analog of high-speed steel - B6Mo5. The specimen dimensions were 2×2 cm^2. The chemical composition of this steel type is similar to that of the specimens supplied by Phygen (M-2). The measured hardness of the initial B6Mo5 and M-2 specimens is shown in Fig. 44.

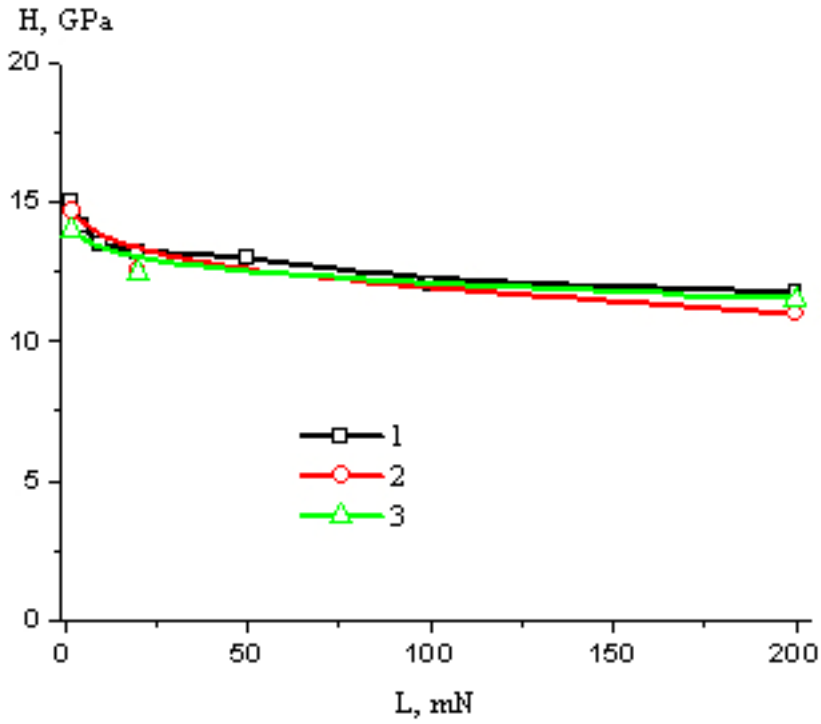

Fig. 44. Hardness versus the nanoindenter load for the initial M-2 (1) and B6Mo5 (2, 3) specimens.

It is seen from the figure that the properties of these steel types are very similar. Therefore, in experimental evaluation of the spatial homogeneity of the deposited films, preference was given to the B6Mo5 specimens for their larger geometrical dimensions.

The DLC film hardness of the initial and N-implanted specimens was investigated for three amplitudes of negative bias voltage -10, -15 and -20 kV. The time of preliminary ion cleaning was 15 min and the negative dc bias voltage applied was 500 V. The parameters of implantation are indicated in Table 4. The results of measurements of the specimen hardness after implantation are shown in Fig. 45.

Table 4. Parameters of implantation for the HSS specimen.

Current of the emitter discharge	11 A
Voltage of the main discharge	100 V
Current of the main discharge	7 A
Plasma density	$2.5 \cdot 10^{10}$ cm^{-3}
Flow rate of argon	25 sccm
Flow rate of nitrogen	25 sccm
Amplitude of negative bias voltage	14 kV
Full pulse width	40 μs
Pulse repetition frequency	500 Hz
Implantation time	60 min

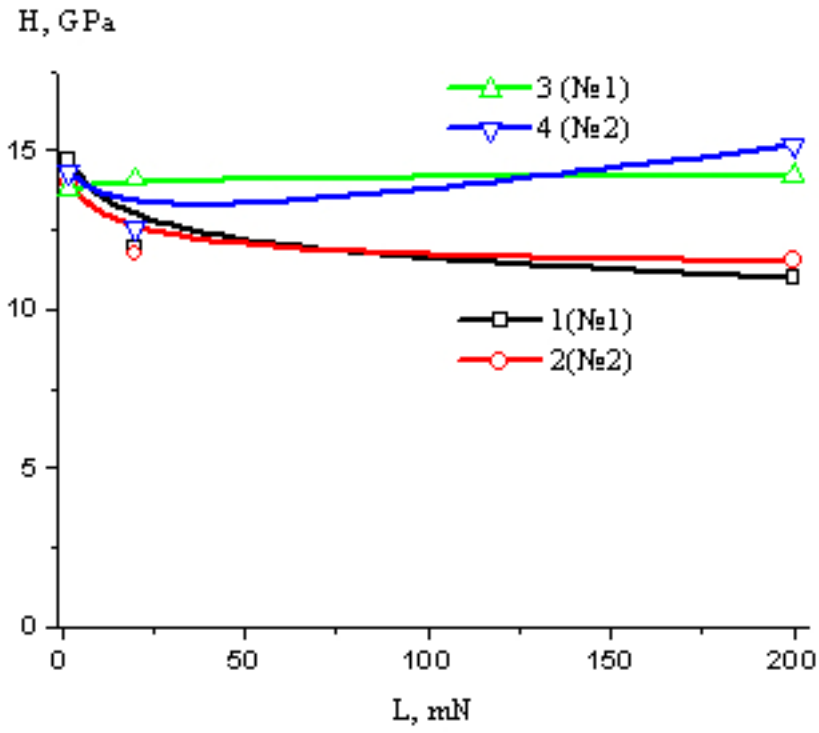

Fig. 45. Hardness versus the nanoindenter load for the initial (1,2) and implanted (3,4) HSS specimens.

The plots suggest that N^+-implantation does little to the hardness of the specimen surface as such. However, penetration of the nanoindenter to a depth of 1 μm at a load of 200 mN shows that the hardness of the N-implanted specimens remains the same and is about 14÷15 GPa, as opposed to that of the initial specimens. The parameters of DLC film deposition on the initial specimen surface are cited in Table 1. The outward appearance of the obtained specimens is shown in Fig. 46. The hardness of the obtained specimens is shown in Fig. 47.

Fig. 46. DLC film on the HSS specimen. Amplitude of negative bias voltage in DLC film deposition: -10 kV (1), -15 kV (2), -20 kV (3).

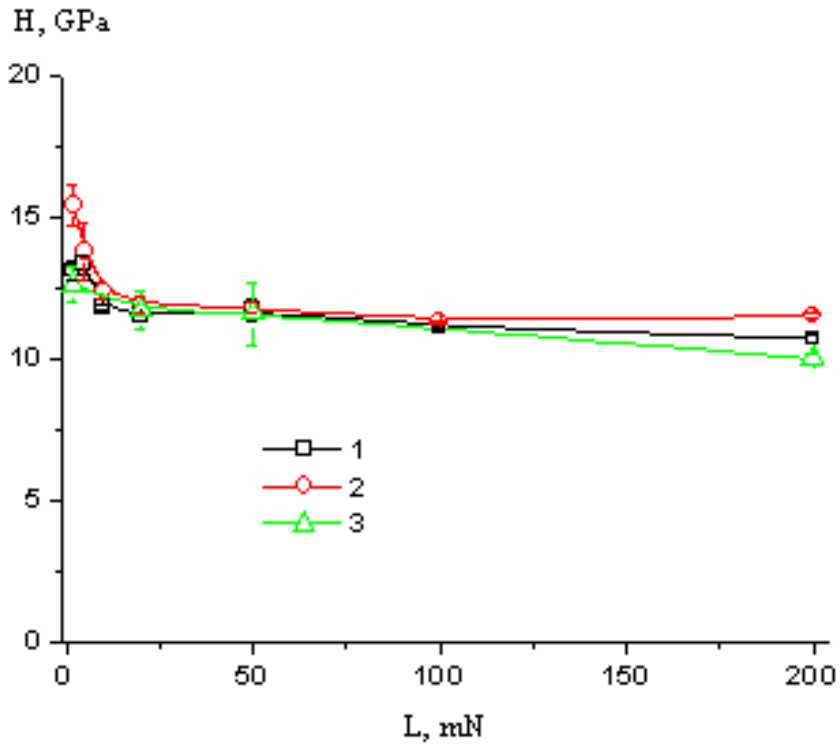

Fig. 47. Hardness versus the nanoindenter load for the untreated specimens with DLC films. Amplitude of negative bias voltage in DLC film deposition: -10 kV (1), -15 kV (2), -20 kV (3).

The deposition of DLC films on the preliminary N^+-implanted specimen surface was realized with parameters similar to those cited in Table 4. The obtained specimens are shown in Fig. 48. The measured hardness of the obtained specimens is shown in Fig. 49.

During the implantation, the specimen temperature can reach 250÷300 °C. Experiments show that before DLC film deposition on the preliminary implanted specimen surface, it is necessary to cool the specimens to a temperature less than 100-150 °C, otherwise no hard adhesive DLC film develops on the specimen surface.

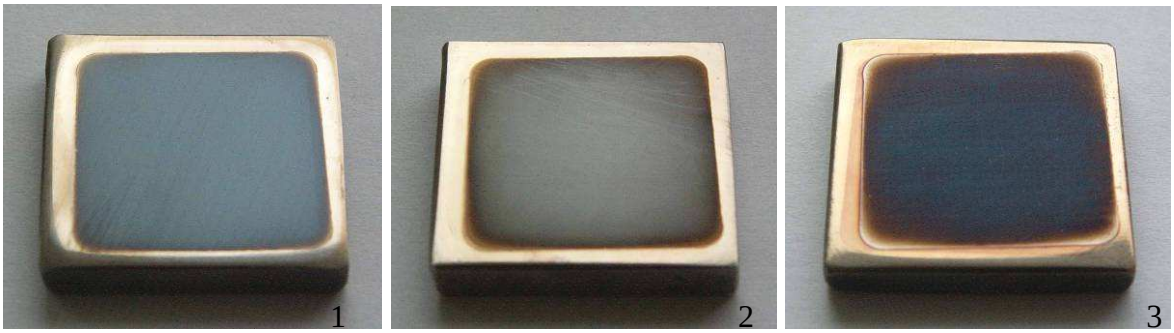

Fig. 48. DLC film on the preliminary N^+-implanted HSS specimen. The amplitude of negative bias voltage in DLC film deposition: -10 kV (1), -15 kV (2), -20 kV (3).

It follows from the dependences that the most significant increase in HSS specimens hardness is found in the case where DLC film is deposited on the preliminary implanted surface at the amplitude of negative bias voltage of -10 and -15 kV. The specimens obtained in this mode display a hardness of 16÷17 GPa which is a greater than the hardness of the initial specimen, of the DLC film on the initial specimen surface, and of the N-implanted specimen without DLC film.

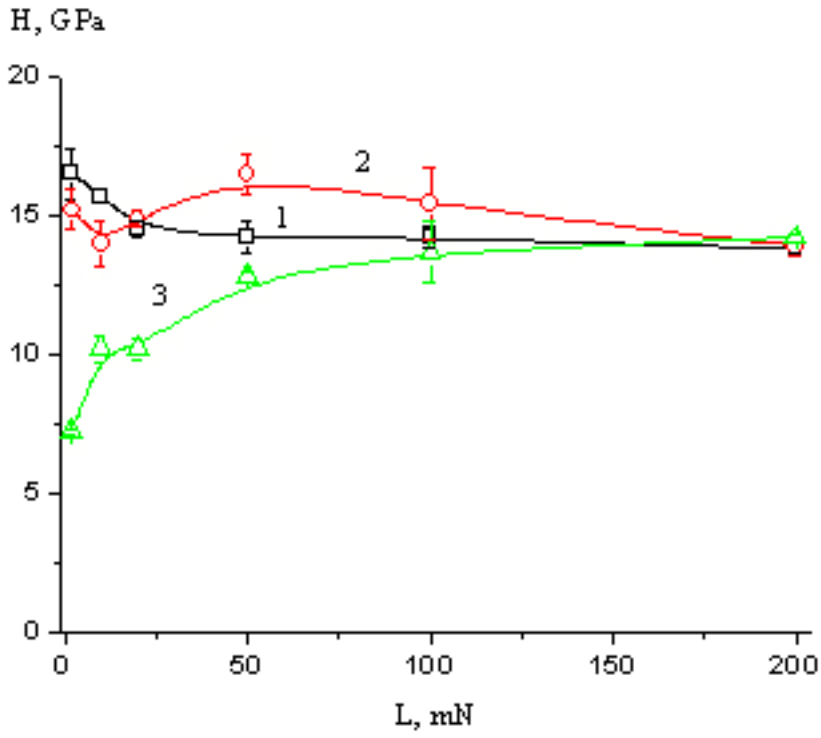

Fig. 49. Hardness versus the nanoindenter load for the implanted specimens with DLC films. Amplitude of negative bias voltage in DLC film deposition: -10 kV (1), -15 kV (2), -20 kV (3).

3.3.2. Adhesion of DLC films.

The adhesion of DLC films was measured on a so-called Sebastian machine by the normal detachment method. The Sebastian machine is a lever of the second order (Fig. 50). The contact plate area was 0.2 cm^2. The ultimate strength of contact adhesive for the “contact plate – clean metal surface” system was 180÷200 kg/cm^2. The adhesion of DLC films was studied on the HSS specimens. In the experiments, the specimens shown in Figs. 46 and 48 were used.

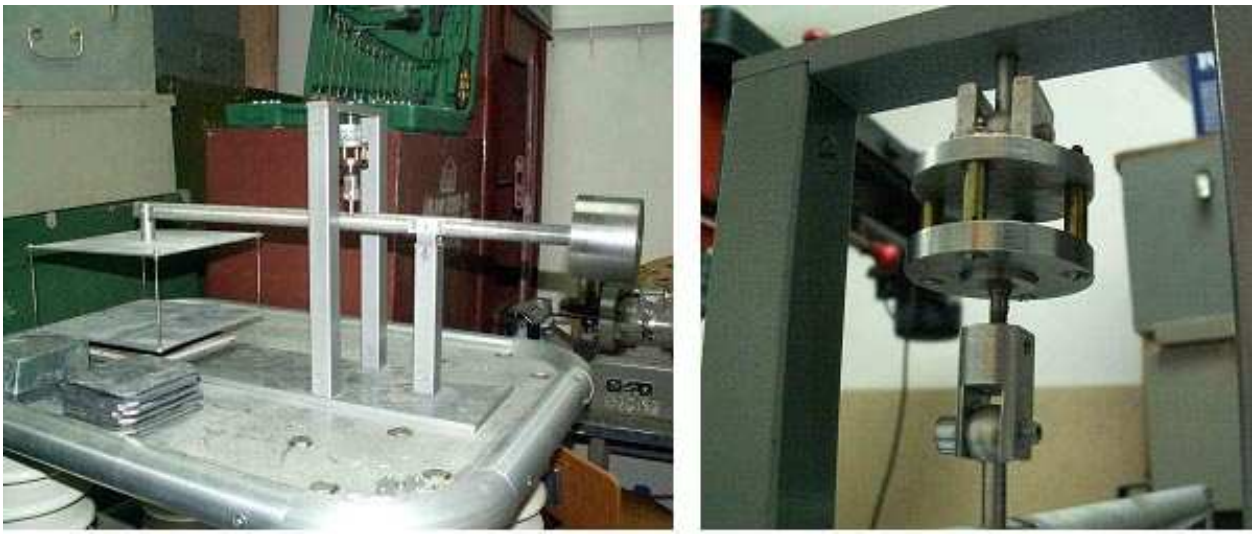

a b

Fig. 50. DLC film adhesion measured on the Sebastian machine: general view (a), specimen attach fitting (b).

The adhesion of each specimen was measured at three or four points. The average values at which the contact plate was broken away from the specimen surface were 150-180 kg/cm^2. In all cases, the separation occurred at the “contact plate-film” interface, and never at the “film – metal surface” interface (Fig. 51,a). The separation of the contact plate at small ultimate loads is presumably associated with low adhesion of the contact adhesive to the DLC film surface. It should be noted that corrosion of the DLC film by the contact adhesive escaped detection. A photo of the specimen surface on removal of the contact adhesive with acetone is shown in Fig. 51,b.

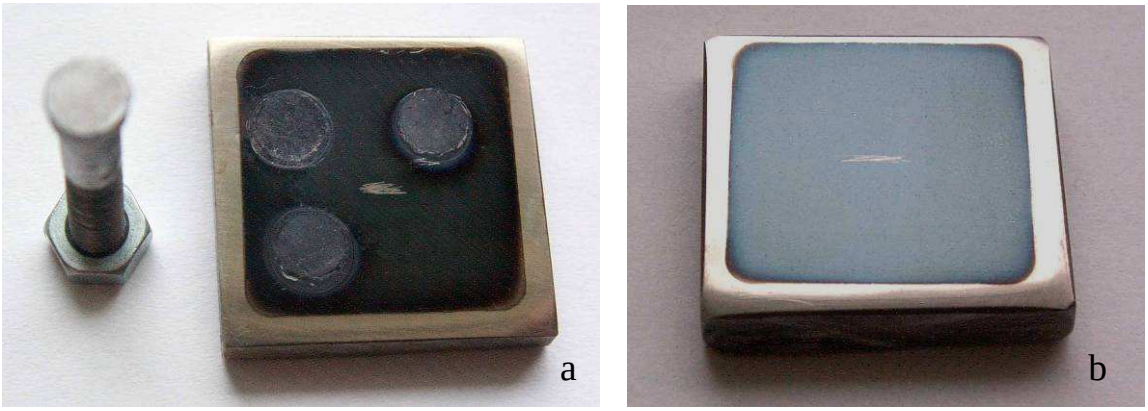

Fig. 51. Specimen after separation of the contact plate (a) and removal of the contact adhesive (b).

The obtained adhesion together with the low friction coefficients and high hardness allows using these films as protective coatings on drills for machining metals such as copper and aluminum [44].

3.4. Corrosion-resistance of DLC films.

In corrosion tests, the specimens with DLC coatings were exposed to sulfuric (H_2SO_4) and hydrochloric (HCl) acids and to a mixture of nitric and hydrochloric acids ($3HCl+HNO_3$), so-called aqua regia.

The attack by sulfuric and hydrochloric acids for 30 min did not reveal any distinction of the black steel and SS specimens with DLC coatings from the initial state, whereas the polished surface of the specimens without coatings starts to erode within a few minute of effect (Fig. 52).

Fig. 52. Specimens with and without DLC films attacked by concentrated sulfuric acids. The upper row – before the attack, the low row - after 30 min of effect.

After 10 min of effect by nitric and hydrochloric acids, the DLC film of the black steel specimens start to separate at the specimen periphery where the film interfaces the metal. After 20 min of effect, the specimen area with DLC coating was less than 50 %. After 20 min of attack by nitric and hydrochloric acids, separation of the DLC coating from the SS specimens was observed in a small periphery region of the specimen.

The HSS specimens effected by sulfuric acid and by a mixture of nitric and hydrochloric acids are shown in Figs 53 and 54. As in the previous case, the specimens without DLC coatings started to erode after 2÷3 min of effect by the acids. The specimens with DLC coatings revealed traces of erosion after 10÷15 min. The erosion centers were the specimen periphery at the film – metal interface and places where cracks were found.

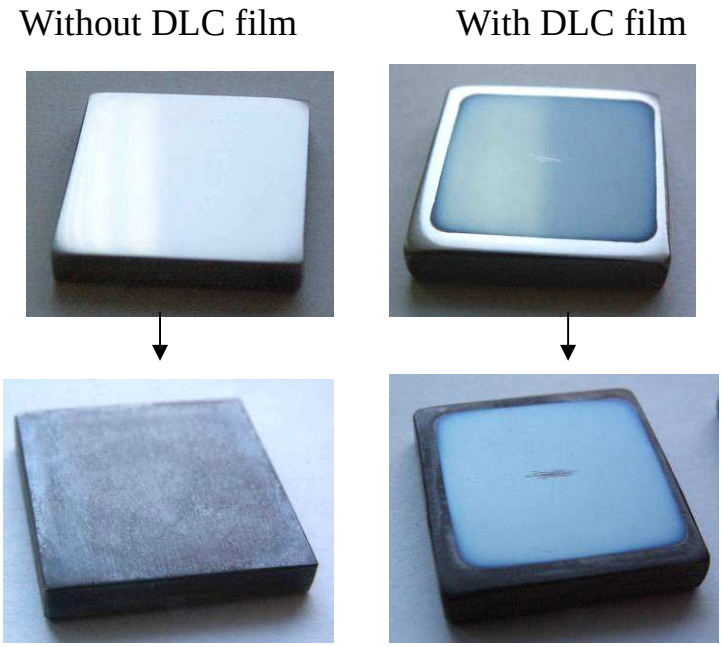

Fig. 53. Specimens with (at the left) and without (at the right) DLC coatings after attack by concentrated sulfuric acid. The upper row – before the attack, the low row – after 30 min of effect.

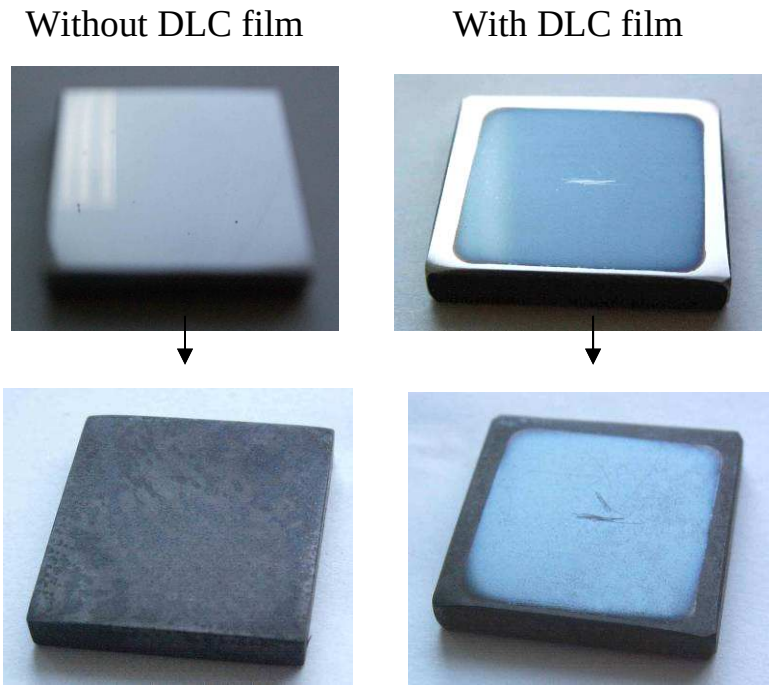

Fig. 54. Specimens with (at the left) and without (at the right) DLC coatings after attack by a mixture of nitric and hydrochloric acids ($3HCl+HNO_3$). The upper row – before the attack, the low row - after 15 min of effect.

Thus, the studies show that the deposition of DLC films allows an increase in corrosion resistance of materials three-five times, compared to the initial specimens without coatings.

3.5. Bias voltage source for electrical displacement of substrate.

Modular bias voltage source produces high and low pulsed bias voltage. The source is used for electrical displacement of substrates. The main parameters of the source are indicated in Table 5. A block diagram of the source is shown in Fig. 55.

Table 5 - Main parameters of the pulse bias power supply

Low-voltage mode	
Output voltage (negative), V	-(50 – 500)
Output voltage step, V	10
Output pulse repetition frequency, kHz	10 – 50
Frequency step, kHz	5
Output pulse duration (pulse ratio), %	20 – 80
Output current (determined by the load), A	0 – 5
High-voltage mode	
Output voltage (negative), kV	-(5 – 15)
Output voltage step, V	500
Output pulse repetition frequency, Hz	100 –1000
Frequency step, Hz	100
Output pulse duration, μs	5 – 15
Output current (determined by the load), A	0 – 30

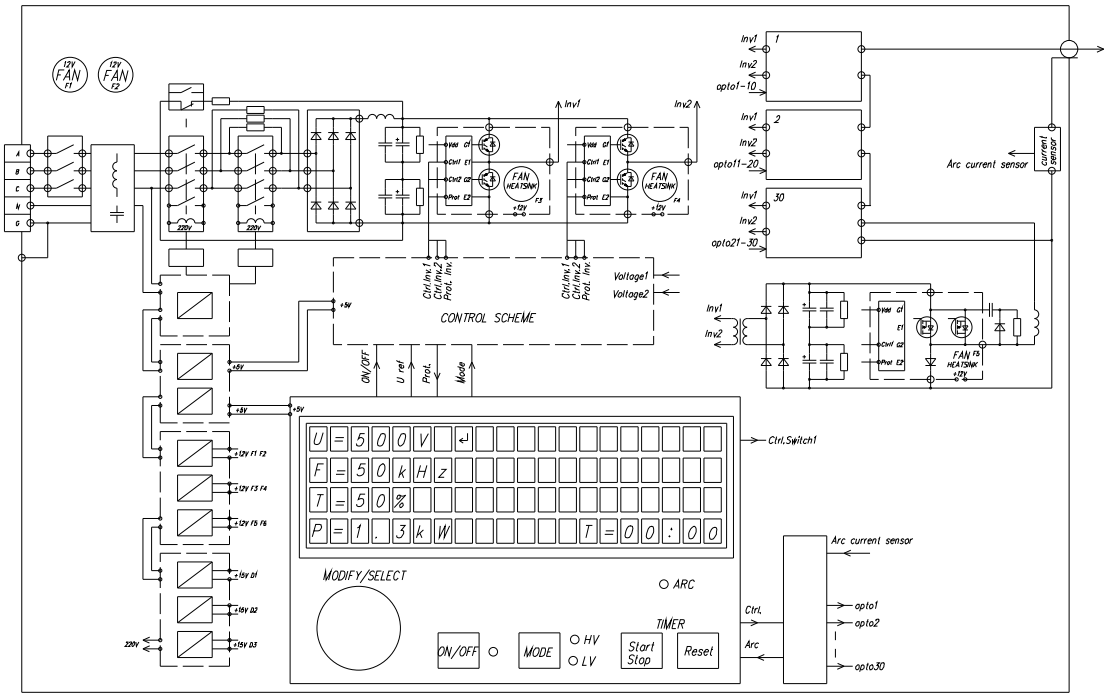

Fig. 55. Block diagram of the source for electrical displacement of substrates.

The source consists of the following main units.

1. Input rectifier is used to convert three-phase supply-line voltage to dc voltage.

2. High-frequency inverter is used to convert rectified voltage to controllable output voltage. The unit comprises a bridge-circuit inverter and a high-frequency transformer. The output voltage is controlled and stabilized by varying the control pulsewidth (pulsewidth modulation).

3. Control unit. The unit comprises a controller board and an inverter control board and controls all systems and communications with the operator.

4. Low-voltage output unit. The unit comprises a rectifier and an output force switch for breakdown and short circuit protections.

5. High-voltage output unit is used to produce output voltage pulses of amplitude from -500 V to -15 kV with a 500 V voltage step. The unit is 30 like cells, each with a stabilized voltage of 500 V at the output. A cell comprises a high-voltage transformer, a rectifier, and an output switch. In the unit, there is also an

output inductance, which specifies the risetime of the output voltage pulse, and shunting diodes for bypassing an inactive cell.

A cell of the high-voltage unit is controlled through an optical fiber independently of the control unit. The amplitude of each output voltage pulse is determined by the number of active cells. In the case of breakdown or shortcircuiting of the output, current protection operates in each active cell and the cells are turned off. Tests show that turn-off of a cell does not affect the protection of the rest of the cells, and hence all cells are turned off at a time that provides fast operation of breakdown protection.

This design has several advantages over traditional versions of high-voltage pulsed power supplies:

1) the absence of an output pulse transformer. This allows elimination of large transformer weight and dimensions, filling of the transformer with oil, demagnetizing of the core, etc.

2) the steep output pulse risetime. The pulse risetime is determined by the output choke in each cell and is independent of the number of active cells (i.e., of the pulse amplitude).

3) the output pulsewidth can take any value, up to direct current, which is impossible in transformer circuits.

4) the absence of parasitic oscillations, ringing, spikes of output voltage pulses.

5) no need for high-voltage or high-current (in the case of large transformation ratios) switches. The output switches and the output diodes in the cells are rated at the maximum output current and at the voltage of a stage (in this case, 500 V). Diodes and transistors (IGBT or MOSFET) with the above parameters are rather cheap and find wide application.

The only unit operating at high voltage is input transformers of the cells, and hence their insulation between the primary and secondary windings must hold the maximum output voltage. However, these transformers are low-power devices and each cell transmits only 1/30 of the total output power. Moreover, the operating

frequency of these transformers is tens of kilohertz (the operating frequency of the inventor). Thus, the transformers have small dimensions and it is not difficult to make winding insulation of the required strength for them. Furthermore, unlike output pulse transformers, input pulse transformers are more variable in pulse shape, which also simplifies their design.

The general view of the source with a partially removed front panel is shown in Fig. 56. Behind the front panel, modules, each containing 10 cells in a common shield, are located. Figure 57 shows a module with 10 cells and a high-voltage transformer. Figure 58 shows the printed circuit board with three cells.

The source is fully controlled from the front panel. The control panel is shown in Fig. 59. The load is connected to the high-voltage outlet in the upper cover of the case (not shown in the figure).

The overall dimensions of the case (without the removable high-voltage outlet) are the following: height 1625 mm, width 600 mm, depth 620 mm.

Fig. 56. General view of the source

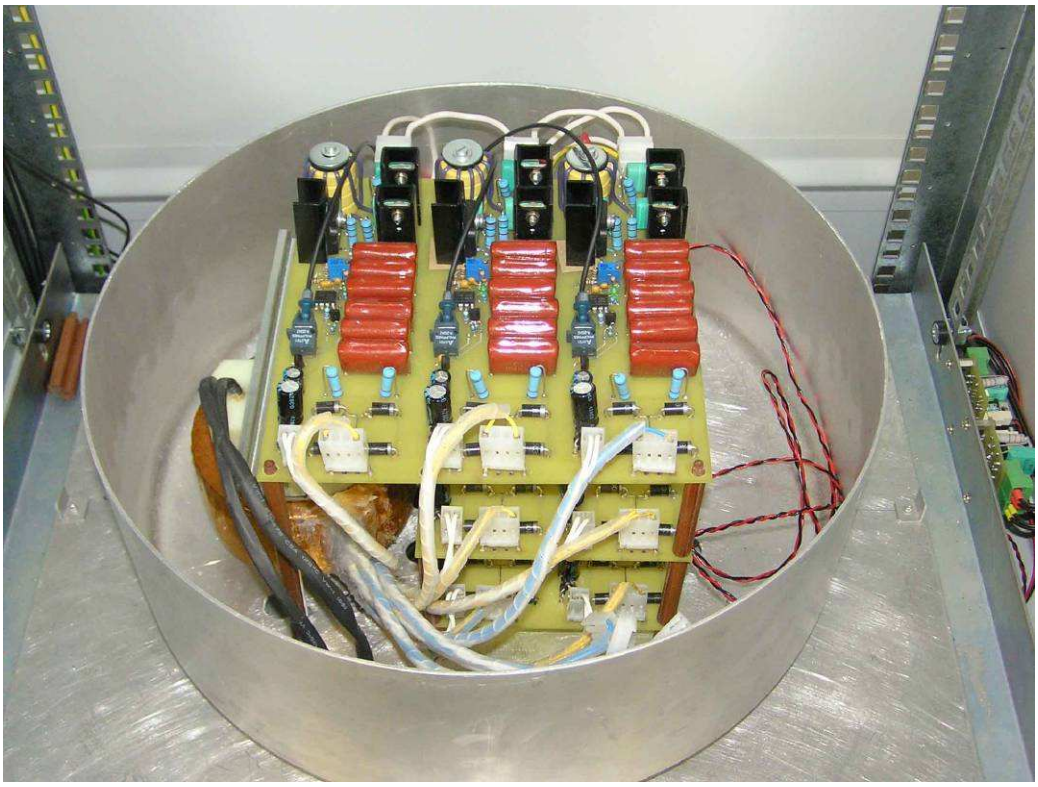

Fig. 57. Assembly of 10 cells (a module) in a shield (the upper part of the shield is removed).

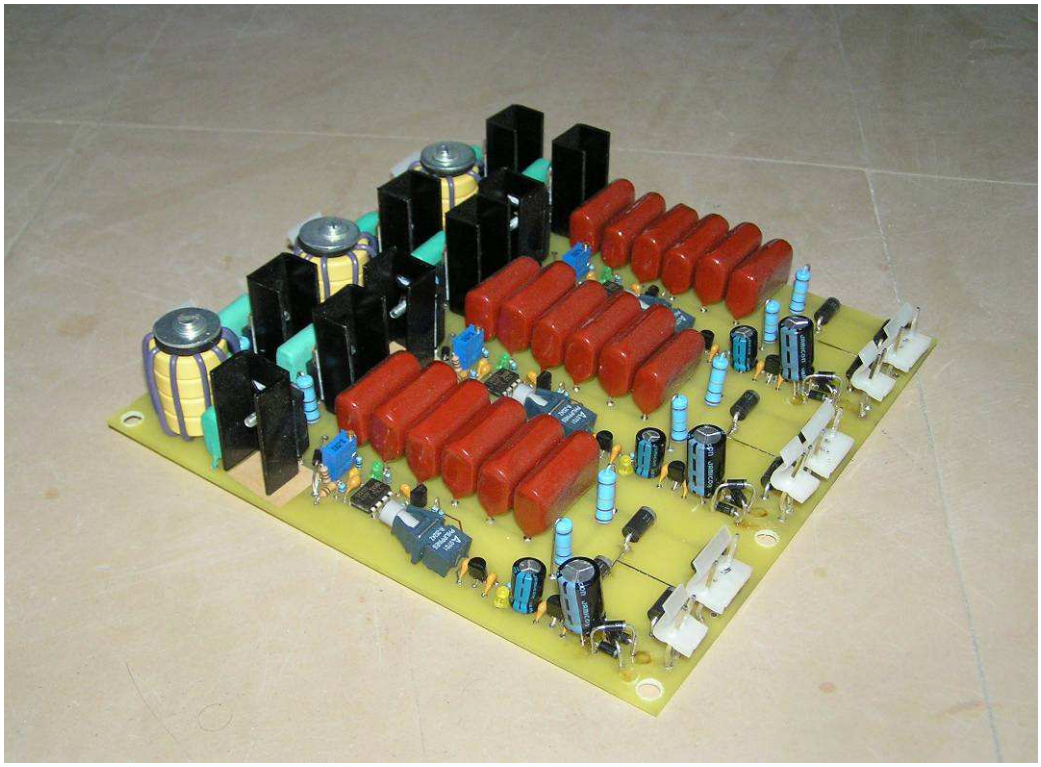

Fig. 58. Printed circuit board with three cells.

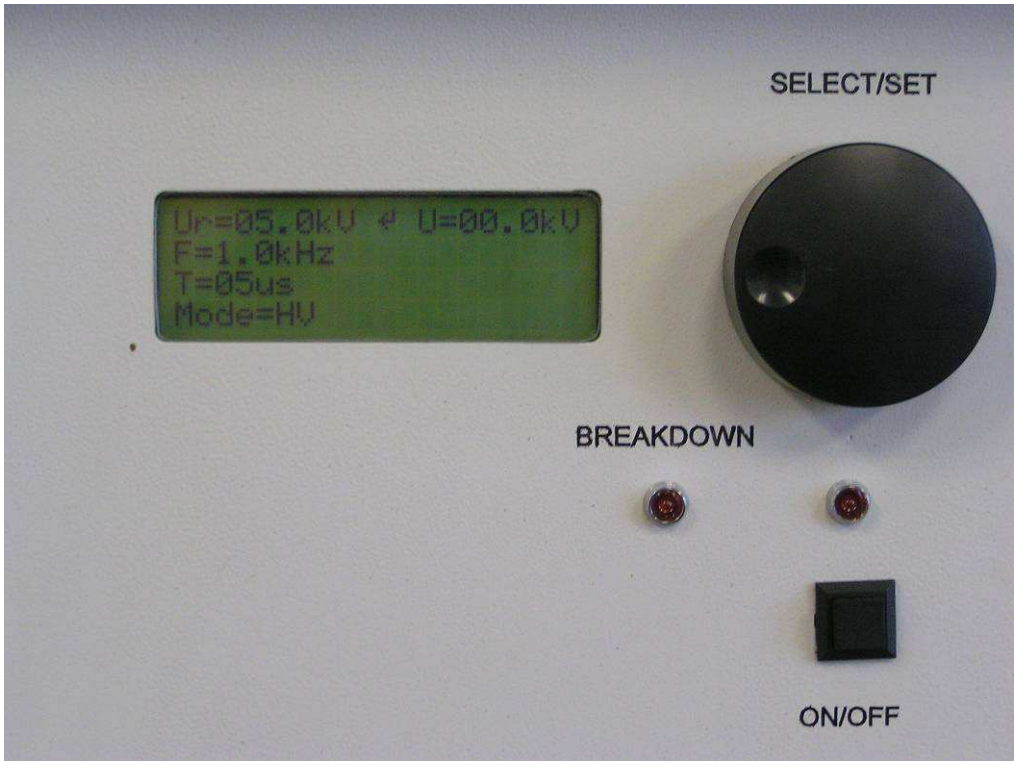

Fig. 59. Control panel.

3.6. Conclusion.

1. The use of only low negative pulsed bias voltage (up to -600 V, 5÷50 kHz) does not allow the formation of amorphous DLC films on the metal surfaces. For hard adhesive DLC films to develop on the metal surface, high negative bias voltage (more than -5 kV) is required.

2. Deposition of DLC films on the SS specimens causes an increase in surface hardness from 4÷5 GPa to 9÷11 GPa and a decrease in friction coefficient from 0.92 to 0.35. The ratio of the measured hardness H to the elastic modulus E (~0.1) is typical of diamond-like films.

3. The mean-squire roughness of the specimens obtained at U_{bias} = -15 and -20 kV (2.5 and 2.6 nm, respectively) is slightly greater than that of the initial specimen (2.4 nm). At the same time, these specimens have smaller friction coefficients due

to the DLC films present on the surface. Comparison of three specimens with DLC films shows that the coating obtained at U_{bias} = -10 kV features not only the greatest roughness (6.2), but also the highest friction coefficient (0.55).

4. For hardening the SS surface, nitriding or N^+ ion implantation from the surrounding bulk plasma can be used before deposition of DLC films.

Nitriding (with negative dc or bipolar bias voltages) for 5 h leads to an increase in SS surface hardness from 4÷5 GPa to 16÷19 GPa. Implantation of the specimens from the bulk N_2-containing plasma for 1 h provides an increase in SS surface hardness from 4÷5 GPa to 13÷15 GPa.

5. The most significant increase in surface hardness is found for N^+-implanted HSS specimens with DLC films deposited at amplitudes of negative bias voltage of -10 and -15 kV. The specimens obtained in this mode display hardness greater than that of the initial specimens, of the DLC film deposited on the initial HSS surface, and of the N-implanted specimens without DLC coatings.

6. The adhesion of the DLC films to the HSS surface is no less than 200 kg/cm^2 (the ultimate strength of the contact adhesive). Separation occurs along the “contact plate – film” interface and never at the “film – metal surface” interface. Erosion of the films by the contact adhesive escapes detection.

7. Deposition of DLC films allows a three-fivefold increase in corrosion resistance of the materials, compared to that of the initial specimens without DLC coatings. The effect by hydrochloric and sulfuric acids for 30 min does not cause any appreciable changes of the specimen surface with DLC coatings, whereas that of the specimens without coatings does. After 15 min of attack by a mixture of hydrochloric and nitric acids ($3HCl+HNO_3$), erosion of the film was observed mainly in periphery regions of the specimen at the “film – metal interface” and where cracks were found.

IV. EQUIPMENT SUPPLY AND FINAL REPORT

4.1. Experimental setup (Phygen Inc.).

Figures 60 and 61 show photos of the facility and mutual arrangement of the plasma generator, specimen holder, and Langmuir probe.

Fig.60. Photo of the facility (Phygen Inc.).

Fig.61. Mutual arrangement of the plasma generator, specimen holder, and probe.

The plasma generator was placed on the upper flange of a water-cooled stainless steel vacuum chamber of volume 0.4 m^3. The walls of the vacuum chamber were the anode of the main discharge. For more uniform plasma production, a scattering electrode was placed on the cathode of the main discharge. For visual control, there was a peephole in the vacuum chamber. DLC coatings were deposited on glass, glass, and high-speed steel specimens. The specimen surface was preliminary cleaned in an ultrasonic bath (Branson 2200) in two stages: cleaning in distilled water solution with additives and finishing cleaning in pure distilled water. The water temperature was 40 C^0. The specimens were placed on a plate of area 200 cm^2 in the vacuum chamber. The plate was located on a high-voltage insulator 45 cm away from the face of the plasma generator. The plasma density was measured using a plane Langmuir probe with a guard ring and a collecting surface area of 0.35 cm^2. The probe was 25 cm away from the plasma generator.

For increasing the lifetime of the cathode grid of the main discharge, the operating current of the emitter discharge was decreased down to 10÷15 A. The voltage of the main discharge was 100 V. Argon was supplied to the cathode cavity of the plasma generator with a flow rate of 30 sccm. Acetylene was supplied in the chamber at a distance of 15 cm from the face of the cathode of the main discharge. The acetylene flow rate was varied between 7 and 30 sccm.

For estimating the density of the produced plasma, the current-voltage characteristic of the Langmuir probe in the substrate (holder) region was measured at an emitter discharge current of 15 A and a main discharge voltage of 100 V. The Argon flow rate was 25 sccm. The current-voltage characteristic of the probe is shown in Fig. 62.

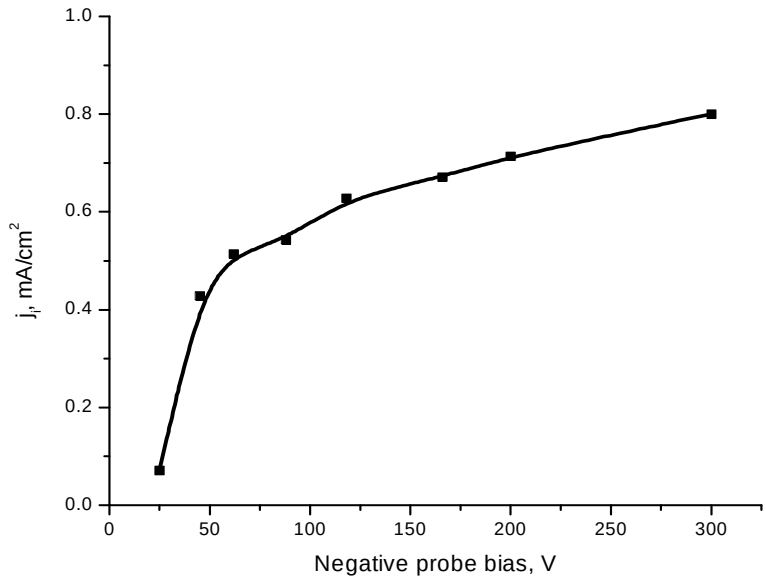

Fig. 62. Current-voltage characteristic of the Langmuir probe ($I_{em.d.}$=15 A, $U_{mn.d.}$=100 V, Q_{Ar}=25 sccm).

Clearly pronounced saturation is absent because for these parameters, the collecting surface area of the probe approximates the thickness of the ion layer, rather than being much greater than it, as required in the probe theory. Thus, the plasma density calculated from the ion current at -300 V will be overestimated. The

plasma density obtained from the position of the characteristic bend (~0.6 A/cm^2) for an electron temperature of 7 eV was about $2 \cdot 10^{10}$ cm^{-3}.

The thickness and the surface of the deposited films were examined using an angsrometer (Sloan) and an optical microscope (Nanometrics) with 100, 400, 1000x magnifications.

Before film deposition, the specimen surface was additionally treated by ion cleaning in the argon plasma. In this process, a negative pulsed (50 kHz) bias of -500 V was applied to the specimen for 30 min.

4.2. Experimental results.

Experiments show that decreasing the cleaning time and the negative bias amplitude at the stage of ion etching considerably impairs the coating adhesion (Fig. 63).

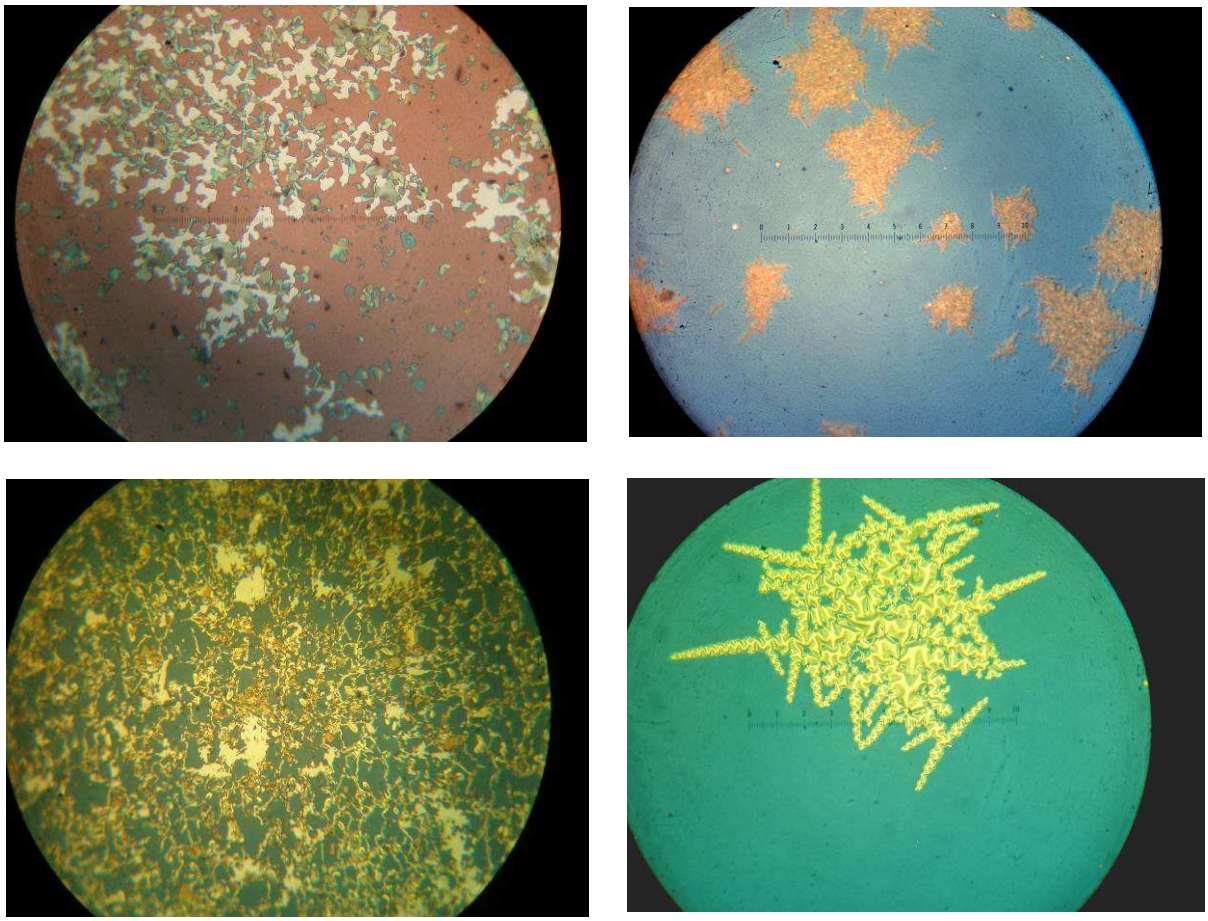

Fig. 63. Film exfoliation from the glass specimen with an insufficient time of preliminary ion etching.

The first experiments also revealed problems with the quality of the deposited coating, visually showing up as many chaotic and variously sized black inclusions on the film surface. Images the specimen surface with inclusions are shown Fig. 64.

It should be noted that most of the contamination is easily removed through wiping the surface as evidenced by the specimen surface shown in Fig. 65 b.

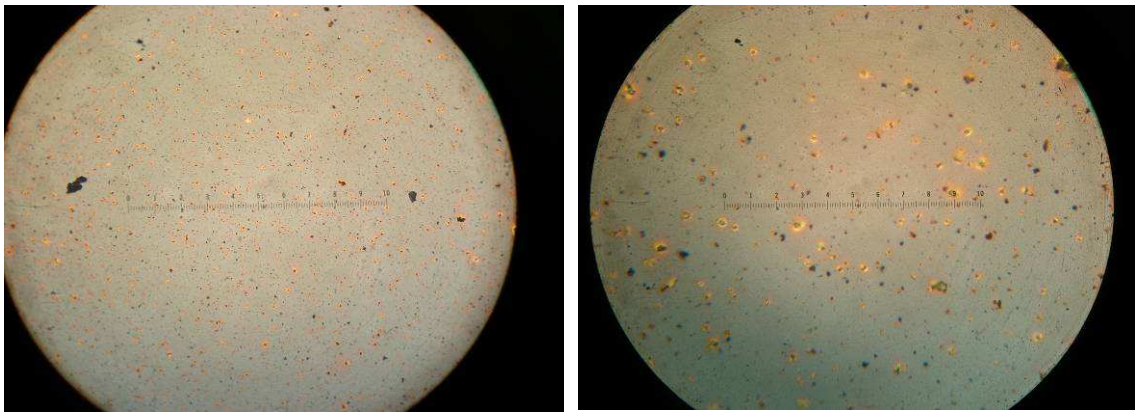

a b

Fig. 64. Surface of the glass specimen after film deposition: 100x (a) and 400x (b) magnifications.

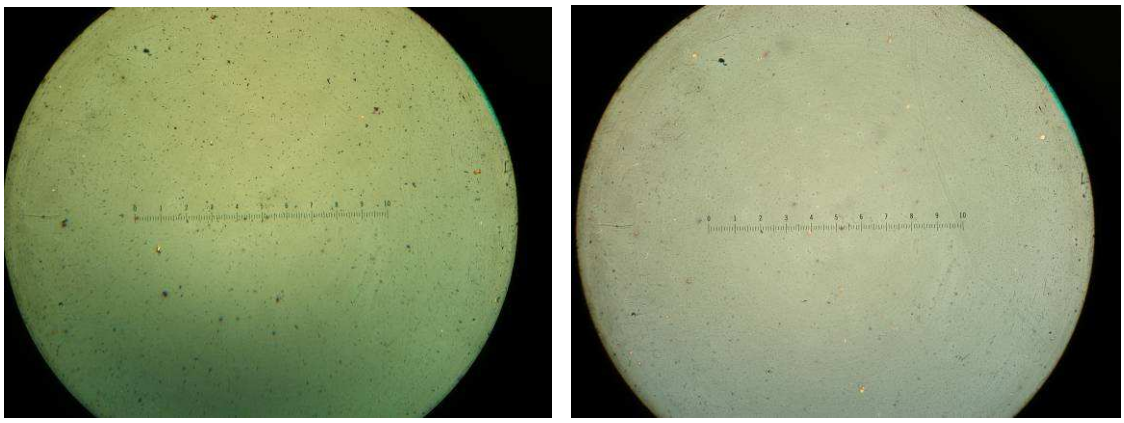

a b

Fig. 65. Surface of the glass specimen after film deposition (100x magnification): before (a) and after (b) wiping of the surface.

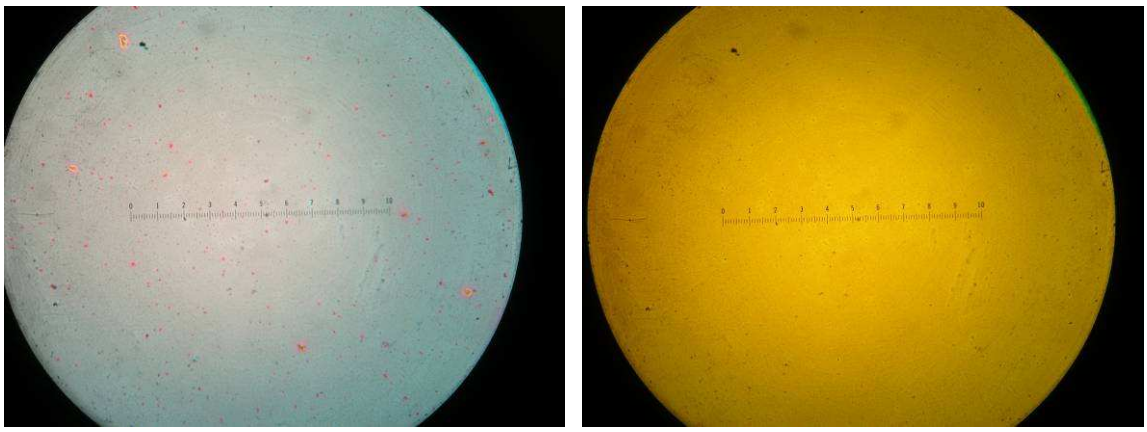

Fig. 66. Film on the glass specimen (100x magnification): with the specimen front side (a) and back side (b) facing the plasma generator.

Experiments with a reference glass specimen show that the number of the inclusions considerably decreases where the back side of the specimen faces the generator, i.e., the specimen front faces the bottom of the chamber (Fig. 66).

Taking into account the foregoing facts, the horizontal position of the holder with specimens, and the position of the plasma generator above the holder, it can be concluded that the inclusions are soot particles. At the same time, it is apparent that most of the contaminations fall on the surface during the pump-down and supply of air to the chamber, rather than during the film growth. For eliminating this effect, it can be recommended to vertically position the generator and the holder with specimens, to regularly clean the walls of the vacuum chamber and the electrodes from soot particles, and also to use a vacuum lock for specimen replacement. The invariable parameters of DLC film deposition are cited in Table 6.

Table 6. Invariable parameters of a-C:H film deposition.

Current of the emitter discharge	14 A
Voltage of the main discharge	100 V
Current of the main discharge	8 A
Plasma density	$2 \cdot 10^{10}$ cm^{-3}
Argon flow rate	30 sccm
Pulse duration	15 μs

The variable parameters were the acetylene flow rate, the deposition time, and the bias in the low-voltage mode (-200÷-500 V) and in the high-voltage mode (-5÷-

15 kV). The pulse repetition rate was 25 and 1 kHz in the low-voltage and high-voltage modes, respectively. The experiments show that for the film deposition rate to increase, the argon to acetylene flow rate ratio should be kept at about 1÷1.5. However, a great part of the graphite-like (sp2) phase is found in the film even with equal argon and acetylene flow rates. These specimens are almost black and their hardness is relatively low (glass specimen #29 and metal specimen #3). For the same reason, the operating frequency in the low-voltage mode was decreased to 5 kHz to obtain high deposition rates (200÷300 nm/h). The experiments show that increasing the interpulse interval in the low-voltage mode (by decreasing the operating frequency from 25 to 5 kHz) allows an increase in film deposition rate to about 200 nm/h (glass specimen #27). Similar films were obtained in the high-voltage mode (5 kV, 1 kHz). In this mode, the time of film deposition on metal and glass specimens was 9 h (glass specimen #31 and metal specimen #5). The specimens were arranged with their front side facing the plasma generator. The deposition parameters are cited in Table 7. Images of the surfaces of the obtained specimens are shown in Figs. 67-69.

Table 7. Parameters of a-C:H film deposition.

Current of the emitter discharge	14 A
Voltage of the main discharge	100 V
Current of the main discharge	8 A
Plasma density	$2 \cdot 10^{10}$ cm^{-3}
Argon flow rate	30 sccm
Acetylene flow rate	20 sccm
Negative bias amplitude	5 kV
Pulse duration	15 μs
Pulse repetition frequency	1 kHz
Deposition time	9 h

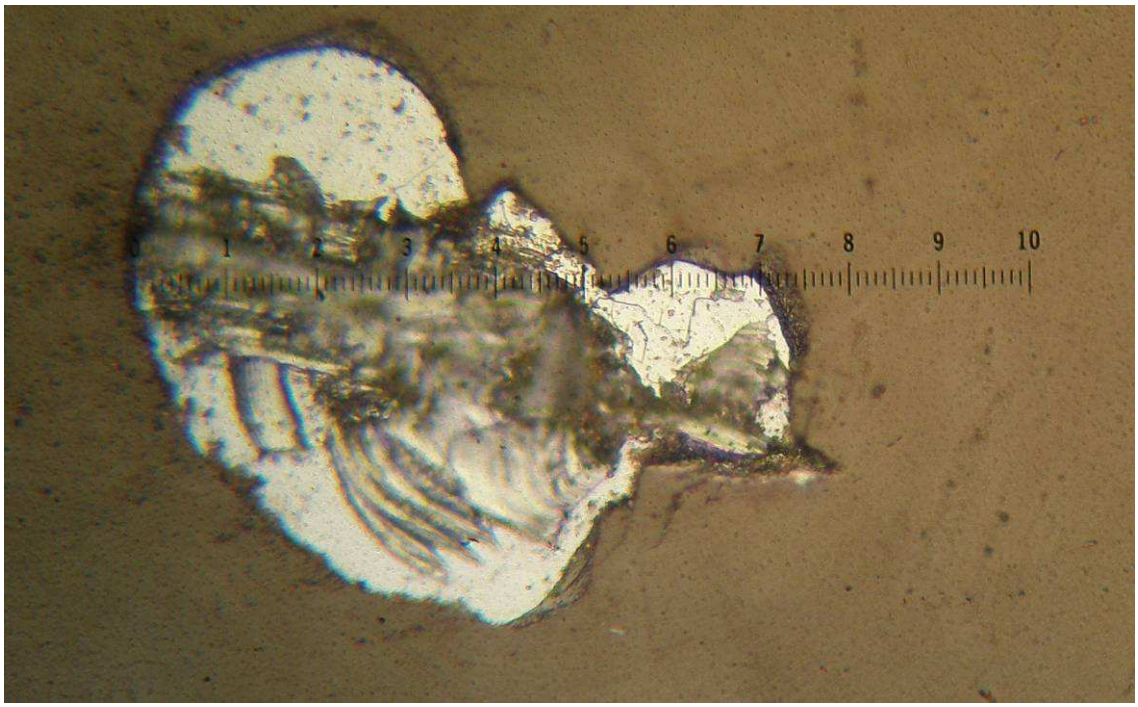

a

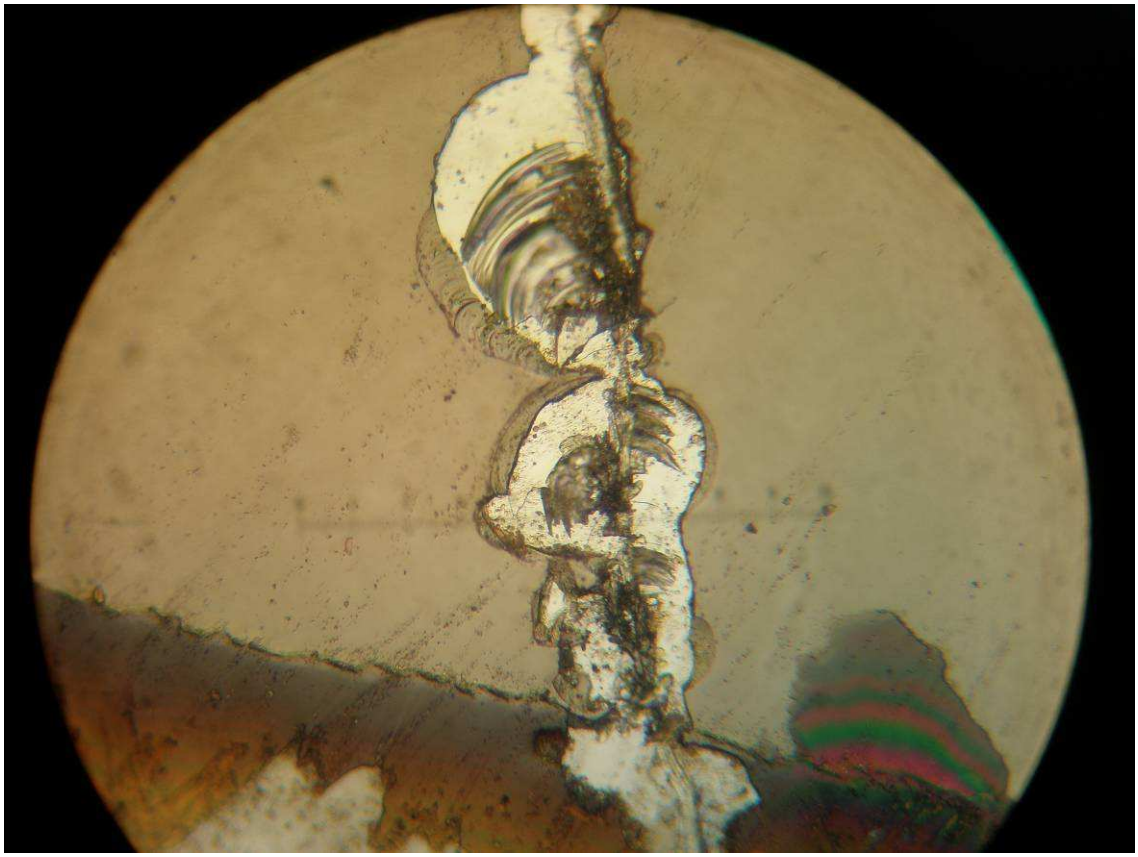

b

Fig. 67. Optical images of the DLC coating on glass at 100x (a) and 400x (b) magnifications (spallation by a diamond point).

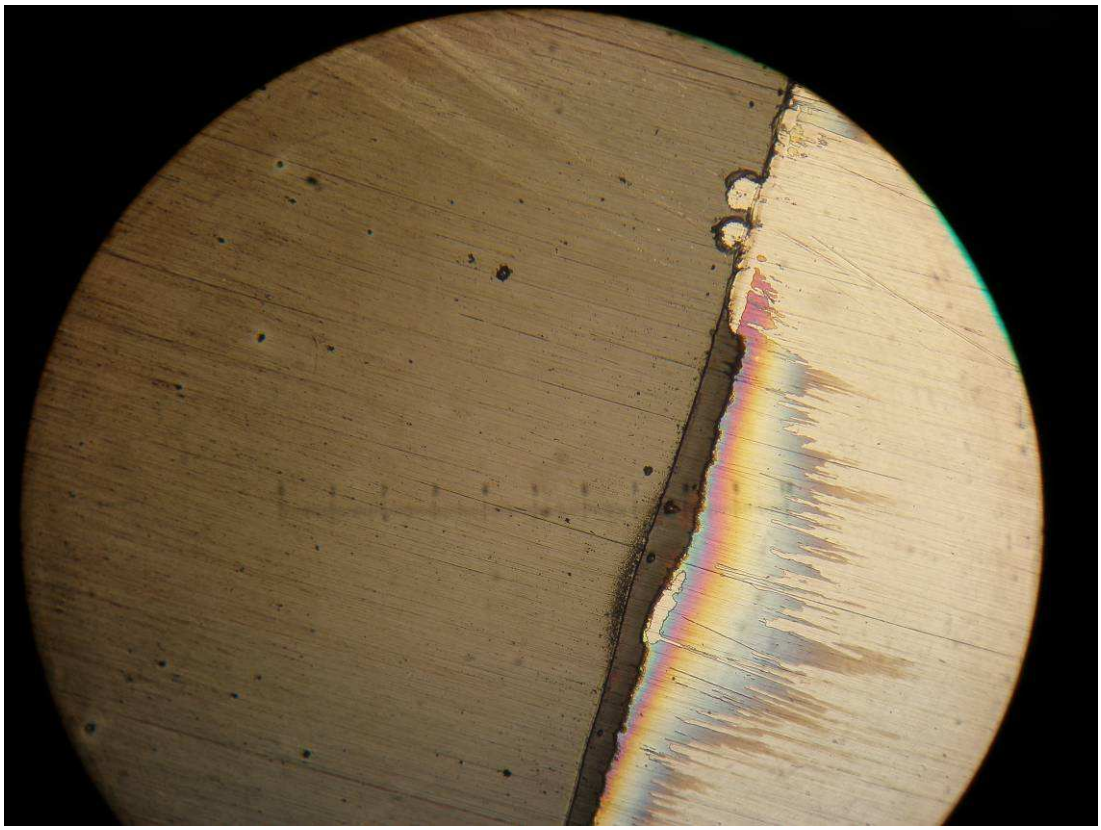

a

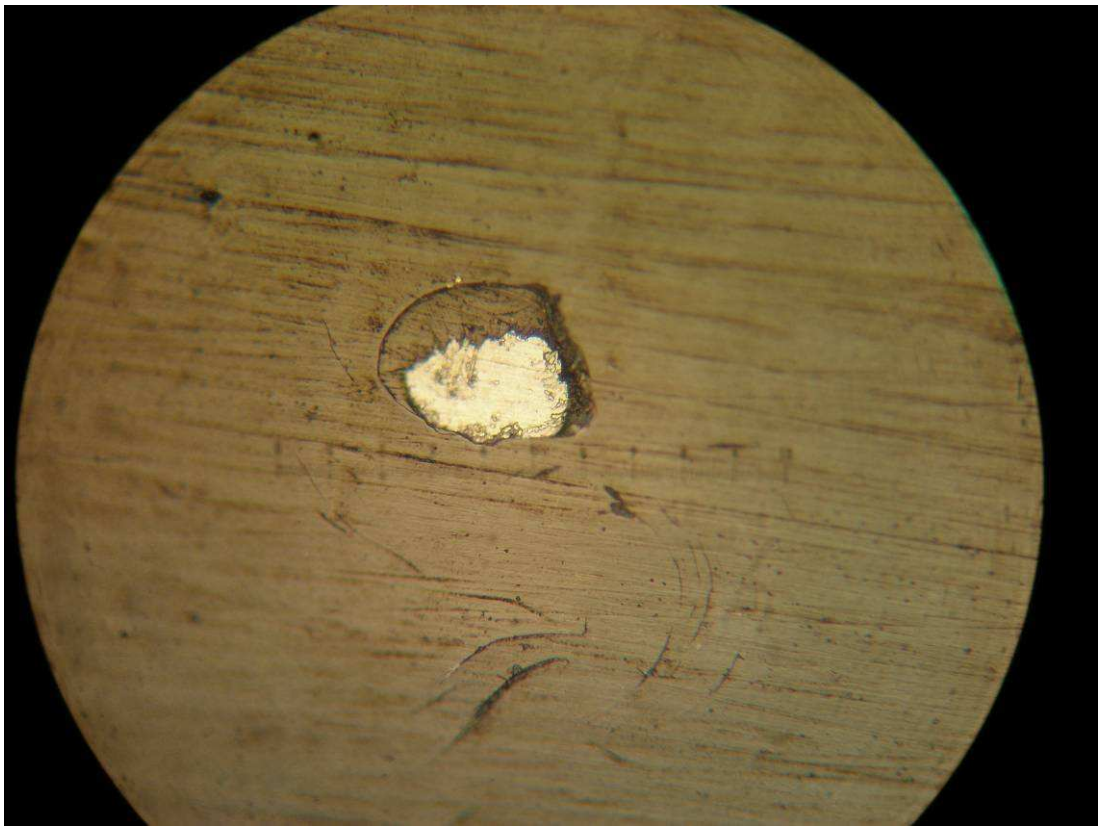

b

Fig. 68. Optical images of the DLC coating on high-speed steel at 100x (a) and 400x (b) magnifications.

Fig. 69. High-speed steel specimen with a DLC coating.

The film on the specimens is uniform over the entire surface and its adhesion is rather high. None of the specimens reveals exfoliation of the film. The film was spalled with a diamond point. It is seen that the coating structure is uniform in thickness with a minimum of defects. Measurements show that the coating thickness is about 1.2÷1.5 μm. The average deposition rate in 9 h was ~150 nm/h.

4.3. Concluding remarks.

The experiments show that:

1. The equipment supplied can successfully be used for ion etching and heating in the inert gas atmosphere before coating deposition as well as for deposition of so-called DLC (amorphous hydrogenated carbon) coatings from the plasma of hydrocarbon gases (methane, propane, acetylene).

2. The additional measures (supply of acetylene directly to the vacuum chamber, replacement of the fine tungsten grid by rods of diameter 0.8 mm) provide a service time of the discharge system up to 50 h even for the operation with hydrocarbons.

3. The precipitation of soot particles on the specimen surface can be precluded by placing the generator and the holder with specimens in a vertical position, regularly cleaning the walls of the vacuum chamber and the electrodes from soot particles, and using a vacuum lock for specimen replacement.

4. For increasing the adhesion, additional ion cleaning of the specimen surface in the argon plasma (-500 V, 50 kHz) for 30 min is required before coating deposition.

5. For deposition of DLC coatings with a rate of ~200 nm/h, it is desirable to use the high-voltage mode of the negative bias source with -5 kV, 15 μs, 1 kHz, or the low-voltage mode with -200 V, 15 μs, 5 kHz. At the same time, the argon to acetylene ratio must be no less than 3/2 to preclude the decrease in film hardness.

References:

1. C.V. Deshpandey, R.F. Bunshah. Diamond and diamond-like films: deposition processes and properties // J. Vac. Sci. Technol. A. - 1989.-V. 7. - №3. - P. 2294 - 2302.

2. H.Y. Ueng, K.-H. Dittrich, C.T. Guo Development of a hybrid coating process for deposition of diamond-like carbon films on microdrills.// Surf.&Coat. Techn. – V.200 – 2006 – P. 2900–2908.

3. H. Tsai, D.P. Bogy. Characterization of diamondlike carbon films and their application as overcoats on thin-film media for magnetic recording // J. Vac. Sci. Technol. A. – 1987. - V. 5. - №6. - P. 3287 - 3312.

4. A. Grill. Electrical and optical properties of diamond-like carbon // Thin Solid Films. – 1999. - V. 355 - 356. - P. 189 - 193.

5. G.Dearnaley атв James H.Arps Biomedical applications of diamond-like carbon (DLC) coatings: A review.// Surf.&Coat.Techn. – V.200 – 2005 – P.2518-2524.

6. B.F. Coll, M. Chhowalla. Amorphous diamond film by enhanced arc deposition // Surf. Coat. Technol.. – 1996. - V. 79. - P. 76 - 86.

7. E. Mounier, E. Quesnel, Y. Pauleau. Plasma diagnostics and characterization of amorphous carbon thin film deposited by magnetron sputtering // New Diamond and Diamond-like Films. Advances in Science and Technology. – 1995. - V. 6. - P. 183 - 190.

8. Pulsed laser deposition of diamond-like amorphous carbon films from graphite and polycarbonate targets/ A.A. Voevodin, S.J.P. Laube, S.D. Walck, J.S. Solomon, M.S. Donley, J.S. Zabinsky // J. Appl. Phys. – 1995. - V. 78. - №3. - P. 4123 - 4130.

9. M. Kitabatake, K. Wasa. Diamond film by ion-assisted deposition at room temperature // J. Vac. Sci. Technol. A. – 1988. - V. 6. - №3. - P. 1793 - 1797.

10. X. Jiang, K. Reichelt, B. Stritzker. Mechanical properties of a-C:H films prepared by plasma decomposition of C_2H_2 // J. Appl. Phys. – 1990. - V. 68. - №3. - P. 1018 - 1022.

11. High rate deposition of ta-C:H using an electron cyclotron wave resonance plasma source / N.A. Morrison, S.E. Rodil, A.C. Ferrari, J. Robertson, W.I. Milne // Thin Solid Films. – 1999. - V. 337. - P. 71 - 73.

12. M. Ham, K.A. Lou. Diamond-like carbon films grown by large-scale DC plasma CVD reactor: system, design, film characteristics, and applications // J. Vac. Sci. Technol. A. – 1990. - V. 8. - №3. - P. 2143 - 2149.

13. Fast deposition of amorphous hydrogenated carbon by an expanding cascaded arc plasma / A.J.M. Buuron, M.C.M. van de Sanden, W.J. van Ooij, D.C. Schram // in proceedings of CIP-93, Antibes, France. – 1993. - P. 89 - 91.

14. Diamond-like carbon./ J.Robertson// Pure&Appl.Chem. - 1994- V.66 - No.9 - P.1789-1796.

15. F. Seitz, J.S. Koehler / in“Progress in Solid State Physics”. - New-York: Academic. - 1957. - V. 2. - P. 30.

16. S. Aisenberg. The role of ion-assisted deposition of diamond-like carbon films // J. Vac. Sci. Technol. A. – 1990. - V. 8. - №3. - P. 2150 - 2154.

17. Y. Lifshitz, G.D. Lempert, E. Grossman. Substantiation of subplantation model for diamondlike film growth by atomic force microscopy // Phys. Rev. Lett. – 1994. - V. 72. - №17. - P. 2753 - 2756.

18. Large-scale implantation and deposition research at Los Alamos National Laboratory / B.P. Wood, I. Henins, W.A. Reass, D.J. Rej, et. al. // Nuclear Instruments and Methods in Physics Research B. – 1995. - V. 96. - P. 429 - 434.

19. Adhesion strength of DLC films on glass with mixing layer prepared by IBAD / Y. Funada, K. Awazu, H. Yasui, T. Sugita // Surf. Coat. Technol. – 2000. - V. 128 – 129. - P. 308 - 312.

20. Effect on intrinsic growth stress on the Raman spectra of vacuum-arc-deposited amorphous carbon films / J.W. Ager III, S. Anders, A. Anders, I.G. Brown // Appl. Phys. Lett. – 1995. - V. 66. - № 25 - P. 3444 - 3446.

21. J. Cui, Y. Ma, R. Fang. Species characterization for a DC biased hot filament growth of diamond using spatial resolved optical emission spectroscopy // Appl. Phys. Lett. – 1996. - V. 69. - №21. - P. 3170 - 3172.

22. J.S. Kim, M.A. Cappelli. Diamond film synthesis in low-pressure premixed methane-oxygen flames // Appl. Phys. Lett. – 1995. - V. 67. - №8. - P. 1081 - 1083.

23. S.Aisenberg, R.Chabot. Ion-beam deposition of thin films of diamondlike carbon // J. Appl. Phys. – 1971. – V. 42. - №7. – P. 2953. – 2958.

24. S.R. Kasi, H. Kang, J.W. Rabalais. Chemically bonded diamondlike films from ion-beam deposition // J. Vac. Sci. Technol. A. – 1988. - V. 6. - №3. - P. 1788 - 1792.

25. I.I. Aksenov, V.A. Belous, V.G. Padalka, V.M. Khoroshikh // Sov. J. Plasma Phys. – 1978. - V. 4. - P. 425.

26. V.E.Strel'nitski, V.G.Padalka, and S.I.Vakula, Properties of the diamond-like carbon films produced by the condensation of a plasma stream with an RF potential// Sov.Phys.Tech.Phys.- V.23 – 1978 - P.222-224.

27. I.I. Aksenov, V.A. Belous, V.G. Padalka, V.M. Khoroshikh Device for vacuum arc cleaning of microparticles. // Sov.Phys.Tech.Phys. – 1978 – V.5 – P.238

28. S. Miyagawa, S.Nakao, K.Saitoh, K.Baba, Y.Miyagawa Deposition of diamond-like carbon films using plasma source ion implantation with pulsed plasmas.// Surf.&Coat.Techn. – V.128-129 – 2000 – P.260-264.

29. K.C.Walter, M.Nastasi, C.Munson Adherent diamond-like carbon coatings on metal via plasma source ion implantation.// Surf.&Coat.Techn. – V.93 – 1997 – P.287-291.

30. K.Baba, R.Hatada Formation of amorphous carbon thin films by plasma source ion implantation.// Surf.&Coat.Techn. – V.103-104 – 1998 – P.235-239.

31. Recent advances in plasma source ion implantation at Los Alamos National Laboratory / C. P. Munson, R. J. Faehl, I. Henins et. al. // Surf. Coat. Technol. – 1996. - V. 84. - P. 528 - 236.

32. Characterization and enhanced properties of plasma immersion ion processed diamond-like carbon films / X.M. Xe, J.-F. Bardeau, K.C. Walter, M. Nastasi // J. Vac. Sci. Technol. A. – 1999. - V. 17. - №5. - P. 2525 - 2530.

33. Yuh-Han Shing, Frederick S.Pool Deposition of diamond-like films by ECR microwave plasma.// U.S.Patent # 5,427,827 (1995).

34. S. F. Yoon, Rusli, J. Ahn, Q. Zhang, Y. S. Wu, and H. Yang Deposition of diamond-like carbon films using the screen grid method in electron cyclotron resonance chemical vapor deposition.// J. Vac. Sci. Technol. - A 171 – 1999 – P.121-124.

35. Noritaka Akite, Satoko Ishii CER plasma CVD apparatus.// U.S. Patent #6,268,582 (2001).

36. Keiichi Kuramoto, Hitoshi Hirano, Yoichi Domoto, Seiichi Kiyama Arc discharge plasma CVD method for forming diamond-like carbon films.// U.S. Patent # 5,691,010 (1997).

37. W. Oliver, G. Phar, An improved technique for determining hardness and elastic modulus using load and displacement sensing indentation experiments.// J. Mater. Res., Vol. 7, 1992, P.1564-83.

38. S. Miyagawa, S.Nakao, K.Saitoh, K.Baba, and Y.Miyagawa, Deposition of diamond-like carbon films using plasma source ion implantation with pulsed plasmas.// Surf.&Coat. Techn., Vol. 128-129, 2000, P.260-264.

39. K.Baba, R.Hatada, Formation of amorphous carbon thin films by plasma source ion implantation.// Surf.&Coat. Techn., Vol. 103-104, 1998, P. 235-239.

40. Fuchigami Kenji, Wazumi Koichiro, Uematsu Kazuo, Sasa Tadashi, Preparation of highly adhesive diamond-like carbon films by plasma CVD combined with ion implantation// IHI Engineering Review, Vol. 37, No. 1, 2004, P.30-34.

41. J. Robertson Diamond-like carbon.// Pure&Appl. Chem., Vol. 66, No. 9, 1994, P.1789-96.

42. K.C.Walter, M Nastasi, H.Kung, P.Kodali, C.Munson, I.Henins, and B.P.Wood, Diamond-like carbon deposition for tribological applications at Los

Alamos National Laboratory// Materials Research Society Symposium Proceedings, Vol. 383, 1995.

43. Q. Jun, L. Jianbin, W.Shizhu, W, Jing, L.Wenzhi, Mechanical and tribological properties of non-hydrogenated DLC films synthesized by IBAD// Surf.&Coat. Techn., Vol. 128-129, 2000, P. 324-328.

44. H.Y. Ueng, K.-H. Dittrich, C.T. Guo, Development of a hybrid coating process for deposition of diamond-like carbon films on microdrills// Surface & Coatings Technology, Vol. 200, 2006, P. 2900–2908.

This document was prepared as an account of work sponsored by the United States Government. While this document is believed to contain correct information, neither the United States Government nor any agency thereof, nor The Regents of the University of California, nor any of their employees, makes any warranty, express or implied, or assumes any legal responsibility for the accuracy, completeness, or usefulness of any information, apparatus, product, or process disclosed, or represents that its use would not infringe privately owned rights. Reference herein to any specific commercial product, process, or service by its trade name, trademark, manufacturer, or otherwise, does not necessarily constitute or imply its endorsement, recommendation, or favoring by the United States Government or any agency thereof, or The Regents of the University of California. The views and opinions of authors expressed herein do not necessarily state or reflect those of the United States Government or any agency thereof or The Regents of the University of California.